Phosphorus Nutrition of Mycorrhizal Plants

A Mathematical Model

Andrea Schnepf

Linacre College

University of Oxford

A thesis submitted for the degree of

MSc Applied and Computational Mathematics

Trinity 2005

Acknowledgements

I would like to thank my supervisor Dr Tiina Roose for her guidance and encouragement throughout the last twelve months, Dr Peter Schweiger for constructive advice about the subject of mycorrhizas, and Dr Willibald Loiskandl and Dr Margarita Himmelbauer for valuable discussions and support.

I would also like to thank my family and friends for always being there for me. I am grateful to Kim Whitear and Stephanie Winterford for proof-reading my draft and to Siddharth Yadav who has been a kind friend and a culinary inspiration.

Finally, I would like to thank my husband Günther, whose continuous support gives me strength and confidence.

Abstract

Arbuscular mycorrhizas, mutualistic symbiotic associations between plant roots and soil fungi, provide an important pathway for phosphorus nutrition of many plants. We are interested in understanding the mechanisms that control and influence this pathway by means of a mathematical model. The scope of this dissertation was to develop a spatially explicit and dynamic model for solute uptake by a mycorrhizal root. To do so, we developed approximate analytical solutions for solute uptake by a single cylindrical hypha based on the standard assumption that the soil can be regarded as continuum as well as based on the assumption that a hypha grows inside individual soil pores. There is up to an order of magnitude of difference between these solutions. This highlights the fact that experiments on the single hyphal scale are needed. Furthermore, we developed a model for fungal growth which we used for upscaling uptake by a single hypha to a fungal colony scale. The result was introduced as sink term in a classical single root uptake model. The differences in calculated total uptake between the different versions of the sink term were large. Our simulation results confirm that mycorrhizas provide the root with a big spatial advantage to access non-mobile solutes in soil. They also confirm that under certain conditions, mycorrhizal fungi may dominate solute uptake completely.

Contents

List of Figures

List of Tables

Chapter 1

Introduction

Phosphorus is one of the essential mineral nutrients for plants. Uptake by plant roots occurs mainly in the chemical form "ortho-phosphate", PO_4^{3-}, the predominant form of phosphorus in soil solution. Phosphate is known to be a non-mobile ion in soil as it is strongly adsorbed to soil solid particles. Under low soil concentrations, it can be the limiting factor for plant growth. Therefore, plants have developed mechanisms to increase their ability to access soil phosphorus. A very important mechanism is the formation of mycorrhizas, a mutualistic symbiotic association between plant roots and soil fungi.

More than 80% of all terrestrial plants form mycorrhizas. They may offer several benefits to the host plant, including faster growth, improved nutrition, greater drought resistance, and protection from pathogens. The fungus benefits from the mycorrhizal symbiosis by receiving photosynthesis products from the plant.

This dissertation concentrates on modelling the phosphate acquisition by plants as effected by mycorrhizal fungi. This knowledge can be used for practical purposes such breeding of plants, development of policy models or design of new experiments. Many plant nutrient uptake models exist (Tinker & Nye 2000). A new aspect of modelling is the incorporation of mycorrhizal effects. The first stage in this process is to start from existing root models and focus on including external fungal hyphae, filaments that extend from the root surface into the soil for several centimeters. This gives mycorrhizal plants an enormous spatial advantage as they could otherwise only access phosphate up to a few millimeters away from the root surface. Spatially explicit plant nutrient uptake models which include nutrient uptake by a dynamic fungal mycelium do not yet exist to our knowledge.

We suggest two spatial scales for a model of nutrient uptake by a mycorrhizal root. Firstly, on the scale of a single hypha, we model nutrient uptake by a single cylindrical hypha. Secondly, on the scale of one root surrounded by a hyphal network

(mycelium), we model nutrient transport towards the plant root in the soil as well as within the hyphal network.

Most experimental data available focus on arbuscular mycorrhizal fungi, a specific kind of mycorrhizal fungi that are obligate symbionts; they cannot survive in the soil on their own, in absence of roots.

1.1 Motivational laboratory experiments

Two experiments motivated our modelling and we will describe them in the following sections. The first experiment is based on measuring the length densities of external hyphae with distance from the root surface. The second experiment is based on measuring the uptake of phosphate by mycorrhizal plants.

1.1.1 Measurements of hyphal length densities

Data that describe the dynamics of a fungal mycelium at different distances from the root surface and at different times are scarce since they are difficult to measure. One of the problems with arbuscular mycorrhizal fungi is that they are obligate symbionts. Therefore, fungal growth cannot be measured in a separate experiment, but always in presence of plants.

Jakobsen *et al.* (1992) measured hyphal length densities of three arbuscular mycorrhizal fungi (*Acaulosphora laevis*, *Glomus sp.* and *Scutellospora calospora*) associated with clover (*Trifolium subterraneum* L.). Plants with a previously established mycorrhiza were transferred in a two-compartment system where root growth into a hyphal only compartment was restricted by a fine nylon mesh around a root compartment. The root compartment was a cylinder with a diameter of $6\,cm$. Spread of external hyphae from the root compartment into the soil was measured at different distances after 0, 7, 14, 28 and 47 days. The measured values represent the total hyphal length density of mycorrhizal and other soil fungi. A control experiment without mycorrhizas was also conducted allowing for the estimation of the length densities of mycorrhizal fungi only.

The data are presented in units of $m\,g^{-1}$ dry soil, but we need the values in units of $cm\,cm^{-3}$ soil volume. To convert the measurements, we need the soil bulk density which was not given in the article. However, from the detailed information about the size of the hyphal compartment and amount of soil used, we estimated the bulk density ρ_b to be $\rho_b = 1.02\,g\,cm^{-3}$. Figure 1.1 shows the data for the three fungal species. At 3 cm and 7 days and 2 cm and 14 days, no control values were available.

We estimated them by linearly interpolating the neighboring values. Our estimates are given in figure 1.1.

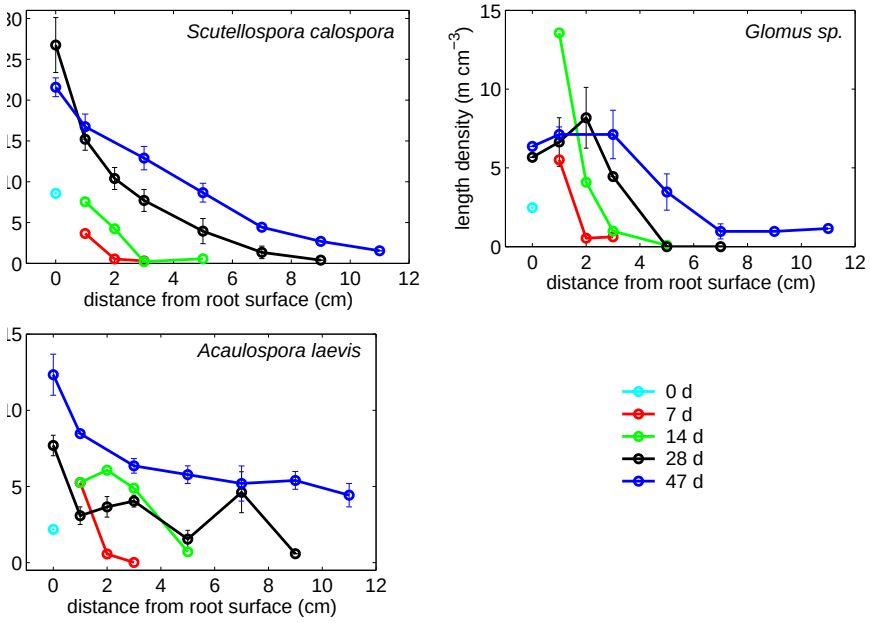

Figure 1.1: Hyphal length densities of *A. laevis*, *Glomus sp.* and *S. calospora* after 0, 7, 14, 28 and 47 days. Data reproduced from tabular and graphical data in Jakobsen *et al.* (1992). Estimated control values at 3 cm and 7 days: 1.06 $m\,g^{-1}$ and at 2 cm and 14 days: 2.00 $m\,g^{-1}$.

1.1.2 Measurements of phosphate uptake by external hyphae

Drew *et al.* (2003) measured phosphate uptake of clover (*T. subterraneum* L.) associated with the arbuscular mycorrhizal fungi *Glomus intraradices* and *G. mosseae*. Similar to Jakobsen *et al.* (1992), they also used a two-compartment system where the plants were grown in a pot with a side arm which was separated from the main compartment with a fine mesh where only fungal hyphae could penetrate. Isotopically labeled phosphate (^{33}P) was added to the side arm and the relative activity of the labeled phosphate in plant shoots was monitored. These data can be used to estimate the total amount of phosphorus taken up by the plant that originally came from the hyphal compartment. Therefore, we know that it must have been taken up by the external hyphae, translocated towards the root surface and transferred into the plant root cells. These processes determine the overall contribution of fungi to plant phosphate uptake. A sketch of the experimental setup is given in Figure 1.2. This experiment will serve to motivate our model on the single root scale.

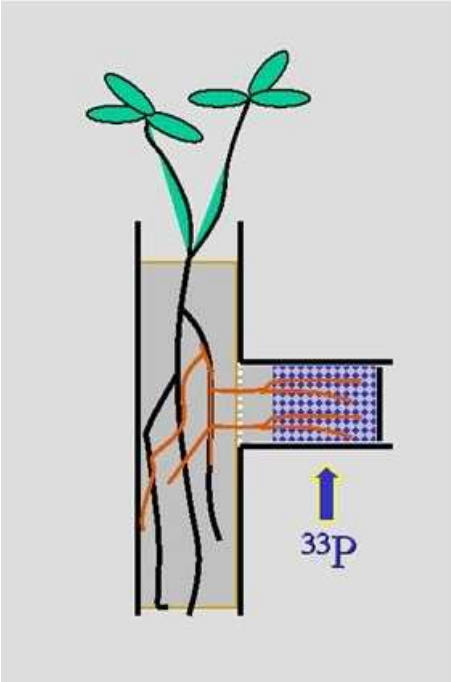

Figure 1.2: Uptake of labeled phosphate from a hyphal only compartment. Sketch of the experimental setup.

1.2 Outline of this dissertation

Our aim is to develop a model for solute uptake by mycorrhizal plants. To do so, we derive a source term to account for solute uptake by external hyphae that can be introduced to existing models on the single root scale (Tinker & Nye 2000).

In chapter 2, we develop a model for growth of arbuscular mycorrhizal fungi. A general model for mycelial fungi (Edelstein 1982) is used as starting point and adapted to the fact that arbuscular mycorrhizal fungi are always attached to a root. Analytical and numerical solutions of the model for different initial and boundary conditions are presented.

In chapter 3, we test the applicability of the model developed in chapter 2 by comparing simulation results to the experimental data of Jakobsen *et al.* (1992) and develop it further as needed. Fitting the model to the data provides us with values for the model parameters.

In chapter 4, we present three different models for solute uptake on the single hyphal scale, each based on different assumptions about the soil. The basic assumption of the first model is that the individual hyphae are present in a soil which which can be described as a continuum, where all three soil phases are present and continuous

at any given point. This is the standard assumption for root models. The basic assumption of the other two models is that the diameter of a hypha is much smaller than an individual soil pore. Depending on the relation between pore and hyphal diameter, we develop this model on a bounded and on a semi-infinite domain. Main focus is on the bounded model in the non-homogenous soil where we use asymptotic expansions to derive an approximate analytical solution. The analytical solutions for the two other models are taken from Roose *et al.* (2001).

In chapter 5 we show how the models of the previous chapters can be used to develop a sink term for solute uptake by mycorrhizas on a single root scale. We present results of numerical simulations to show the effect of external hyphae on total plant uptake.

In the conclusions in chapter 6, we outline what we have achieved, what the limitations are, and what future work could be done.

Chapter 2

Growth model for arbuscular mycorrhizal fungi

2.1 Introduction

One of the first mathematical models for the growth of filamentous fungi was proposed by Edelstein (1982). Mycorrhizal fungi are also filamentous and we therefore expect that the model is, in general, applicable to them. In this chapter, we develop a growth model for mycorrhizal fungi based on the original model of Edelstein (1982) and present analytical and numerical solutions. This provides the basis for testing the fungal growth model against experimental data in chapter 3.

Our final aim is to develop a model for the growth of mycorrhizal fungi which we can use to create a source term in a single root model to account for nutrient uptake by the mycelium. Therefore, we will focus on the external hyphae that grow in the soil. Arbuscular mycorrhizal fungi also develop internal hyphae that enter the root cortical cells and form structures called arbuscules where the transfer of phosphorus from fungus to root is thought to occur. In a first approximation, we will only deal with the influence of the root in the form of a boundary condition and not go into the detail of what is happening inside it.

As in the original model, we assume that fungal growth can be described by two variables: the hyphal length density ρ and the hyphal tip density n. The hyphal length density is the variable that can be compared to experimental data. The hyphal tips are important because growth is thought to occur due to elongation of the region just behind the hyphal tips. Therefore we can describe a flux of hyphal tips, with the tips leaving a "trail" of newly created hyphae behind them.

Edelstein (1982) describes in general biological processes such as the creation of new branches, the fusion of a tip with another tip or its neighboring hypha (anasto-

mosis) and hyphal death. Mycorrhizal fungi are known to branch mainly apically, *i.e.* one tip splits up into two. It is less clear whether anastomosis occurs in arbuscular mycorrhizal fungi. There are reports that it does (Giovanetti *et al.* 2001), but this seems to be more the exception than the rule (P. Schweiger, personal communication 2005). We will start with the most simple model here, and include additional processes as necessary when we test the model against experimental data in chapter 3.

2.2 Model formulation

We derive the equation describing fungal tip density as a conservation law. Consider an arbitrary finite volume V, which is bounded by the surface S. Let n be the hyphal tip density in that volume, $\mathbf{v}$ be the vector of elongation rates, $(n\mathbf{v})$ be the tip flux through the surface and $\mathbf{u}_n$ the unit outward normal vector to S. The total amount of tips contained in V is

$$\int_V n(x,t)dV.$$

The flux of tips into V is

$$-\int_S (n\mathbf{v})\cdot\mathbf{u}_n dS.$$

Note that the minus sign is due to the fact that $\mathbf{u}_n$ points outward. The number of tips created or destroyed in V per unit time is described by

$$\int_V f dV.$$

The change in tip density in V with time must be equal to the flux of tips into V plus the number of tips created or destroyed, *i.e.*,

$$\frac{d}{dt}\int_V n dV = -\int_S (n\mathbf{v})\cdot\mathbf{u}_n dS + \int_V f dV.$$

Because V does not change with time we can swap the integration and differentiation operators, and using the divergence theorem, we get

$$\int_V \frac{\partial n}{\partial t} dV = -\int_V \nabla\cdot(n\mathbf{v})dV + \int_V f dV.$$

Since the above expression must be true for every volume V, we conclude that

$$\frac{\partial n}{\partial t} = -\nabla\cdot(n\mathbf{v}) + f. \tag{2.1}$$

As a simplest case, we consider the new tip creation to be linearly proportional to the existing tip density, *i.e.* $f = bn$, where b is the tip branching rate. This would, in biological terms, correspond to apical branching, where one tip splits into two. The other type of branching would be lateral branching where a new hypha grows from the side of an existing hypha. However, mycorrhizal fungi are known to branch mainly apically.

The hyphal length density is dependent on hyphal growth and death. Hyphal growth occurs due to elongation of a small region just behind the hyphal tip. Therefore, the hyphae can be viewed as the "trail" left behind the tips and the increase of hyphal density can be written as $n|\mathbf{v}|$[1]. The simplest way to describe the death rate is to consider it linearly proportional to the hyphal length density ρ, *i.e.* the rate of death is $d\rho$ where d is the hyphal death rate. Hence, the equation describing the hyphal length density is

$$\frac{\partial \rho}{\partial t} = n|\mathbf{v}| - d\rho. \tag{2.2}$$

To close the growth model described by equations (2.1) and (2.2) we need to apply initial and boundary conditions. For that we will distinguish between two cases which we call the "Initial Condition Model" and the "Boundary Flux Model". For both models, let Ω be the domain where the growth of fungus is observed. It could be a petri dish in the case of non-mycorrhizal fungi or the hyphal compartment in the experiments of Drew *et al.* (2003) and Jakobsen *et al.* (1992). Let $\partial\Omega$ be the boundary of this domain.

The Initial Condition Model is the original model of Edelstein (1982) which we include here for completeness. It is motivated by an experimental setup where the growth of an initial "blob" of fungi in a petri dish is observed. We take that there is a part of the domain Ω where the hyphal tip and length density is initially greater than zero and that there are no new tips created at the boundary of the domain, $\partial\Omega$. Let $\Omega_0 \subset \Omega$ be the part of the domain where the initial hyphal length and tip density are $\rho_0 > 0$ and $n_0 > 0$, respectively, and $\mathbf{x} \in \Omega$. Then the initial and boundary conditions can be written as

[1]This corresponds also to "local time" argument known from stochastic analysis where the trail density of particle paths at any given point corresponds to the time the particle spent at that location.

$$\rho(x,0) = \begin{cases} \rho_0, & \mathbf{x} \in \Omega_0, \\ 0, & \mathbf{x} \in \Omega \backslash \Omega_0, \end{cases} \tag{2.3}$$

$$n(x,0) = \begin{cases} n_0, & \mathbf{x} \in \Omega_0, \\ 0, & \mathbf{x} \in \Omega \backslash \Omega_0, \end{cases} \tag{2.4}$$

$$(n\mathbf{v}) \cdot \mathbf{u}_n = 0, \quad t \geq 0, \mathbf{x} = \partial\Omega. \tag{2.5}$$

This model cannot be applied to mycorrhizal fungi, since they are obligate symbionts. We will consider the root surface to be a part of the domain boundary in the Boundary Flux Model.

The Boundary Flux Model is motivated by the experiment of Jakobsen *et al.* (1992) where the growth of fungal hyphae in an initially fungus free compartment is observed. We take that the interface between root and hyphal compartment is mimicking the root surface and serves as a boundary where new tips are born. Let us assume that $\partial\Omega_1 \subset \partial\Omega$ is the part of the boundary where the tip flux is $(n\mathbf{v}) = k > 0$. Then, the initial and boundary conditions can be written as

$$\rho(x,0) = 0, \quad \mathbf{x} \in \Omega, \tag{2.6}$$

$$n(x,0) = 0, \quad \mathbf{x} \in \Omega, \tag{2.7}$$

$$(n\mathbf{v}) \cdot \mathbf{u}_n = \begin{cases} k, & t \geq 0, \mathbf{x} \in \partial\Omega_1, \\ 0, & t \geq 0, \mathbf{x} \in \partial\Omega \backslash \partial\Omega_1. \end{cases} \tag{2.8}$$

Having written down the models, we will now non-dimensionalise them to find the dimensional grouping that influences the solution.

2.3 Non-dimensionalisation

We scale the variables by $t = t^*[t]$, $\mathbf{x} = \mathbf{x}^*[x]$, $n = n^*[n]$ and $\rho = \rho^*[\rho]$. If we let $[t] = \frac{1}{b}$, $[x] = \frac{|\mathbf{v}|}{b}$ and $[\rho] = [n]|\mathbf{v}|b$, equations (2.1)-(2.2) become (dropping asterisks)

$$\frac{\partial \rho}{\partial t} = n - \delta\rho, \tag{2.9}$$

$$\frac{\partial n}{\partial t} = -\nabla \cdot (n\nu) + n, \tag{2.10}$$

where $\delta = \frac{d}{b}$ and $\nu = \frac{\mathbf{v}}{|\mathbf{v}|}$. The dimensionless parameter $\delta = \frac{d}{b}$ describes the ratio between the hyphal death rate and tip branching rate. Note that the dimensionless parameter ν becomes one in the one-dimensional case.

In the Initial Condition Model, we choose $[n]$ from the initial condition, *i.e.* $[n] = n_0$ and $[\rho] = \frac{n_0|\mathbf{v}|}{b}$. The non-dimensional initial and boundary conditions are

$$\rho(x,0) = \begin{cases} \mu, & \mathbf{x} \in \hat{\Omega}_0, \\ 0, & \mathbf{x} \in \hat{\Omega} \backslash \hat{\Omega}_0, \end{cases} \tag{2.11}$$

$$n(x,0) = \begin{cases} 1, & \mathbf{x} \in \hat{\Omega}_0, \\ 0, & \mathbf{x} \in \hat{\Omega} \backslash \hat{\Omega}_0, \end{cases} \tag{2.12}$$

$$(n\nu) \cdot \mathrm{u}_n = 0, \quad t \geq 0, \mathbf{x} \in \hat{\Omega}, \tag{2.13}$$

where $\mu = \frac{b\rho_0}{|\mathbf{v}|n_0}$ and the hat ($\hat{}$) indicates that Ω has been scaled by the length scale $[x]$.

In the Boundary Flux Model, we choose $[n]$ from the boundary condition, *i.e.* $[n] = \frac{k}{|\mathrm{v}|}$ and $[\rho] = \frac{k}{b}$. The non-dimensional initial and boundary conditions are

$$\rho(x,0) = 0, \quad \mathbf{x} \in \hat{\Omega}, \tag{2.14}$$

$$n(x,0) = 0, \quad \mathbf{x} \in \hat{\Omega}, \tag{2.15}$$

$$(n\nu) \cdot \mathrm{u}_n = \begin{cases} 1, & t \geq 0, \mathbf{x} \in \partial\hat{\Omega}_1, \\ 0, & t \geq 0, \mathbf{x} \in \partial\hat{\Omega} \backslash \partial\hat{\Omega}_1. \end{cases} \tag{2.16}$$

To solve both the Initial Condition and the Boundary Flux Model, we need to choose the appropriate coordinate system. Some experimental setups, such as the one of Drew *et al.* (2003), require cartesian coordinates. Others, such as the one of Jakobsen *et al.* (1992) require cylindrical coordinates. Both situations will be dealt with in the sections below.

2.4 One-dimensional model in cartesian coordinates

In the experiment described by Drew *et al.* (2003), there is a planar interface between the hyphal and non-hyphal compartment. The hyphal tip and length densities at that boundary might be a function of time or regarded constant if the roots and fungi are well established in the main compartment. For this experimental setup, we can consider hyphal and tip length densities to depend only on the horizontal distance from the root-fungus interface. Hence we have to solve the one dimensional problem in cartesian coordinates. Let us consider a semi-infinite domain. The non-dimensional equations are

$$\frac{\partial \rho}{\partial t} = n - \delta\rho, \tag{2.17}$$

$$\frac{\partial n}{\partial t} = -\frac{\partial n}{\partial x} + n. \tag{2.18}$$

Let us assume that the soil initially containing hyphal tips is in the interval $[0, x_1]$ and that initially, there are only hyphal tips present (*i.e.* spores) so that the initial hyphal length density is zero. Let $\hat{x_1}$ be the dimensionless parameter $\hat{x_1} = \frac{x_1}{[x]} = \frac{x_1 b}{v}$. Then the initial and boundary conditions of the Initial Condition Model are

$$n(x,0) = \begin{cases} 1, & 0 \le x \le \hat{x_1}, \\ 0, & \hat{x_1} < x < \infty, \end{cases} \tag{2.19}$$

$$\rho(x,0) = \begin{cases} 0, & 0 < x < \infty, \end{cases} \tag{2.20}$$

$$n(0,t) = 0, \quad t > 0. \tag{2.21}$$

The initial and boundary conditions of the Boundary Flux Model are

$$n(x,0) = 0, \quad 0 < x < \infty, \tag{2.22}$$

$$\rho(x,0) = 0, \quad 0 < x < \infty, \tag{2.23}$$

$$n(0,t) = 1, \quad t > 0. \tag{2.24}$$

2.4.1 Analytical solutions

Equation (2.18) is a hyperbolic equation and can be solved using the method of characteristics. Let x and t be functions of a parameter τ, *i.e.* $x = x(\tau)$, $t = t(\tau)$. Then the characteristic equations are

$$\frac{\partial t}{\partial \tau} = 1, \tag{2.25}$$

$$\frac{\partial x}{\partial \tau} = 1, \tag{2.26}$$

and the partial differential equation (2.18) becomes the ordinary differential equation

$$\frac{\partial n}{\partial \tau} = n. \tag{2.27}$$

From equations (2.25) and (2.26) we find that the characteristics are straight parallel lines (figure 2.1). The dashed line in figure 2.1 separates the regions determined by the initial and boundary conditions. The characteristic equations are valid for both the Initial Condition and the Boundary Flux Model.

Initial Condition Model

We first solve the equation for n in the Initial Condition Model. We parameterise the initial condition (2.19), so that at $\tau = 0$, $x = s$, $t = 0$ and

$$n(s,0) = \begin{cases} 1, & 0 \le s < \hat{x_1}, \\ 0, & \hat{x_1} < s < \infty, \end{cases}$$

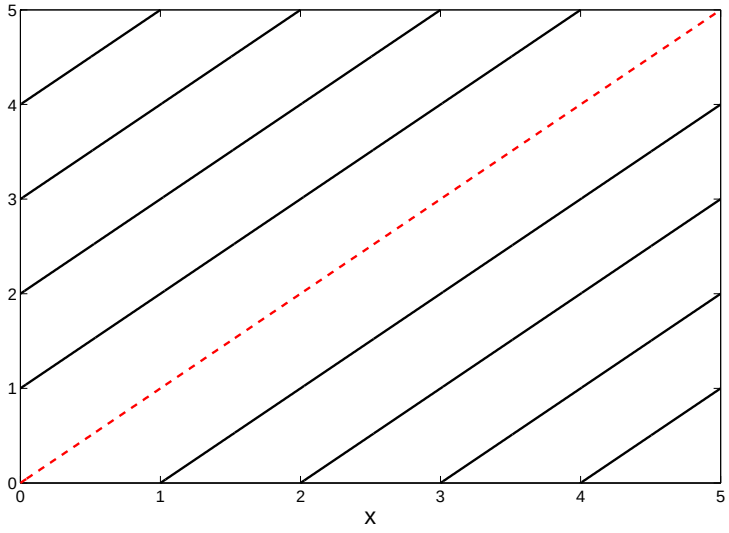

Figure 2.1: Characteristics of equation (2.18).

where $s = x(0)$. Then, integrating equations (2.25)-(2.27) gives the parametric solution in the region influenced by the initial condition,

$$t = \tau, \tag{2.28}$$

$$x = \tau + s, \tag{2.29}$$

$$n(s) = \begin{cases} e^{\tau}, & 0 \leq s < \hat{x_1}, \\ 0, & \hat{r_1} < s < \infty. \end{cases} \tag{2.30}$$

We parameterise the boundary condition (2.21) so that at $\tau = 0$, $x = 0$, $t = s$, $n(s, 0) = 0$, $s \geq 0$, and integrating equations (2.25)-(2.27) gives the parametric solution influenced by the boundary condition,

$$t = \tau + s, \tag{2.31}$$

$$x = \tau, \tag{2.32}$$

$$n(s) = 0, \ s \leq 0. \tag{2.33}$$

Combining the solutions of the two regions and eliminating the parameters τ and s, we have the solution for n,

$$n(x,t) = \begin{cases} 0, & x - t \leq 0, \\ e^{t}, & 0 \leq x - t < \hat{x_1}, \\ 0, & \hat{x_1} < x - t < \infty. \end{cases} \tag{2.34}$$

To find ρ, we solve

$$\frac{d\rho}{dt} + \delta\rho = n(x,t), \tag{2.35}$$

on the interval $[0, t]$ with initial condition $\rho(x, 0) = 0$, for $0 \leq x \leq \infty$, to get

$$\rho(x,t) = e^{-\delta t} \int_0^t n(x,\xi) e^{\delta t} d\xi, \qquad 0 < x < \infty. \tag{2.36}$$

The solution is

$$\rho(x,t) = \frac{e^{-\delta t}}{1+\delta} \begin{cases} e^{(1+\delta)t} - 1, & x \leq \hat{x_1} \text{ and } 0 \leq t \leq x, \\ e^{(1+\delta)x} - 1, & x \leq \hat{x_1} \text{ and } 0 \leq x \leq t, \\ e^{(1+\delta)t} - e^{(1+\delta)(x-\hat{x_1})}, & x > \hat{x_1} \text{ and } x - \hat{x_1} < t < x, \\ e^{(1+\delta)x} - e^{(1+\delta)(x-\hat{x_1})}, & x > \hat{x_1} \text{ and } x - \hat{x_1} < x < t, \\ 0, & t \leq x - \hat{x_1} < \infty. \end{cases} \tag{2.37}$$

Figure 2.2 shows the result of the dimensionless model for different values of the parameter δ. The left graph shows the hyphal tip density at time $t = 0$ and $t = 1$. We see that the initial "blob" of tips has moved due to the elongation rate and that the number of tips has increased due to branching. The parameter δ has no effect on this increase, because we have scaled the model so that the branching rate is always one. The effect of δ is visible in the right graph of figure 2.2, where the hyphal length density at time $t = 1$ is shown. (At $t = 0$, $\rho = 0$.) The larger δ, the greater is the death rate and the more pronounced is the decrease of length density.

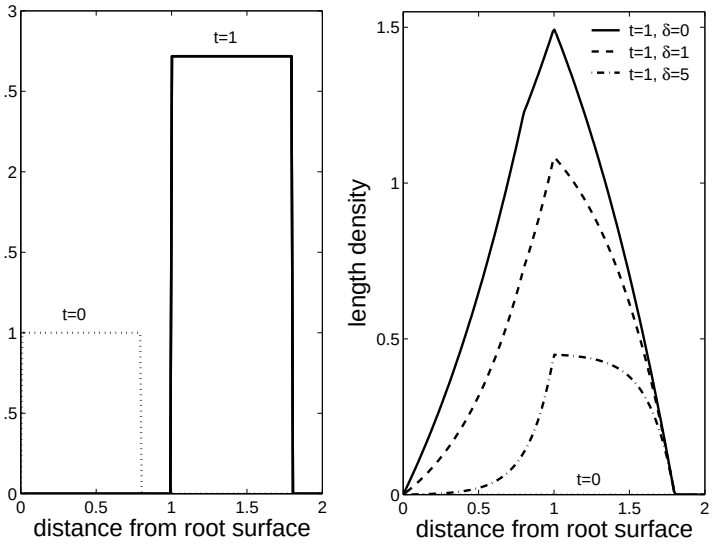

Figure 2.2: Plot of equations (2.34) and (2.37). Analytical solution for hyphal tip and length density of the Initial Condition Model in one-dimensional cartesian coordinates for different values of the dimensionless parameter δ.

Boundary Flux Model

We now solve for n in the Boundary Flux Model. Equations (2.25)-(2.27) are still valid, but we use the initial and boundary conditions given by equations (2.22)-(2.24). We parameterise the initial condition (2.22) so that at $\tau = 0$, $x = s$, $t = 0$ and

$$n(s, 0) = \ 0, \qquad 0 < s < \infty.$$

Integrating equations (2.25)-(2.27) gives the parametric solution in the region influenced by the initial condition,

$$t = \tau, \tag{2.38}$$

$$x = \tau + s, \tag{2.39}$$

$$n(s) = 0, \qquad x - t \geq 0. \tag{2.40}$$

Parameterising the boundary condition (2.24) so that at $\tau = 0$, $x = 0$, $t = s$ and $n(s, 0) = 1$ for $s \geq 0$ and integrating equations (2.25)-(2.27) gives the parametric solution in the region influenced by the boundary condition,

$$t \ = \ \tau + s, \tag{2.41}$$

$$x \ = \ \tau, \tag{2.42}$$

$$n(s) \ = \ e^{\tau}, \ x - t \leq 0. \tag{2.43}$$

Combining the solutions of the two regions and eliminating the parameters τ and s, we have the solution for n,

$$n(x, t) = \begin{cases} e^{x}, & x - t \leq 0, \\ 0, & x - t \geq 0. \end{cases} \tag{2.44}$$

To find ρ, we solve

$$\frac{d\rho}{dt} + \delta\rho = n(x, t), \tag{2.45}$$

on the interval $[0, t]$ with initial condition $\rho(x, 0) = 0$, for $0 \leq x \leq \infty$, to get

$$\rho(x, t) = \begin{cases} \frac{1}{\delta} e^{x} \left(1 - e^{\delta(x-t)}\right), & 0 \leq x < t, \\ 0, & t \leq x < \infty. \end{cases} \tag{2.46}$$

Figure 2.3 shows the result for different values of the parameter δ. The left graph shows the hyphal tip density at time $t = 1$. As in the result for the previous model, the parameter δ has no effect on the hyphal tip density, because we have scaled the model so that the branching rate is always 1. The effect of δ is again visible in the

right graph of figure 2.3, where the hyphal length density at time $t = 1$ is shown. The hyphae have arrived at the same position, but the larger δ, the greater is the death rate and the more pronounced is the decrease of length density. When the death rate is small, the largest length density is at the root surface. The larger δ, the further this peak moves away from the root surface. If we assume that all hyphae are active, that would mean that the highest activity is at the front of the colony when the death rate is high.

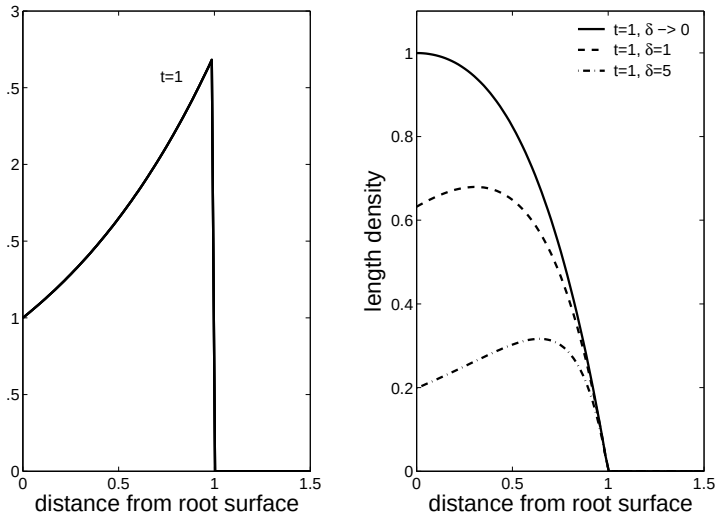

Figure 2.3: Plot of Equations (2.44) and (2.46). Analytical solution for hyphal tip and length density of the Boundary Flux Model in one-dimensional cartesian coordinates for different values of the dimensionless parameter δ.

2.4.2 Numerical solutions

Our final aim is to fit the Boundary Flux Model to the data given by Jakobsen *et al.* (1992), who measured hyphal length densities at different distances from a root compartment at several points in time. The data suggest that we might have to introduce non-linearities into the model which could require a numerical solution. In anticipation of this, we will now solve these linear equations numerically so we can compare the results to the analytical solutions derived above and determine the most preferred numerical scheme. We will do this for both the Initial Condition and Boundary Flux Model. We compare three numerical schemes for solving the hyperbolic equation for the hyphal tip density n: an Upwind scheme, a Lax-Friedrich scheme and a Lax-Wendroff scheme (Morton & Mayers 1994). The equation describing hyphal length density, equation (2.17), can be solved with any scheme for an ordinary differential

equation. We use the explicit Euler method in time for simplicity, using the same time step as the scheme for the hyperbolic equation. Below, we describe the different schemes. Let T_f be the final time, M the number of time steps, Δx the grid spacing, J the number of grid points and $\Delta t = \frac{T_f}{M}$. Let $n(x_j, t_m) \approx U_j^m$ and $\mu = \frac{\Delta t}{\Delta x}$.

The upwind scheme is derived by replacing the derivatives with divided differences. Equation (2.18) becomes

$$\frac{U_j^{m+1} - U_j^m}{\Delta t} = -\frac{U_j^m - U_{j-1}^m}{\Delta x} + U_j^m, \qquad j = 1, 2, ..., J \tag{2.47}$$

$$U_j^0 = U_0, \qquad j = 0, ..., J \tag{2.48}$$

$$U_0^{m+1} = U_b, \qquad m = 0, ..., M-1. \tag{2.49}$$

Equation (2.47) can be written as

$$U_j^{m+1} = (1 - \mu + \Delta t)U_j^m + \mu U_{j-1}^m. \tag{2.50}$$

The Lax-Friedrich scheme is derived by using a centered difference for the space derivative and replacing U_j^m in the time difference by the average of its neighboring points, $\frac{1}{2}(U_{j+1}^m + U_{j-1}^m)$. Then equation (2.18) becomes

$$\frac{U_j^{m+1} - \frac{1}{2}(U_{j+1}^m + U_{j-1}^m)}{\Delta t} = -\frac{U_{j+1}^m - U_{j-1}^m}{2\Delta x} + U_j^m, \tag{2.51}$$

for $j = 1, 2, ..., J$, which can be rearranged to

$$U_j^{m+1} = (\frac{1}{2} - \frac{\mu}{2})U_{j+1}^m + (\frac{1}{2} + \frac{\mu}{2})U_{j-1}^m + \Delta t U_j^m. \tag{2.52}$$

For the derivation of the Lax-Wendroff scheme, we use the fact that

$$n_t = -n_x + n, \tag{2.53}$$

$$\begin{aligned} n_{tt} &= -\frac{\partial}{\partial x}(n_t) + n_t, \\ &= n_{xx} - 2n_x + n. \end{aligned} \tag{2.54}$$

Substituting these into the Taylor series expansion

$$U_j^{m+1} = U_j^m + \Delta t[U_t]_j^m + \frac{(\Delta t)^2}{2}[U_{tt}]_j^m + O((\Delta t)^3),$$

and neglecting higher order terms gives

$$U_j^{m+1} = U_j^m + \Delta t(-U_x + U_j^m) + \frac{(\Delta t)^2}{2}(U_{xx} - 2U_x + U_j^m). \tag{2.55}$$

Replacing the space derivatives by centered differences and rearranging gives the Lax-Wendroff scheme

$$\begin{aligned} U_j^{m+1} = (1 + \Delta t - \mu^2 + \frac{(\Delta t)^2}{2})U_j^m \\ +(-\Delta t\frac{\mu}{2} - \frac{\mu}{2} + \frac{\mu^2}{2})U_{j+1}^m \\ +(\Delta t\frac{\mu}{2} + \frac{\mu}{2} + \frac{\mu^2}{2})U_{j-1}^m. \end{aligned} \tag{2.56}$$

The initial and boundary conditions for the Initial Condition Model are $U_j^0 = n_0(x_j)$ for $j = 0, ..., J$, $U_0^{m+1} = 0$ for $m = 0, 1, ..., M-1$, and for the Boundary Flux Model $U_j^0 = 0$ for $j = 0, ..., J$, $U_0^{m+1} = 1$ for $m = 0, 1, ..., M-1$.

Figures 2.4(a)-2.6(b) show comparisons of the numerical and analytical solutions for the hyphal tip and length densities for both the Initial Condition and the Boundary Flux Model. In general, all three schemes performed reasonably well. Judging from the graphs, the numerical solutions are closest to the analytical solution in the case of the Lax-Wendroff scheme. The scheme for the computation of the length density seems to smooth out the typical oscillations around the sharp edges that can be seen in the left graphs of figures 2.5(a) and 2.5(b).

In the following paragraph, we perform stability analysis and give the accuracy for each of the three schemes for the hyperbolic equation. Let us assume the Courant-Friedrichs-Lewy (CFL) condition, so that $0 \leq \mu \leq 1$, where $\mu = \frac{\Delta t}{\Delta x}$. By inserting the Fourier mode $U_j^m = (\lambda(k))^m e^{ikj\Delta x}$ into each scheme, we find, after some algebra, the amplification factor λ. The modulus squared of the amplification factor of the Upwind scheme is

$$|\lambda|^2 = (1 + \Delta t)^2 - 4\mu \sin^2 \frac{k\Delta x}{2} \left((1 + \Delta t) - \mu\right). \tag{2.57}$$

If $|\mu| \leq 1$, we have $|\lambda| \leq 1 + \Delta t$, the scheme is von Neumann stable. The modulus squared of the amplification factor of the Lax-Friedrich scheme is

$$|\lambda|^2 = (1 + \Delta t)^2 - ((1 + \Delta t)^2 - \mu^2) \sin^2 k\Delta x. \tag{2.58}$$

If $|\mu| \leq 1$, we have $|\lambda| \leq 1 + \Delta t$, the scheme is von Neumann stable. The modulus squared of the amplification factor of the Lax-Wendroff scheme is

$$\begin{aligned} |\lambda|^2 &= 1 - 4\mu^2(1 - \mu^2) \sin^4 \frac{k\Delta x}{2} - (\mu^2(\Delta t)^2 + 2\mu^2\Delta t) \cos^2(k\Delta x) + \\ &+ \Delta t(2 + \mu^2) + (\Delta t)^2(2 + \mu^2) + (\Delta t)^3 + \frac{(\Delta t)^4}{4}. \end{aligned} \tag{2.59}$$

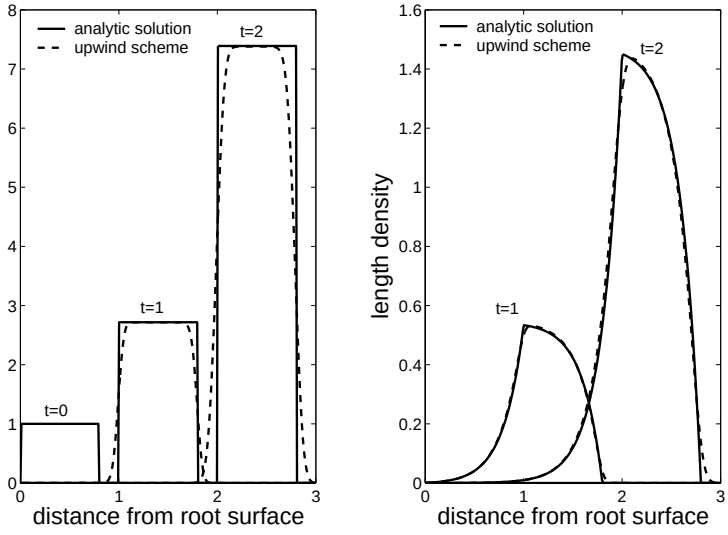

(a) Initial Condition Model

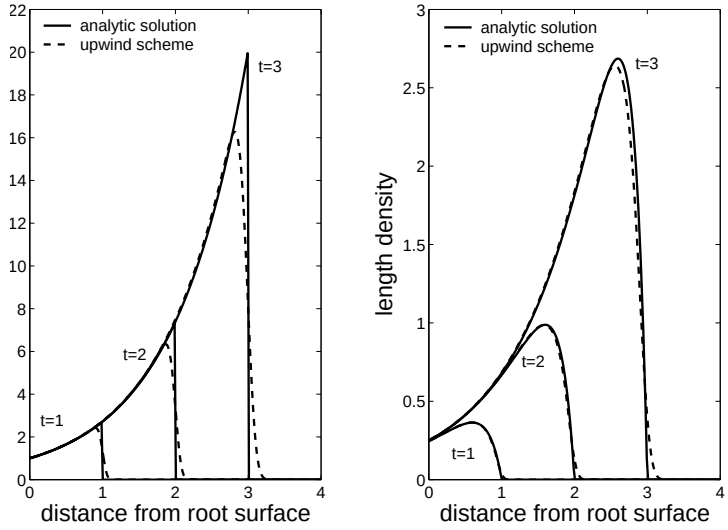

(b) Boundary Flux Model

Figure 2.4: Comparison of Upwind scheme to analytical solutions at three different points in time. $\delta = 4$, $J = 300$, $\frac{\Delta t}{\Delta x} = 0.8$, dt=0.0027.

If $|\mu| \leq 1$, we have $|\lambda| \leq 1 + \Delta t + \frac{(\Delta t)^2}{2}$. If $\Delta t \leq 1$, we have $|\lambda| \leq 1 + \frac{3}{2}\Delta t$, the scheme is von Neumann stable. The accuracy of the the Upwind scheme is $O(\Delta t + \Delta x)$, the accuracy of the Lax-Friedrich scheme is $O(\Delta t + \frac{(\Delta x)^2}{\Delta t}(\Delta x)^2)$ and the accuracy of the Lax-Wendroff scheme is $O((\Delta t)^2 + (\Delta x)^2)$. All three schemes considered are von Neumann stable. If $\mu \leq 1$, the largest constant in front of Δt is found in the Lax-Wendroff scheme. However, in the numerical examples considered, stability was not a problem. Therefore, we will select the scheme with the highest accuracy if a

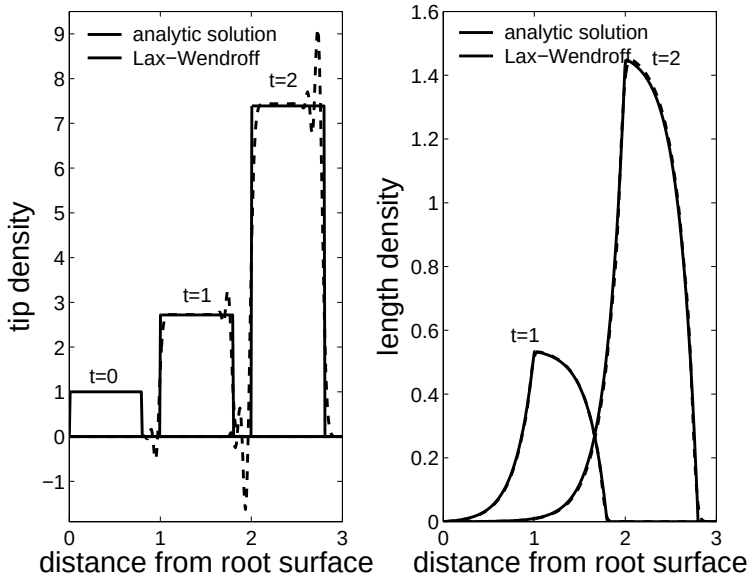

(a) Initial Condition Model

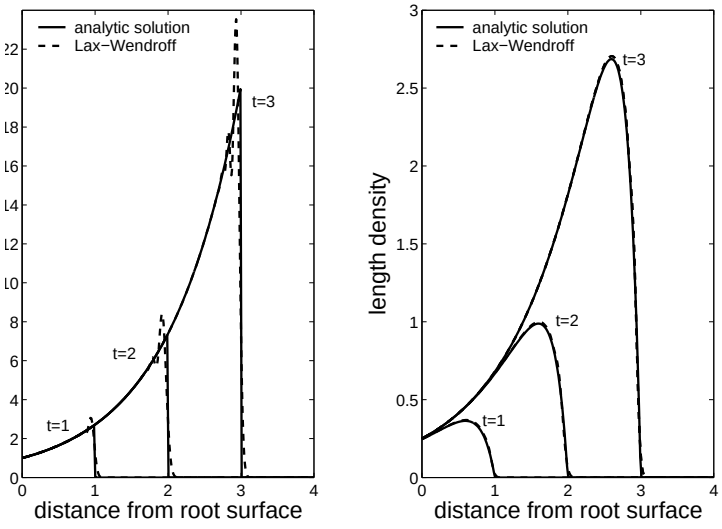

(b) Boundary Flux Model

Figure 2.5: Comparison of Lax-Wendroff scheme to analytical solutions at three different points in time. $\delta = 4$, $J = 300$, $\frac{\Delta t}{\Delta x} = 0.8$, dt=0.0027.

numerical solution is required, which is the Lax-Wendroff scheme.

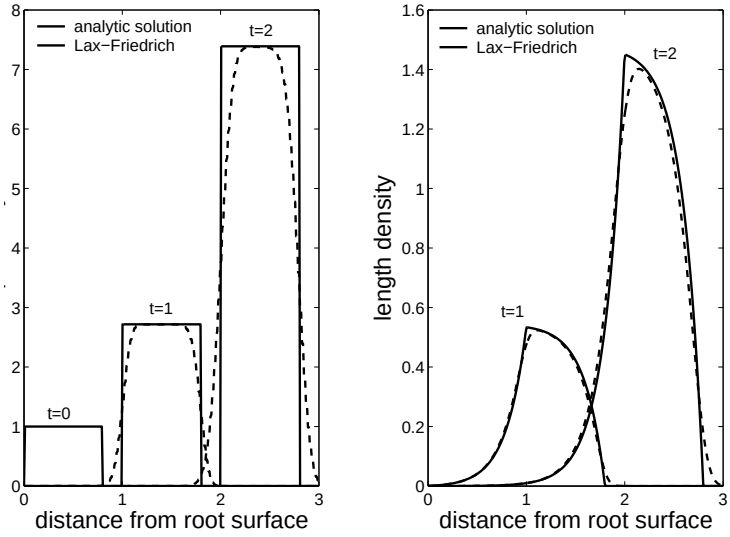

(a) Initial Condition Model

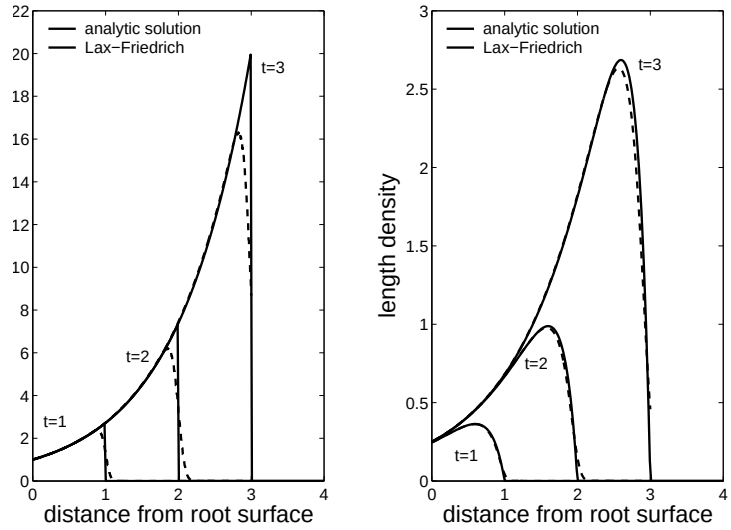

(b) Boundary Flux Model

Figure 2.6: Comparison of Lax-Friedrich scheme to analytical solutions at three different points in time. $\delta = 4$, $J = 300$, $\frac{\Delta t}{\Delta x} = 0.8$, dt=0.0027.

2.5 One-dimensional model in radial polar coordinates

Radial polar coordinates are suitable when we consider a cylindrical root from which the fungal hyphae start growing into the soil. This situation is mimicked in the experiment of Jakobsen *et al.* (1992), where a cylindrical root compartment is placed in an initially fungus free soil. In polar coordinates, the divergence operator ($\nabla\cdot$) is

given by $\frac{1}{r}\frac{\partial}{\partial r}r$. If r_0 is the root radius and $\hat{r_0} = \frac{r_0 b}{v}$, equation (2.10) becomes

$$\frac{\partial n}{\partial t} = -\frac{1}{r}\frac{\partial (rn)}{\partial r} + n, \qquad t \geq 0,\, \hat{r_0} \leq r \leq \infty. \tag{2.60}$$

The initial and boundary conditions for n of the Initial Condition Model in radial coordinates are

$$n(r,0) = \begin{cases} 1, & \hat{r_0} \leq r \leq \hat{r_1}, \\ 0, & \hat{r_1} < r < \infty, \end{cases} \tag{2.61}$$

$$n = 0, \qquad t > 0, r = \hat{r_0}, \tag{2.62}$$

where $\hat{r_1} = \frac{r_1 b}{v}$ and $[\hat{r_0}, \hat{r_1}]$ is the interval initially containing hyphal tips. The initial and boundary conditions of the Boundary Flux Model are

$$n(r,0) = 0, \qquad \hat{r_0} < x < \infty, \tag{2.63}$$

$$n = 1, \qquad t > 0,\, r = \hat{r_0}. \tag{2.64}$$

2.5.1 Analytical solutions

As before, we use the method of characteristics to solve the hyperbolic equation (2.60). The characteristic equations are

$$\frac{\partial t}{\partial \tau} = 1, \tag{2.65}$$

$$\frac{\partial r}{\partial \tau} = 1, \tag{2.66}$$

and the partial differential equation 2.60 becomes the ordinary differential equation

$$\frac{\partial n}{\partial \tau} = (1 - \frac{1}{r})n. \tag{2.67}$$

Initial Condition Model

We parameterise the initial condition (2.61) so that at $\tau = 0$, $r = s$, $t = 0$ and

$$n(s,0) = \begin{cases} 1, & \hat{r_0} \leq s < \hat{r_1}, \\ 0, & \hat{r_1} < s < \infty. \end{cases}$$

Integrating equations (2.65)-(2.67) gives the parametric solution for the region influenced by the initial condition,

$$t = \tau, \tag{2.68}$$

$$r = \tau + s, \tag{2.69}$$

$$n(s) = \begin{cases} \frac{s}{\tau + s}e^{\tau}, & \hat{r_0} \leq s < \hat{r_1}, \\ 0, & \hat{r_1} < s < \infty. \end{cases} \tag{2.70}$$

Parameterising the boundary condition (2.62) so that at $\tau = 0$, $r = \hat{r_0}$, $t = s$, $n(s,0) = 0$, $s \geq 0$, and integrating equations (2.65)-(2.67) gives the parametric solution in the region influenced by the boundary condition,

$$t = \tau + s, \tag{2.71}$$

$$r = \tau + \hat{r_0}, \tag{2.72}$$

$$n(s) = 0 \text{ for } s \leq \hat{r_0}. \tag{2.73}$$

Combining the solutions of the two regions and eliminating the parameters τ and s, we have the solution for n,

$$n(r,t) = \begin{cases} 0, & r - t \leq \hat{r_0}, \\ \frac{r-t}{r} e^t, & \hat{r_0} \leq r - t < \hat{r_1}, \\ 0, & \hat{r_1} < r - t < \infty. \end{cases} \tag{2.74}$$

To find ρ, we solve

$$\frac{d\rho}{dt} + \delta\rho = n(r,t), \tag{2.75}$$

on the interval $[0,t]$ with initial condition $\rho(r,0) = 0$, for $\hat{r_0} \leq r \leq \infty$, to get

$$\begin{aligned} \rho(r,t) &= \frac{e^{-\delta t}}{r(1+\delta)} \times \\ &\times \begin{cases} (r - t + \frac{1}{1+\delta})e^{(1+\delta)t} - (r + \frac{1}{1+\delta}), & r \leq \hat{r_1},\ 0 \leq t \leq r - \hat{r_0}, \\ (\hat{r_0} + \frac{1}{1+\delta})e^{(1+\delta)(r-\hat{r_0})} - (r + \frac{1}{1+\delta}), & r \leq \hat{r_1},\ 0 \leq r - \hat{r_0} \leq t, \\ (r - t + \frac{1}{1+\delta})e^{(1+\delta)t} - (\hat{r_1} + \frac{1}{1+\delta})e^{(1+\delta)(r-\hat{r_1})}, & r > \hat{r_1},\ r - \hat{r_1} < t < r - \hat{r_0}, \\ (\hat{r_0} + \frac{1}{1+\delta})e^{(1+\delta)(r-\hat{r_0})} - (\hat{r_1} + \frac{1}{1+\delta})e^{(1+\delta)(r-\hat{r_1})}, & r > \hat{r_1},\ r - \hat{r_1} < r - \hat{r_0} < t, \\ 0, & t \leq r - \hat{r_1} < \infty. \end{cases} \end{aligned} \tag{2.76}$$

In Figure 2.7, the effect of varying the dimensionless parameter δ is shown. The left graph shows the hyphal tip density at times $t = 0$ and $t = 1$. Similar to the cartesian case, the initial "blob" of hyphal tips has propagated, due to elongation of hyphae, and that the hyphal tip density has increased, due to branching. The parameter δ does not effect the result, since we scaled the model such that the branching rate is always 1. On the right graph, the hyphal length density at time $t = 1$ is shown for different values of δ. If $\delta \to 0$, which would correspond to a situation where there is no hyphal death, the length density increases as the tips are propagated and the colony increases in width. If the death rate is high, not only the tips but the whole fungal colony is propagated with time.

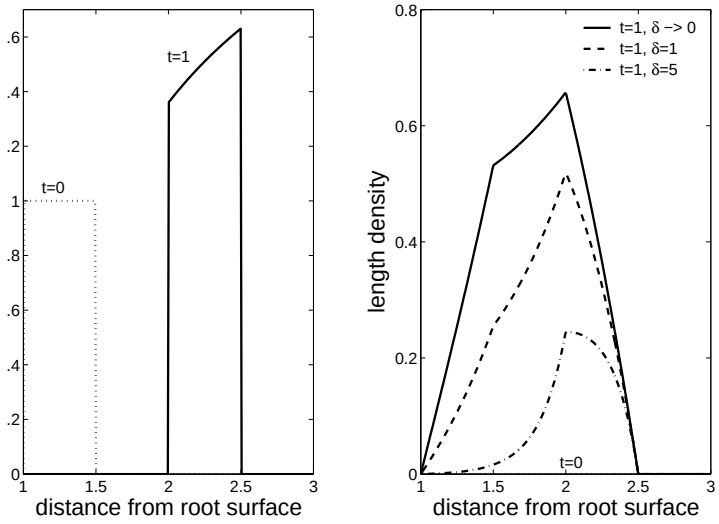

Figure 2.7: Plot of Equations (2.74) and (2.76). Analytical solution for hyphal tip and length density in the Initial Condition Model in polar radial coordinates of different values of the dimensionless parameter δ.

Boundary Flux Model

We parameterise the initial condition (2.63) so that at $\tau = 0$, $r = s$, $t = 0$ and $n(s, 0) = 0$ for $\hat{r_0} < s < \infty$. Integrating the characteristic equations (2.65)-(2.67) gives the parametric solution in the region influenced by the initial condition,

$$t = \tau, \tag{2.77}$$

$$r = \tau + s, \tag{2.78}$$

$$n(s) = 0, \qquad s \geq \hat{r_0}. \tag{2.79}$$

We parameterise the boundary condition (2.64) so that at $\tau = 0$, $r = \hat{r_0}$, $t = s$, and $n(s, 0) = 1$ for $s \geq 0$. Integrating equations (2.65)-(2.67) gives the parametric solution in the region influenced by the boundary condition,

$$t = \tau + s, \tag{2.80}$$

$$r = \tau + \hat{r_0}, \tag{2.81}$$

$$n(s) = \frac{\hat{r_0}}{r} e^{\tau}, \text{ for } s \leq \hat{r_0}. \tag{2.82}$$

Combining the solutions of the two regions and eliminating of the parameters τ and s, we have the solution for n,

$$n(r, t) = \begin{cases} \frac{r_0}{r} e^{(r - \hat{r_0})}, & r - t \leq \hat{r_0}, \\ 0, & r - t \geq \hat{r_0}. \end{cases} \tag{2.83}$$

To find ρ, we solve

$$\frac{d\rho}{dt} + \delta\rho = n(r,t), \tag{2.84}$$

on the interval $[0,t]$ with initial condition $\rho(r,0) = 0$, for $\hat{r_0} \leq r \leq \infty$, to get

$$\rho(x,t) = \begin{cases} \frac{1}{\delta}\frac{\hat{r_0}}{r}e^{(r-\hat{r_0})}\left(1 - e^{\delta(r-\hat{r_0}-t)}\right), & \hat{r_0} \leq r < t + \hat{r_0}, \\ 0, & t + \hat{r_0} \leq r < \infty. \end{cases} \tag{2.85}$$

Figure 2.8 shows the result for varying the dimensionless parameter δ. On the left graph, we see the hyphal tip density at time $t = 1$. Again, δ has no effect on the tip density, because we scaled the model such that the branching rate is always 1. On the right graph, we see how the hyphal length density decreases with increasing δ. If δ is small, the highest value of ρ is at the root surface. As δ becomes larger, the peak moves away from the root surface. If we assume, like in the cartesian case, that hyphae take up nutrients along their entire length, the front of the colony is the most active region, when δ is large.

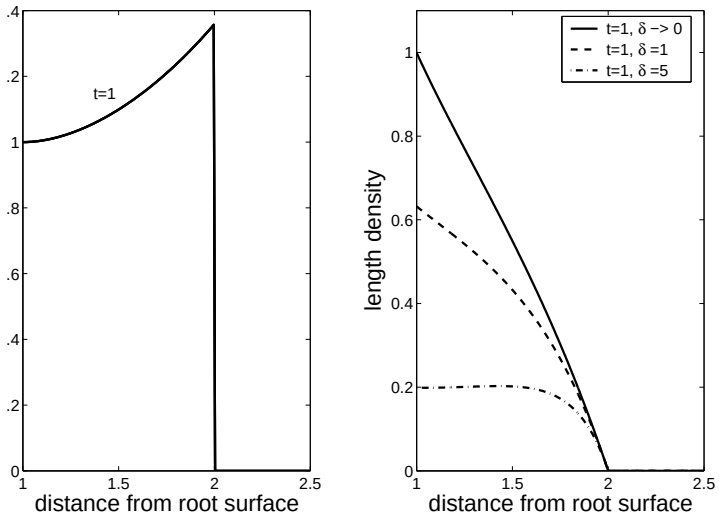

Figure 2.8: Plot of Equations (2.83) and (2.85). Analytical solution for hyphal tip and length density of the Boundary Flux Model in polar radial coordinates for different values of the dimensionless parameter δ.

Below, we adapt the numerical schemes used in the cartesian case to polar radial coordinates.

2.5.2 Numerical solutions

The numerical schemes for the computation of the hyphal tip density n have to be adapted to radial polar coordinates. Following on from section 2.4.2, the upwind

scheme is now derived from

$$\frac{U_j^{m+1} - U_j^m}{\Delta t} = -\frac{1}{r_j^m}\frac{r_j^m U_j^m - r_{j-1}^m U_{j-1}^m}{\Delta r} + U_j^m, \qquad j = 1, 2, ..., J. \tag{2.86}$$

Equation (2.86) can be rearranged to

$$U_j^{m+1} = (1 - \mu + \Delta t)U_j^m + \left(\frac{r_{j-1}^m}{r_j^m}\mu\right) U_{j-1}^m. \tag{2.87}$$

The Lax-Friedrich scheme for radial coordinates is derived from equation (2.60) by using centered differences for every space derivative and by averaging every U_j^m by its neighboring points, *i.e.*

$$\frac{U_j^{m+1} - \frac{1}{2}(U_{j+1}^m + U_{j-1}^m)}{\Delta t} = -\frac{1}{r_j^m}\frac{r_{j+1}^m U_{j+1}^m - r_{j-1}^m U_{j-1}^m}{2\Delta r} + U_j^m. \tag{2.88}$$

This can be rearranged to give

$$U_j^{m+1} = (\frac{1}{2} - \frac{\mu}{2}\frac{r_{j+1}^m}{r_j^m})U_{j+1}^m + (\frac{1}{2} + \frac{\mu}{2}\frac{r_{j-1}^m}{r_j^m})U_{j-1}^m + \Delta t U_j^m. \tag{2.89}$$

The Lax-Wendroff scheme is again based on substituting for the time derivatives in the Taylor series expansion. We have

$$\begin{aligned} U_t &= -\frac{1}{r}\frac{\partial}{\partial r}(rU) + U, & (2.90)\\ U_{tt} &= -\frac{1}{r}\frac{\partial}{\partial r}(rU_t) + U_t = \\ &= \frac{1}{r}\frac{\partial^2}{\partial r^2}(rU) - 2\frac{1}{r}\frac{\partial}{\partial r}(rU) + U. & (2.91) \end{aligned}$$

Substituting these into the Taylor series expansion, neglecting higher order terms, replacing the space derivatives by centered differences and rearranging gives the Lax-Wendroff scheme

$$\begin{aligned} U_j^{m+1} = (1 + \Delta t - \mu^2 + \frac{(\Delta t)^2}{2})U_j^m \\ +(-\Delta t\frac{\mu}{2} - \frac{\mu}{2} + \frac{\mu^2}{2})\frac{r_{j+1}^m}{r_j^m}U_{j+1}^m \\ +(\Delta t\frac{\mu}{2} + \frac{\mu}{2} + \frac{\mu^2}{2})\frac{r_{j-1}^m}{r_j^m}U_{j-1}^m. \end{aligned}$$

Figures 2.9(a)-2.11(b) show comparisons of the numerical and analytical solutions of both the Initial Condition Model and the Boundary Flux Model in radial polar coordinates. As in the cartesian case, the Lax-Wendroff scheme gives the best numerical approximation to the analytical solution of the hyphal length density.

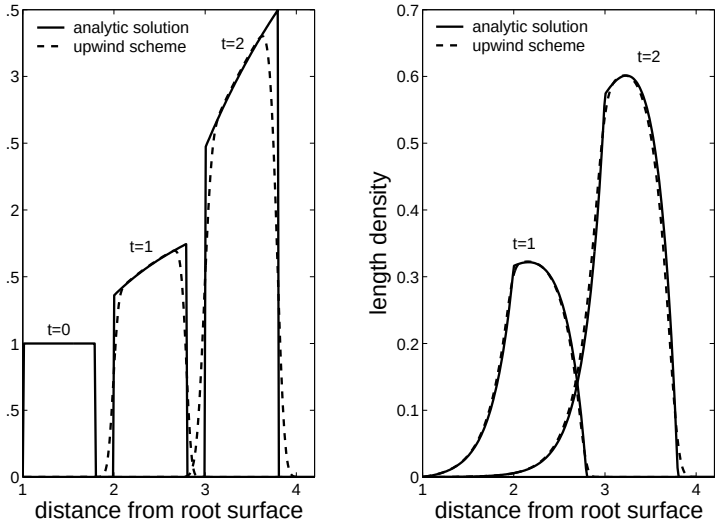

(a) Initial Condition Model

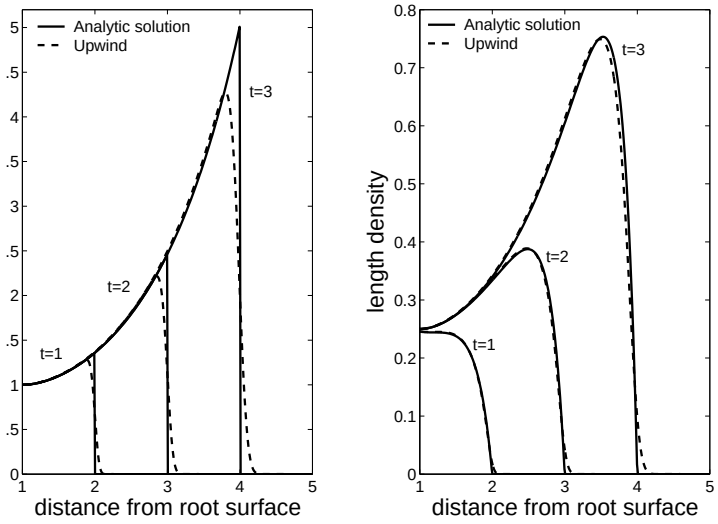

(b) Boundary Flux Model

Figure 2.9: Comparison of Upwind scheme to analytical solution at three different points in time. $\delta = 4$, $J = 300$, $\frac{\Delta t}{\Delta r} = 0.8$, dt=0.0027.

2.6 Conclusions

In this chapter, we provide analytical and numerical solutions for a fungal growth model. The model of Edelstein (1982) was our starting point and we showed how to apply it to the case of arbuscular mycorrhizal fungi by means of defining a flux of tips at the boundary. This should mimic the fact that arbuscular mycorrhizal fungi are attached to the root surface that acts as a continuous source of new tips. We provided the numerical schemes in anticipation of the fact that comparison with experimental

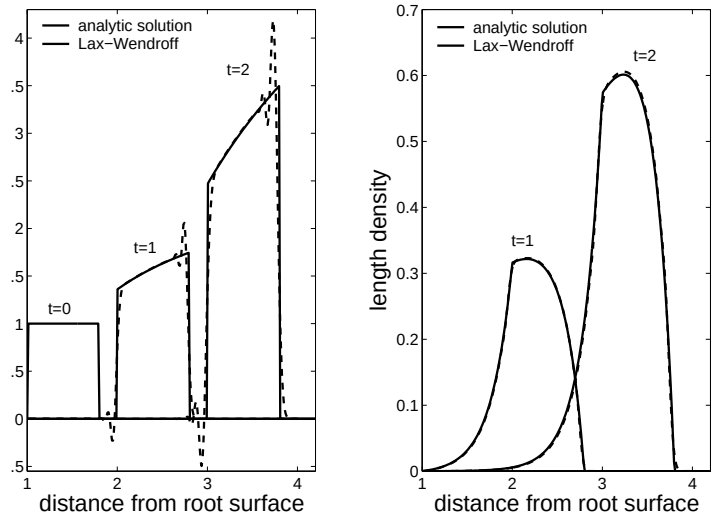

(a) Initial Condition Model

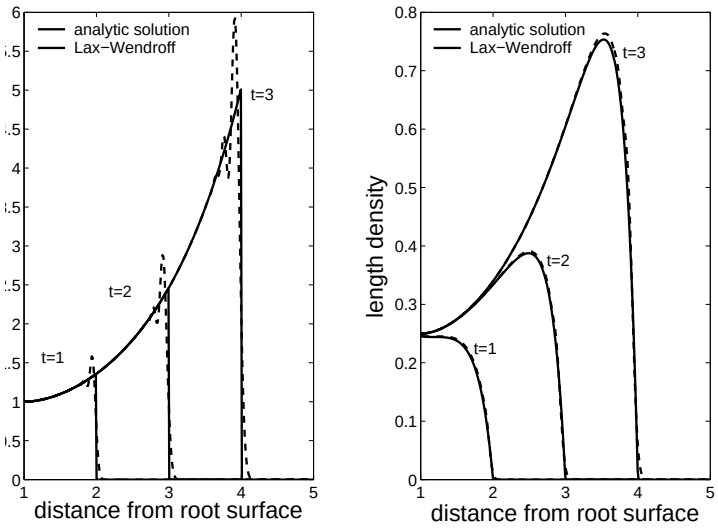

(b) Boundary Flux Model

Figure 2.10: Comparison of Lax Wendroff scheme to analytical solution at three different points in time. $\delta = 4$, $J = 300$, $\frac{\Delta t}{\Delta r} = 0.8$, dt=0.0027.

data may necessitate a more complicated model. From the numerical schemes tested, we prefer the Lax-Wendroff scheme to the Upwind and the Lax-Friedrich scheme, because its accuracy is highest.

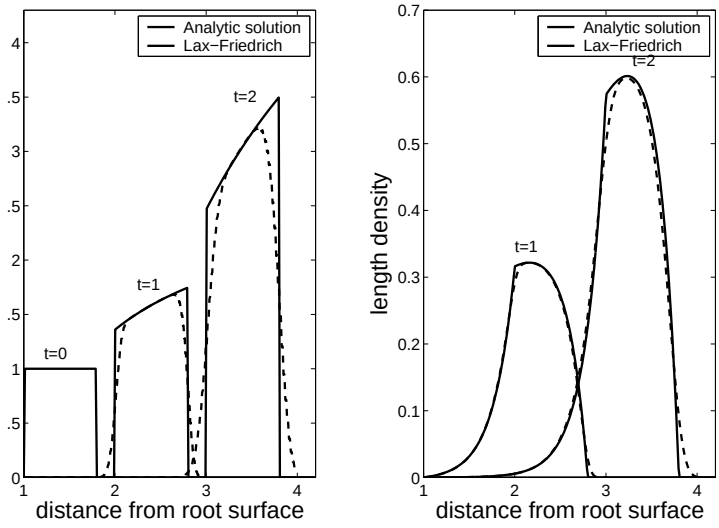

(a) Initial Condition Model

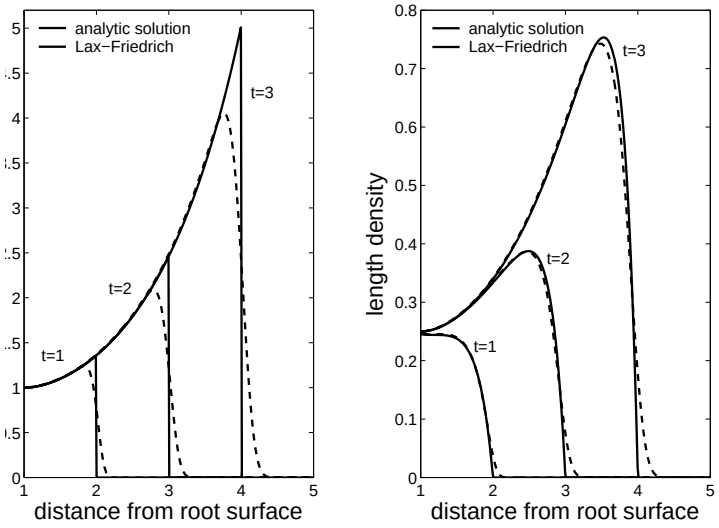

(b) Boundary Flux Model

Figure 2.11: Comparison of Lax Friedrich scheme to analytical solution at three different points in time. $\delta = 4$, $J = 300$, $\frac{\Delta t}{\Delta r} = 0.8$, dt=0.0027.

Chapter 3

Testing the fungal growth model against experimental data

In this chapter, we test the modelling approach developed in chapter 2 against experimental data. We hope that by adjusting the input parameters, we will be able to reproduce the measurements with the model. If successful, we can confidently use this fungal growth model to create the sink term for solute uptake by a fungal mycelium in the single root model (chapter 5). We will take our starting guesses for the input parameters from literature. If necessary, we will adapt the model by altering some of the model assumptions. The data which we use for comparison are from Jakobsen *et al.* (1992). The experiment is described in section 1.1.1. Hyphal length densities of three arbuscular-mycorrhizal fungi associated with clover (*Trifolium subterraneum* L.) are measured at different times and distances from a cylindrical root compartment in an initially fungus free soil. It is therefore appropriate to use radial polar coordinates, and an initial value of zero for both hyphal length and tip density. We are going to solve the Boundary Flux Model described by equations (2.1)-(2.2) and (2.6)-(2.8) in radial polar coordinates. If we take that the measurements of hyphal length density inside the root compartment represent the value at the interface between root and fungal compartment, we have to make our first adjustment to the model in terms of a time dependent boundary condition, $nv = k(t)$. The model equations are

$$\frac{\partial \rho}{\partial t} = vn - \mu\rho, \qquad t \geq 0,\ r_0 \leq r \leq \infty, \tag{3.1}$$

$$\frac{\partial n}{\partial t} = -\frac{1}{r}\frac{\partial (vrn)}{\partial r} + bn, \qquad t \geq 0,\ r_0 \leq r \leq \infty, \tag{3.2}$$

where we now write μ instead of d for the death rate, so as not to confuse the product μt with the differential operator dt later. The initial and boundary conditions are

$$\rho(r,0) = 0, \qquad r_0 \leq r \leq \infty, \tag{3.3}$$

$$n(r,0) = 0, \qquad r_0 \leq r \leq \infty, \tag{3.4}$$

$$n(r_0,t) = f(t), \qquad t > 0. \tag{3.5}$$

To determine the time dependent boundary condition, we consider that arbuscular mycorrhizal fungi are attached to the plant root cells via so-called "entry points". Because there is only a certain number of cells, it would make sense to assume that the hyphal length density at the root surface can increase with time until it reaches a maximum value. We propose the following equation for the hyphal length density at the boundary $r = r_0$,

$$\frac{d\rho}{dt} \quad = \quad a(1 - \frac{\rho}{\rho_{max}}), \tag{3.6}$$

with initial condition $\rho(r_0, 0) = \rho_{0,b}$, where ρ_{max} is the maximum hyphal length density, $\rho_{0,b}$ is the initial hyphal length density at the boundary and a is a rate constant. The hyphal length density at the boundary is thus

$$\rho(r_0,t) = \rho_{max} + e^{-\frac{a}{\rho_{max}}(\rho_{0,b} - \rho_{max})}. \tag{3.7}$$

Equation (3.7) was fitted to the boundary data values using the Matlab function `lsqcurvefit`. Results for the three fungal species are shown in figure 3.1 and table 3.1. Equation (3.7) could be fitted to the data for the fungal species *Glomus*

Table 3.1: Fitting results for the non-linear equation (3.7).

	$\rho_{max}\,(m\,cm^{-3})$	$\rho_0\,(m\,cm^{-3})$	$a\,(m\,cm^{-3}d^{-1})$	RMSE
S. calospora	24.16	8.57	21.63	13.37
Glomus sp.	6.85	2.48	0.32	1.10×10^{-6}
A. laevis	2200.23	2.04	0.22	0.19

sp. and *A. laevis* with a root mean squared error (RMSE) of 1.10×10^{-6} and 0.32, respectively. However, the fitted curve for *S.calospora* shows a steep increase of hyphal length density near $t = 0$. From a biological perspective it is not very likely that the maximum value of hyphal length density is reached so soon. More data points could have forced the curve to be less steep. However, in absence of additional data, we

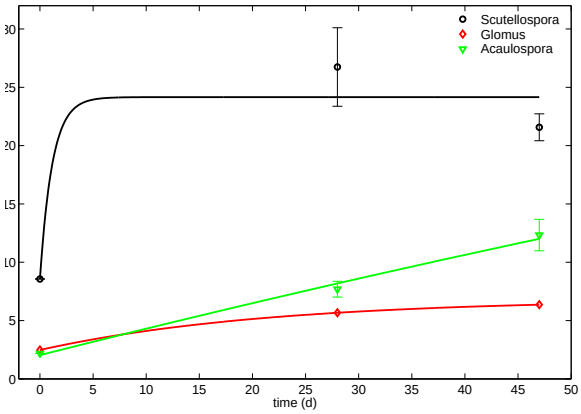

Figure 3.1: Resulting curves when fitting equation (3.7) to the boundary data.

will use a more conservative approach and assume a linear increase of hyphal length density with time for this fungal species. For completeness, we fit equation

$$\rho(r_0, t) = at + \rho_{0,b}, \tag{3.8}$$

to the data for all three fungal species. The results are shown in Figure 3.2 and table 3.2. From a biological perspective, it makes more sense to use the more conservative linear equation for the fungal species *S. calospora*. The non-linear equation gives the best fit for *Glomus sp.* Both the linear and non-linear boundary condition can be fitted to *A. laevis*. We now have time dependent functions for the hyphal length

Table 3.2: Fitting results for the linear equation (3.8)

	$\rho_0\,(m\,cm^{-3})$	$a\,(m\,cm^{-3}d^{-1})$	RMSE
S. calospora	11.34	0.30	71.63
Glomus sp.	2.71	0.09	0.51
A. laevis	2.04	0.21	0.19

density at the root surface, however, we need to supply the model with a boundary condition for the hyphal tip density. Therefore, we use the model equations to infer the tip density at the boundary when the hyphal length density at the boundary is given by either equation (3.7) or (3.8). Integrating the equation for the hyphal length density, equation (3.1), at $r = r_0$, we get that

$$\rho(r_0, t) = ve^{-\mu t} \int_0^t n(\xi) e^{\mu \xi} d\xi. \tag{3.9}$$

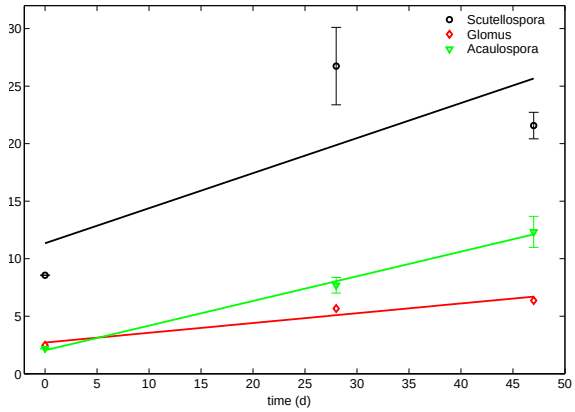

Figure 3.2: Resulting curves when fitting equation (3.8) to the boundary data.

Setting this equal to the nonlinear equation (3.7), we infer $n(r_0, t)$ to be

$$n(r_0, t) = \frac{\mu\rho_{max}}{v} + \frac{\rho_{0,b} - \rho_{max}}{v}(\mu - \frac{a}{\rho_{max}})e^{-\frac{a}{\rho_{max}}t}. \tag{3.10}$$

Likewise, in the case of the linear equation (3.8), we infer $n(r_0, t)$ to be

$$n(r_0, t) = \frac{a}{v}(1 + \mu t) + \frac{\mu\rho_{0,b}}{v}. \tag{3.11}$$

Values of the parameters ρ_{max}, a and $\rho_{0,b}$ are obtained for each specific fungus by fitting the respective equation for ρ to the boundary data. In the following section, we present analytical solutions for the hyphal length density for both the nonlinear and linear boundary condition.

3.1 Analytical solutions

We non-dimensionalised the model using the same scales for time, length and hyphal length density as in section 2.3 and $[n] = \max(n(r_0, t))$ for the tip density. Using the method of characteristics as described in chapter 2, we solved for n and then solved the linear first order ordinary differential equation for ρ. Below, we present the dimensional solutions for ρ, since this is the variable which we can compare to

experimental data. For the nonlinear boundary condition, it is

$$\begin{aligned}\rho(r,t) &= \frac{1}{\mu}\frac{r_0}{r}e^{\frac{b}{v}(r-r_0)} \times \\ &\times \begin{cases} \rho_{max}\mu\left(1-e^{\frac{\mu}{v}(r-r_0-tv)}\right)+ \\ +(\rho_{0,b}-\rho_{max})\left(\mu-\frac{a}{\rho_{max}}\right)\frac{\rho_{max}b}{\rho_{max}b-a}e^{\frac{a}{\rho_{max}v}(r-r_0)}\times \\ \times\left(e^{-\frac{a}{\rho_{max}}t}-e^{(\frac{\mu}{v}-\frac{a}{\rho_{max}v})(r-r_0)-\mu t}\right), & r_0 \le r \le tv+r_0, \\ 0, & tv+r_0 < r < \infty, \end{cases}\end{aligned} \tag{3.12}$$

and for the linear boundary condition, it is

$$\begin{aligned}\rho(r,t) &= \frac{1}{\mu}\frac{r_0}{r}e^{\frac{b}{v}(r-r_0)} \times \\ &\times \begin{cases} \frac{a\mu}{v}(tv-r+r_0-\frac{v}{\mu})+\rho_{0,b}\mu+a+ \\ +\rho_{0,b}\,\mu\,e^{\frac{\mu}{v}(r-r_0-tv)}, & r_0 \le r \le tv+r_0, \\ 0, & tv+r_0 < r < \infty. \end{cases}\end{aligned} \tag{3.13}$$

To check the validity of these analytical solutions, we compared them to the numerical solution calculated with the Lax-Wendroff scheme developed in chapter 2, using several combinations of parameter values. One example is shown in figure 3.3. Analytical and numerical solutions for both nonlinear and linear boundary conditions agree well.

3.2 Parameterisation

In this section, we try to find values for the parameters v, b and μ such that the results of equation (3.13) or (3.12) fit to the data of Jakobsen *et al.* (1992). Our initial guess for v comes from the article of Jakobsen *et al.* (1992) itself, where they measured the spread of each fungal species with time. The mean value was $0.08\,cm\,d^{-1}$ for *S. calospora*, $0.07\,cm\,d^{-1}$ for *Glomus sp.* and $0.31\,cm\,d^{-1}$ for *A. laevis*. Our initial guess for the death rate μ is motivated by Staddon *et al.* (2003) who reported that a hypha lives approximately six days. Branching is often measured in number of branches per unit length of hyphae (Giovanetti *et al.* 2001), but we did not find any values for the branching rate. Therefore, we used an arbitrary value as initial guess.

Consider first the fungal species *S. calospora*. Equations (3.12) and (3.13) were plotted against the data and the parameter values varied until a good fit was obtained

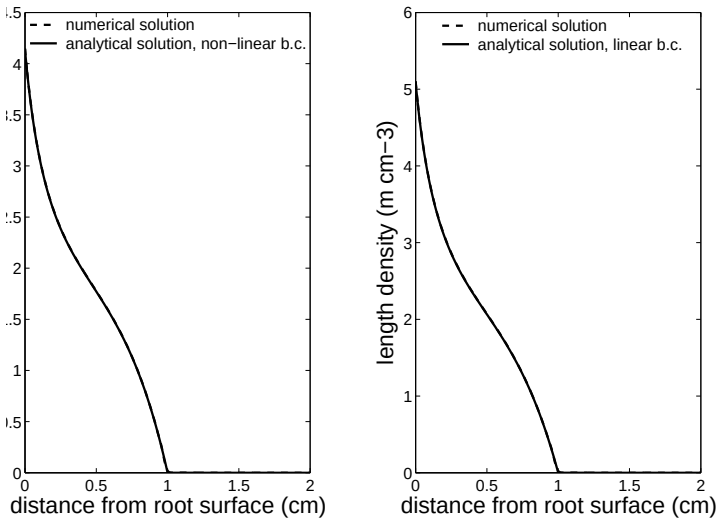

Figure 3.3: Comparison of analytical solution for ρ for nonlinear (left graph, equation (3.12)) and linear (right graph, equation (3.13)) boundary condition with numerical solution. Model parameters: $\mu = 0.2\,d^{-1}$, $b = 0.5\,d^{-1}$, $v = 0.25\,d^{-1}$, $\rho_{max} = 15\,m\,cm^{-3}$, $\rho_0 = 2\,m\,cm^{-3}$, $a = 100\,m\,cm^{-3}d^{-1}$, final time: $4\,d$, numerical parameters: J=300, mu=0.8, dt=0.005.

(see figure 3.4). As expected, simulated values overestimated measured ones, at early times in particular, when the nonlinear boundary condition was applied. This corresponds to our previous assumption that the fast increase of boundary tip density is biologically not meaningful. However, when the solution based on the linear boundary condition was used, we found good agreement between simulated and measured values. The parameter values that produced the best fit are given in figure 3.4. Note that the fitted value for v is approximately three times larger than the value given by Jakobsen *et al.* (1992).

For both other fungal species, *Glomus sp.* and *A. laevis*, the difference in results when using the non-linear or linear boundary condition is negligible. Therefore, we proceed using only the solution based on the nonlinear boundary condition, equation (3.12) when testing the model against the data for these fungal species. We applied equation (3.12) to both species and found that we could not fit it to either of them. Figure 3.5 shows the best result that could be obtained for *Glomus sp.* We observe that the solution underestimates the data at early times (7 and 14 days) and overestimates it at large times (47 days).

We anticipate that other mechanisms are important for the growth of these two fungi and test the effect of two new mechanisms: non-linear branching and anastomosis. Consider first the effect of non-linear branching. From a biological point of view,

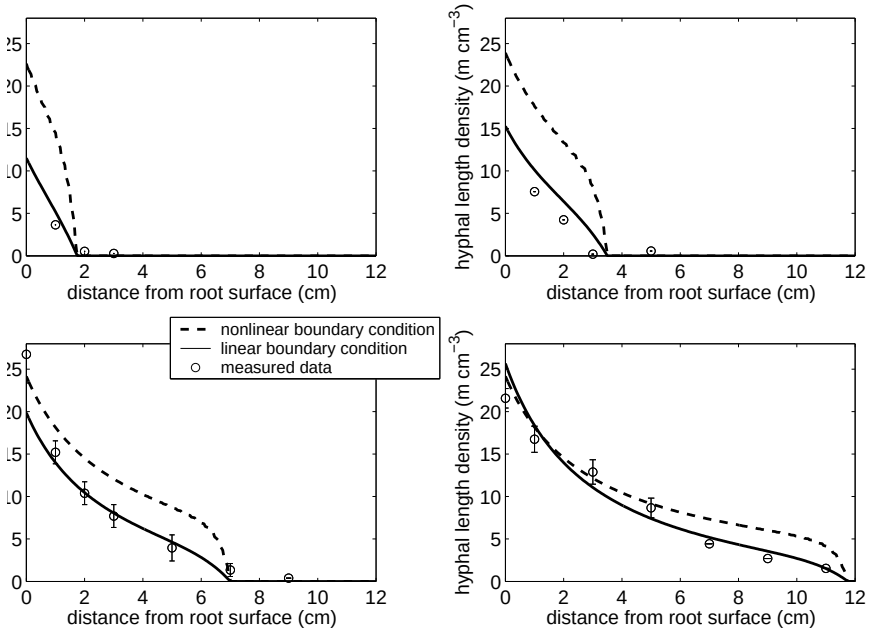

Figure 3.4: Plot of equations (3.12) and (3.13), comparison to data for *S. calospora*. Solutions based on linear and nonlinear boundary conditions. $v = 0.25d^{-1}$, $\mu = 0.25d^{-1}$, $b = 0.005d^{-1}$

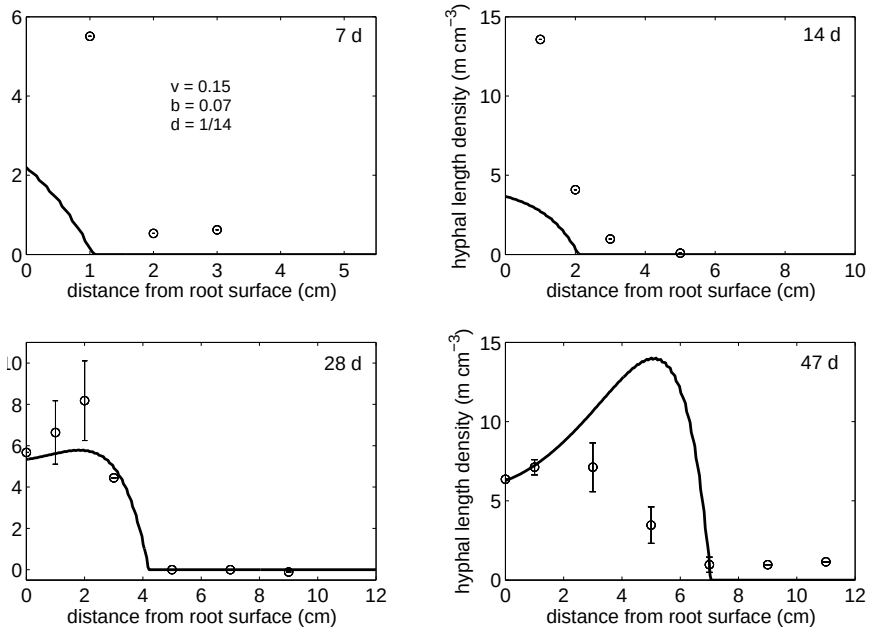

Figure 3.5: Plot of equation (3.12), comparison to data for *Glomus sp.*

it seems reasonable that there might be a maximal tip density at which no further branching occurs. Therefore, we extend the linear model equation for the tip density,

equation (3.2), by assuming that the branching ceases at a maximal tip density n_{max}. We propose the following equation for the hyphal tip density,

$$\frac{\partial n}{\partial t} = -\frac{1}{r}\frac{\partial (vrn)}{\partial r} + bn\left(1 - \frac{n}{n_{max}}\right), \qquad t \geq 0,\, r_0 \leq r \leq \infty. \tag{3.14}$$

This equation together with initial condition (3.4) and boundary condition (3.10) was solved numerically using the Lax-Wendroff scheme described in chapter 2. The numerical solution for ρ was computed using an explicit Euler scheme. Figure 3.6 shows in general the effect of varying the parameter n_{max}. If n_{max} is large, the result is close to the linear branching model. The smaller it gets, the more the hyphal length density is decreased at larger times because the production of new tips and hence hyphae is suppressed. Figure 3.7 shows that the nonlinear branching model

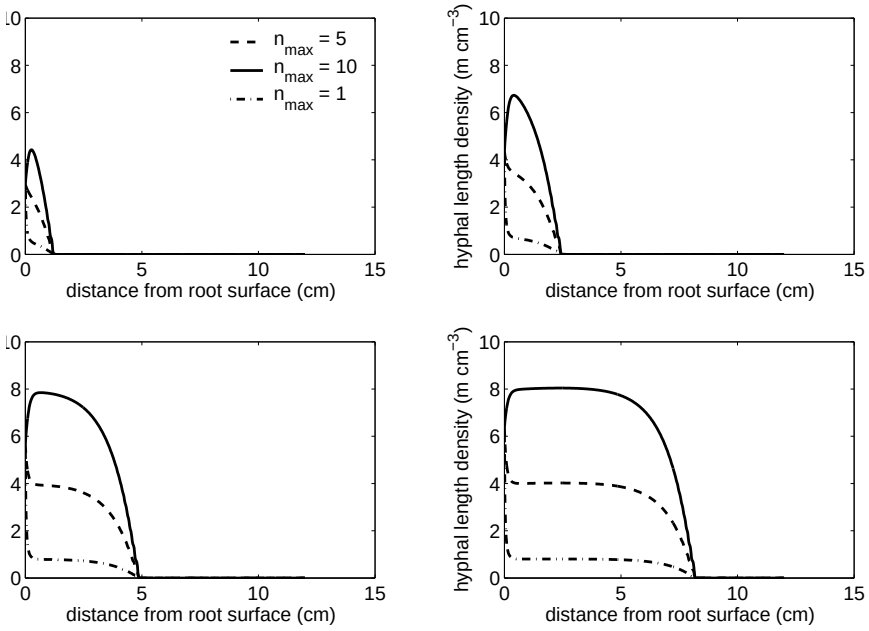

Figure 3.6: Model including non-linear branching, effect of varying n_{max}. Numerical parameters: $J = 300, mu = 0.8, dt = 0.01$.

fits to the data of *Glomus sp.* much better than the linear branching model. In the first few days of the experiment, it still slightly underestimates measured values. In particular, the data point after $7\,d$ at a distance of $1\,cm$ is not reached. However, because the tip density at this point is much larger than any of the other values, we think that this data point may be an experimental outlier. The non-linear branching model could not be fitted to the data for the fungal species *A. leavis* (results not shown). From figure 1.1, it appears that the hyphal length density of *A. leavis* at

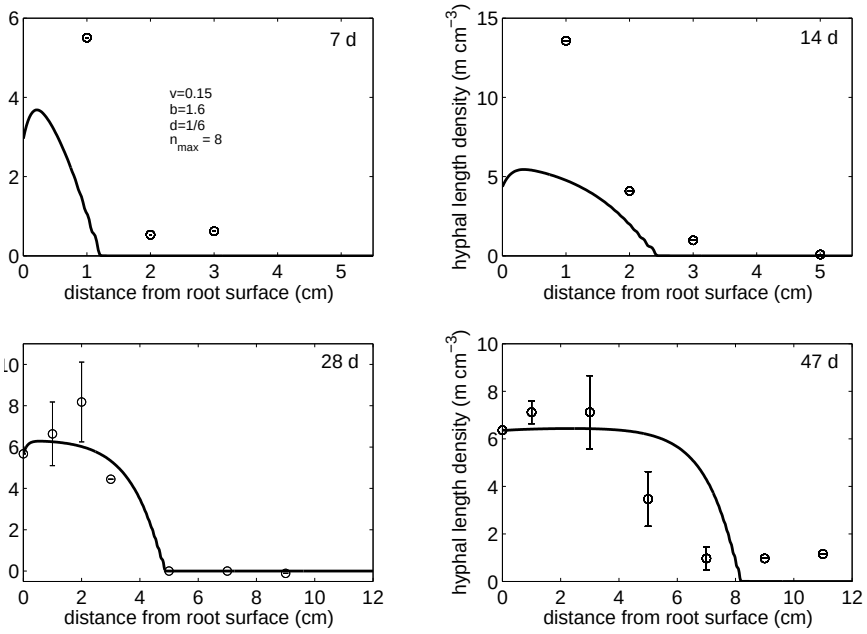

Figure 3.7: Comparison of numerical solution of nonlinear branching model to data for *Glomus sp.* Numerical parameters: J=300, mu=0.8, dt=0.01

28 d shows a small local maximum at a distance of 7 cm. Such a behavior is captured by the model when anastomosis is taken into account (figure 3.8). Anastomosis is a biological mechanism where hyphae and tips can fuse together and thus reduce the number of tips. The equation for n becomes

$$\frac{\partial n}{\partial t} = -\frac{1}{r}\frac{\partial (vrn)}{\partial r} + bn - a_2 n\rho, \qquad t \geq 0,\ r_0 \leq r \leq \infty. \tag{3.15}$$

where a_2 is the anastomosis rate. This equation is now coupled with equation (3.1) for ρ. They were solved numerically together with initial conditions (3.3) and (3.4) and boundary condition (3.10). As before, n was approximated by the Lax-Wendroff scheme and ρ by an explicit Euler scheme. However, the model including anastomosis could not be fitted to the data for *A. leavis*. The agreement is better than with the linear model, but in particular after 47 d, the model underestimates the hyphal length density at positions near the root surface. Therefore, we cannot conclude that anastomosis alone can explain the behavior of the data. There may be other processes that are important, such as a varying value of v or sporation.

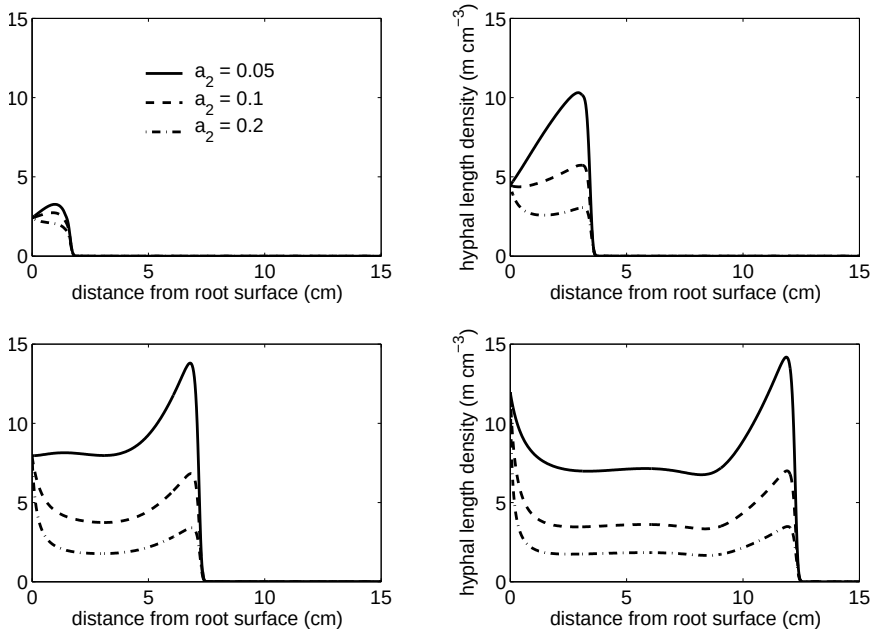

Figure 3.8: Model including anastomosis, effect of varying a_2. Numerical parameters: $J = 300, mu = 0.8, dt = 0.01$.

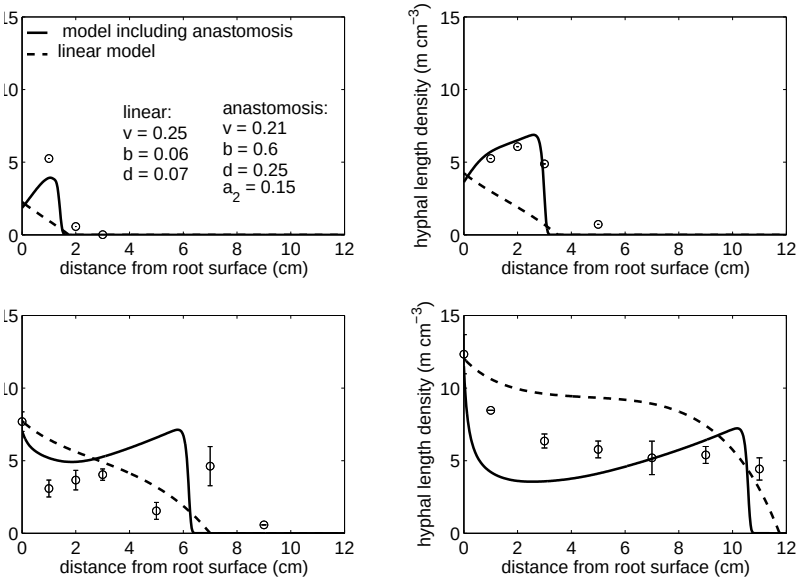

Figure 3.9: Simulated hyphal length density of *A. laevis* including and not including anastomosis and comparison to measured data. Numerical parameters: $J = 300, mu = 0.8, dt = 0.01$.

3.3 Conclusions

In this chapter we have extended the modelling approach of chapter 2 by using time dependent boundary conditions to make it applicable to the specific fungi considered

by Jakobsen *et al.* (1992). We found good agreement between the linear model and the data for *S. calospora*. We also found that it was necessary to adapt the original model equations for the two other fungal species considered. The non-linear branching model could be fitted to the data for *Glomus sp.* but not to *A. laevis*. None of the models performed particularly well for *A. laevis*; the model which performed best was the one including anastomosis.

Reasons for deviations between model simulation and data could be that other mechanisms need to be included in the model. Sporation may be important under some circumstances, or there might be a strongly varying elongation rate. The differences could also be due to an error in the boundary condition. When we did the data conversion from mass to volume basis, we used the bulk density of the soil in the hyphal compartment. This value might not be valid for the root compartment, we used it in absence of other information. Lastly, there is the possibility of experimental outliers. In particular, we consider the data point for *Glomus sp.* at $1\,cm$ after $14\,d$. The value for the hyphal length density of almost $15\,m\,cm^{-3}$ seems very large and is never found again at later times. Therefore, we think that this could be an artefact.

In summary, we have shown that a modelling approach originally developed for mycelial fungi is applicable to arbuscular mycorrhizal fungi, depending on the specific species. The new important feature is the boundary condition that provides a flux of hyphal tips which stands for the effect of the root on fungal growth. We have developed a library of solutions that could be useful for biologists. Additional information that would improve the model includes more and accurate data for the boundary condition, as well as quantitative experimental evidence about additional biological mechanisms that could possibly be incorporated into the model. Results of this chapter give us confidence to use the fungal growth models presented here for the derivation of the sink term for mycorrhizal solute uptake in chapter 5.

Chapter 4

Solute uptake on the single hyphal scale

4.1 Introduction

The contribution of mycorrhizal fungi to plant phosphate uptake can be considerable (Smith *et al.* 2003), yet no spatially explicit plant nutrient uptake model takes this into account. In addition to the direct uptake of phosphate by the root, there is an additional pathway where it is taken up by the external hyphae, translocated within the mycelium and then transferred into the root. In this chapter, we develop expressions for hyphal solute uptake on the scale of a single hypha. Our final aim is to use these expressions to create a source term for fungal colony uptake in a root uptake model.

Most root uptake models use a continuum description of the soil, where it is assumed that all three soil phases are present and continuous at each point. We present an expression for solute influx into hyphae based on this assumption in section 4.2. In most soils, the diameter of a hypha is smaller than the soil pore diameter. Because of this, we relax the assumption that the soil can be described as a continuum and consider hyphae growing in the pore space between the soil particles. We present two expressions for solute influx into hyphae based on this assumption in section 4.3. A comparison of the resulting influxes in presented in section 4.4.

4.2 Solute uptake by a single hypha from a continuum soil

In this section we follow the assumption that the soil can be described as a continuum. We develop a model for radial flow of solutes towards the surface of a single cylindrical

hypha and uptake of solute at that surface.

4.2.1 Model formulation

We assume that the soil consists of a solid phase, a liquid phase and a gas phase, and that the volume fraction of each phase stays constant, so that we have

$$\theta_s + \theta_l + \theta_a = 1, \tag{4.1}$$

where θ_s is the volume fraction of the soil solid phase, θ_l is the volumetric water content and θ_a is the volume fraction of the air phase. The sum of θ_l and θ_a is the soil porosity Φ. Typical values of Φ are $0.3 - 0.6$ and typical values for θ_l in soils at field capacity are $0.15 - 0.4$ (Scheffer *et al.* 2002). We assume that solute is present in the solid (C_s) and liquid (C_l) phase. As is conventional, C_s is expressed in moles per unit total soil volume whereas C_l is expressed in moles per unit volume of liquid phase. We consider the sum of the concentrations in solution and adsorbed onto the solid phase as the total concentration of solute present in soil ($C_{T,soil}$). It is given by

$$C_{T,soil} = C_s + \theta_l C_l. \tag{4.2}$$

In the following paragraphs, we develop equations for the rate of change of concentration in each soil phase. We assume that soil air phase is not taking part in any transport or reaction mechanisms. Assuming equilibrium sorption according to a linear Freundlich isotherm, and neglecting intra-particle diffusion, the rate of change of C_s with respect to t is given by (Atkins 1998; Barber 1995; Tinker & Nye 2000)

$$\frac{\partial C_s}{\partial t} = b_p \frac{\partial C_l}{\partial t}, \tag{4.3}$$

where b_p is the buffer power of the soil. The rate of change of C_l with respect to t is dependent on diffusive and convective transport in the soil solution. Consider an arbitrary volume of soil V with concentration θC_l. The rate of change of θC_l in V must be equal to the flux of solutes, q, across its boundary ∂V plus the contribution from any internal sources or sinks. Let us assume that there are no internal sources or sinks. Then, applying the conservation law stated in equation (2.1), we get

$$\theta \frac{\partial C_l}{dt} + \nabla \cdot q = 0,$$

where the dependent variable is now the solution concentration C_l instead of the hyphal tip density n. The flux q is derived by assuming diffusive and convective

transport. Diffusion is given by Fick's law that describes the movement of solutes in the direction of decreasing concentration gradient:

$$q_{diff} = -D_l \theta_l f_l(\theta_l) \nabla C_l,$$

where D_l is the diffusion coefficient of the solute in free water, and $f_l(\theta_l)$ is the impedance factor of solute in the liquid phase. It can be described by the empirical relation $f_l = 1.6\,\theta_l - 0.172$ for most agricultural soils (Barber 1995). The convective movement of solutes is given by

$$q_{con} = \mathbf{v} C_l,$$

where $\mathbf{v}$ is the Darcy flux of water. With $q = q_{diff} + q_{con}$, we can write our model for radial flow of solutes towards the hypha as

$$\frac{\partial(\theta_l C_l)}{\partial t} = \nabla \cdot (\theta_l D_l f_l \nabla C_l) - \nabla \cdot (\mathbf{v}\, C_l), \tag{4.4}$$

The rate of change of $C_{T,soil}$ with time is given by the sum of equations (4.3) and (4.4),

$$\frac{\partial\left((b_p + \theta_l) C_l\right)}{\partial t} = \nabla \cdot (\theta_l D_l f_l \nabla C_l) - \nabla \cdot (\mathbf{v}\, C_l). \tag{4.5}$$

Let us assume that the concentration in soil solution is initially constant, so that the initial condition is given by

$$C_l = C_{l,0}, \qquad t = 0, \tag{4.6}$$

where $C_{l,0}\,(\mu mol\, cm^{-3})$ is the initial concentration of solute in soil solution. Let us assume that the uptake of solute at the hyphal surface follows Michaelis-Menten kinetics (Barber 1995), so that the boundary condition at the hyphal surface is given by

$$\theta_l D_l f_l \frac{\partial C_l}{\partial n} - v_n C_l = \frac{F_m C_l}{K_m + C_l}, \tag{4.7}$$

where $\frac{\partial}{\partial n}$ is the operator for the outward normal derivative, v_n is the Darcy flux of water normal to the hyphal surface, $F_m\,(\mu mol\, cm^{-2}\, s^{-1})$ is the maximal hyphal uptake rate and $K_m\,(\mu mol\, cm^{-3})$ is the Michaelis Menten constant. Following an equation given by Reginato *et al.* (2000) for roots, we calculate the half distance between two hyphae, r_1, as

$$r_1 = \frac{1}{\sqrt{\pi \rho}}, \tag{4.8}$$

where ρ is the hyphal length density. With this equation, we assume that the hyphae are evenly distributed in soil. In chapter 3, the highest hyphal length density was in the order of $1000\,cm\,cm^{-3}$, hence r_1 is in the order of $0.01\,cm$ or or more. The diameter of one hypha is in the order of $10^{-4}\,cm$ (Ezawa *et al.* 2002). Thus, since the distance between two hyphae is much larger than the hyphal diameter, we will assume there is no competition between hyphae and thus the concentration far away from the hyphal surface stays constant. So, the boundary condition far away from the hyphal surface is

$$C_l = C_{l,0}, \qquad |\mathbf{x}| \to \infty. \tag{4.9}$$

We are interested in simulating radial flow into a cylindrical hypha. In radial polar coordinates, the model is

$$\begin{aligned}
(b+\theta_l)\frac{\partial(\theta_l C_l)}{\partial t} &= \theta_l D_l f_l \frac{1}{r}\frac{\partial}{\partial r}\left(r\frac{\partial C_l}{\partial r}\right) + \frac{v_0}{r}\frac{\partial C_l}{\partial r}, && (4.10)\\
\theta_l D_l f_l \frac{\partial C_l}{\partial r} + q_0 C_l &= \frac{F_m C_l}{K_m + C_l},\ r = r_0, && (4.11)\\
C_l &= C_{l,0},\ r = r_1, && (4.12)
\end{aligned}$$

where r_0 is the radius of the hypha and v_0 is the Darcy flux of water into the hyphal surface. The convection term is due to conservation of water. We need $2r\pi v(r)$ constant, and hence $2r\pi v(r) = 2r_0\pi v_0$. Note that the change of sign is due to the fact that v_0 represents the flux of water into the hypha.

4.2.2 Non-dimensionalisation and parameter estimation

Let $r = r_0 r^*$, $t = \frac{r_0^2(b_p+\theta_l)}{\theta_l D_l f_l} t^*$ and $C_l = K_m C_l^*$. Then the non-dimensional model is (dropping asterisks)

$$\begin{aligned}
\frac{\partial C_l}{\partial t} &= \frac{1}{r}\frac{\partial}{\partial r}\left(r\frac{\partial C_l}{\partial r}\right) + Pe\frac{1}{r}\frac{\partial C_l}{\partial r}, && (4.13)\\
\frac{\partial C_l}{\partial r} + P_e C_l &= \lambda\frac{C_l}{1+C_l},\ r = r_0, && (4.14)\\
C_l &\to c_\infty,\ r \to \infty. && (4.15)
\end{aligned}$$

The dimensionless parameters are $Pe = \frac{r_0\, v_0}{D_l\theta_l f_l}$, $\lambda = \frac{F_m r_0}{K_m D_l \theta_l f_l}$ and $c_\infty = \frac{C_{l,0}}{K_m}$, where Pe is the Péclet number, λ is the dimensionless uptake parameter and c_∞ is the dimensionless concentration in the bulk soil solution.

Typical values for the dimensional parameters are given in table 4.1. Based on these values, the dimensionless parameters are $Pe = 5.43 \times 10^{-5}$, $\lambda = 0.3$ and $c_\infty = 0.1 - 1$.

Table 4.1: Typical values of the dimensional parameters for the continuum scale model.

Parameter	Units	Value for P	Reference
D_l	$cm^2\ s^{-1}$	10^{-5}	Lide (2000)
θ	$cm^3\ cm^{-3}$	0.3	Barber (1995)
v	$cm^2\ s^{-1}$	10^{-7}	Barber (1995)
f_l	$cm^2\ s^{-1}$	0.308	Barber (1995)
r_0	cm	5×10^{-4}	Ezawa *et al.* (2002)
F_m	$\mu mol\ cm^{-2}\ s^{-1}$	3.26×10^{-6}	Tinker & Nye (2000)
K_m	$\mu mol\ cm^{-3}$	5.8×10^{-3}	Tinker & Nye (2000)
b_p	$cm^3\ cm^{-3}$	239	Barber (1995)
C_{l0}	$\mu mol\ cm^{-3}$	$10^{-4} - 10^{-3}$	low to medium concentration (Barber 1995)

Because $Pe << 1$, we can, at the leading order, neglect convective transport and the model becomes

$$\frac{\partial C_l}{\partial t} = \frac{1}{r}\frac{\partial}{\partial r}\left(r\frac{\partial C_l}{\partial r}\right), \tag{4.16}$$

$$\frac{\partial C_l}{\partial r} = \lambda\frac{C_l}{1+C_l},\ r = r_0, \tag{4.17}$$

$$C_l \rightarrow c_\infty,\ r \rightarrow \infty. \tag{4.18}$$

4.2.3 Approximate analytical solution by Roose *et al.* (2001)

Using asymptotic expansions, Roose *et al.* (2001) provide an approximate analytical solution to the model described by equations (4.16)-(4.18). It is in fact their solution for nutrient uptake by a single cylindrical root from soil. With the previous sections we have arrived at the conclusion that we can use their solution for calculating influx into a single cylindrical hypha, as long as our assumption, that the soil can be described as a continuum, is valid. The expression for the influx into hypha is (Roose *et al.* 2001)

$$F(t) = \frac{2\lambda c_\infty}{1 + c_\infty + \frac{\lambda}{2}\ln(4e^{-\gamma}t + 1) + \sqrt{4c_\infty + [1 - c_\infty + \frac{\lambda}{2}\ln(4e^{-\gamma}t + 1)]^2}}, \tag{4.19}$$

where $\gamma \approx 0.57722$ is Euler's constant. We obtain the dimensional influx by multiplying equation (4.19) with the scale for the flux, $\frac{K_m D_l \theta_l f_l}{r_0} = \frac{F_m}{\lambda}$.

If $\lambda << 1$, we may neglect the change of solute concentration in the liquid phase at the hyphal surface. In that case, the influx into hyphae is determined only by the bulk soil solution concentration and simply given by

$$F = \lambda\frac{c_\infty}{1 + c_\infty}, \tag{4.20}$$

or in dimensional form,

$$F_D = \frac{F_m C_{l,0}}{K_m + C_{l,0}}. \tag{4.21}$$

4.3 Solute uptake by a single hypha from a soil pore

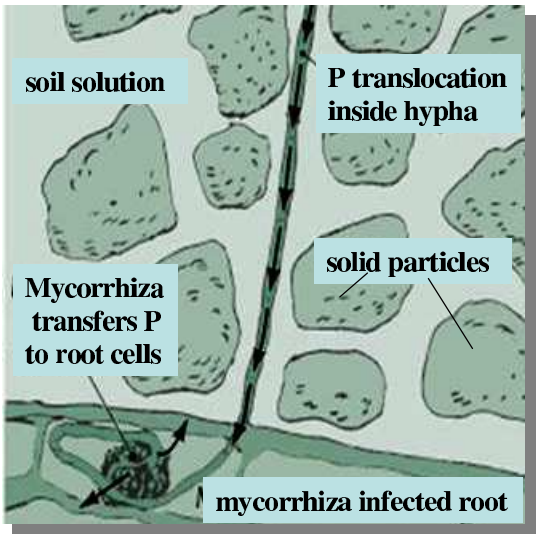

Figure 4.1: Sketch of fungal hypha in soil. The diameter of a mycorrhizal hypha is smaller than the soil pore diameter.

Hyphal diameter are in the order of micrometers whereas the diameter of soil pores can be up to the order of millimeters (Ezawa *et al.* 2002; Scheffer *et al.* 2002). If the soil pore diameter is much larger than the diameter of a single hypha, the assumption that the soil can be described as a continuum is no longer valid. Consider a single hypha growing within a soil pore (Figure 4.1). The space between the hypha and the solid particle surface is filled with either soil solution or air. Solute uptake only occurs from soil solution. We consider radial diffusion through the soil solution towards the hyphal surface where solutes are taken up according to Michaelis-Menten kinetics. Because of their thin radius, we expect the water uptake rate of hyphae to be less than the rate for roots. Hence, we can expect the Péclet number to be even smaller than the one derived in section 4.2.2 and we can neglect convective solute transport. At the interface between liquid phase and soil pore wall, we need to account for ad- and desorption reactions. A simple approach to describe chemical non-equilibrium is

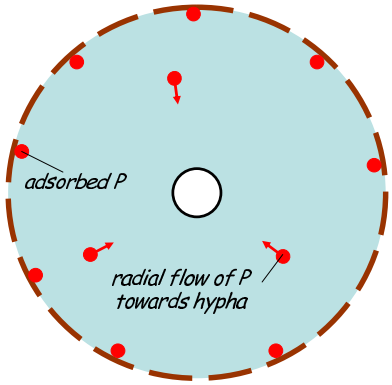

Figure 4.2: Model domain on the single hyphal scale. A cylindrical hypha is surrounded by the solution within a soil pore.

a linear first order kinetic reaction

$$\frac{dC_S}{dt} = \frac{k_a\theta}{\rho_b}C_l - k_dC_S \tag{4.22}$$

$$\frac{dC_l}{dt} = \frac{k_d\rho_b}{\theta}C_S - k_aC_l \tag{4.23}$$

where C_S $(mol\ g^{-1})$ is the concentration adsorbed onto the soil solid phase, C_l $(mol\ cm^{-3})$ is the soil solution concentration, k_a (s^{-1}) is the adsorption rate constant, k_d (s^{-1}) is the desorption rate constant, ρ_b $(g\ cm^{-3})$ is the soil bulk density and θ (cm^3cm^{-3}) is the volumetric water content. At equilibrium, this turns into the linear Freundlich isotherm

$$C_S = K_dC_l \tag{4.24}$$

where $K_d = \frac{k_a\theta}{k_d\rho_b}$ $(cm^3\ g^{-1})$ is the distribution coefficient. K_d is related to the buffer power b_p of equation (4.3) by $b_p = \rho_bK_d$.

4.3.1 Model formulation

Consider a cylindrical hypha surrounded by a hollow cylinder filled with soil solution which is bounded by the pore wall (Figure 4.2). To model the movement of solutes in the soil solution, consider an arbitrary volume of solution V with concentration C_l. The rate of change of C_l in V must be equal to the flux of solutes, q, across its boundary ∂V plus the contribution from any internal sources or sinks. Let us assume that there are no internal sources or sinks. Then, again applying the conservation law stated in equation (2.1), we get

$$\frac{\partial C_l}{dt} + \nabla \cdot q = 0,$$

Neglecting convective solute transport as stated before, the flux q is given by Fick's law,

$$q = -D_l \nabla C_l,$$

where D_l is the diffusion coefficient ($cm^2\ s^{-1}$) in free water. Hence we can write the model for radial diffusion of solutes towards the hypha as

$$\frac{\partial C_l}{dt} = D_l \frac{1}{r} \frac{\partial}{\partial r}(r \frac{\partial C_l}{\partial r}). \tag{4.25}$$

For the initial condition, we assume that there is a uniform concentration C_{l0}. We further assume that the hyphae take up solutes according to Michaelis-Menten kinetics, so that the boundary condition at the hyphal surface is

$$D \frac{\partial C_l}{dr} = \frac{F_m C_l}{K_m + C_l}, \qquad r = r_0, \tag{4.26}$$

where r_0 is the hyphal radius, F_m ($mol\ cm^{-2}\ s^{-1}$) is the maximal hyphal uptake rate and K_m ($mol\ cm^{-3}$) is the Michaelis-Menten constant. At the solution-solid interface ($r = r_1$, $r_1 > r_0$), we assume that the flux of solute is equal to the rate of change in the density of solute bound to the solid surface. Here, we make the assumption that the surface of a pore can be regarded as homogeneous and we express the adsorbed concentration per unit area of pore wall, C_a ($mol\, cm^{-2}$). We derive the boundary condition using conservation of mass. Consider the surface area A of the cylinder with radius $r = r_1$ and length h. In absence of any source or sink terms, and assuming that we can neglect intra-particle diffusion or surface diffusion, the rate of change of adsorbed concentration must be equal to the flux across the solid-solution interface. Therefore,

$$\frac{d}{dt} \int_A C_a dA = - \int_A q \cdot \mathbf{u}_n dS.$$

Since C_a is homogeneous on the surface, $\int_A C_a dA = 2r_1 \pi h C_a$. Also, we have $q = -D\frac{\partial C_l}{\partial r}$, $\mathbf{u}_n = -1$ and $A = 2r_1\pi h$ at $r = r_1$, so that $-\int_A q \cdot \mathbf{u}_n dS = -2r_1 \pi h D \frac{\partial C_l}{\partial r}$. Hence, the boundary condition at $r = r_1$ is

$$\frac{\partial C_a}{\partial t} = -D \frac{\partial C_l}{\partial r}. \tag{4.27}$$

The rate of change of C_a is given by the kinetic reaction stated in equation (4.22), but with the adsorbed concentration expressed per unit surface area:

$$\frac{dC_a}{dt} = \frac{k_a \theta}{\rho_b A_s} C_l - k_d C_a. \tag{4.28}$$

where A_s ($cm^2\ g^{-1}$) is the specific surface area. Equation (4.28) has the additional parameter A_s as compared to equation (4.22), because the adsorbed concentration is now expressed per unit particle surface area and not per unit mass of soil. We now have two equations for the boundary condition at $r = r_1$,

$$D\frac{\partial C_l}{\partial r} = -(\frac{k_a\theta}{\rho_b A_s}C_l + k_d C_a), \tag{4.29}$$

$$\frac{dC_a}{dt} = \frac{k_a\theta}{\rho_b A_s}C_l - k_d C_a. \tag{4.30}$$

According to these equations, it is possible that the fungus depletes a pore completely. In principal we could add processes that resupply C_l to the pore, such as intra-particle diffusion. However, the diffusion coefficient of phosphate in water is in the order of $10^{-5}\,cm\,s^{-1}$ (Lide 2000) and intra-particle diffusion coefficients are the order of $10^{-11}\,cm\,s^{-1}$. Therefore, as a first approximation, we neglect resupply of C_l to the pore. Let us assume that the initial condition for C_l is $C_l = C_{l,0}$ and that, initially, C_{a0} is in equilibrium with C_{l0}, so that $C_{a0} = \frac{k_a\theta}{k_d\rho_b A_s}C_{l0}$.

In summary, we developed the following model in radial polar coordinates:

$$\frac{\partial C_l}{\partial t} = D_l\frac{1}{r}\frac{\partial}{\partial r}(r\frac{\partial C_l}{\partial r}), \qquad r_0 < r < r_1,\ t > 0, \tag{4.31}$$

$$D_l\frac{\partial C_l}{\partial r} = \frac{F_m C_l}{K_m + C_l}, \qquad r = r_0, \tag{4.32}$$

$$\begin{cases} D_l\frac{\partial C_l}{\partial r} = -\left(\frac{k_a\theta}{\rho_b A_s}C_l - k_d C_a\right), \\ \frac{dC_a}{dt} = \frac{k_a\theta}{\rho_b A_s}C_l - k_d C_a, \end{cases} \qquad r = r_1, \tag{4.33}$$

$$C_l = C_{l0}, C_a = \frac{k_a\theta}{k_d\rho_b A_s}C_{l0}, \qquad t = 0, \tag{4.34}$$

where C_l ($mol\ cm^{-3}$) is the concentration of solute in soil solution, C_a ($mol\ cm^{-2}$) is the adsorbed concentration of solute per unit surface area of soil solid particles, D_l ($cm^2\ s^{-1}$) is the diffusion coefficient of the solute in free water, F_m ($mol\ cm^{-2}\ s^{-1}$) is the maximum hyphal uptake rate, K_m ($mol\ cm^{-3}$) is the Michaelis-Menten constant for hyphal uptake, r_0 (cm) is the hyphal radius, r_1 (cm) is the distance to the pore wall.

4.3.2 Non-dimensionalisation

Let $t = [t]t^*$, $r = [r]r^*$, $C_l = [C_l]C_l^*$ and $C_a = [C_a]C_a^*$. An intrinsic length scale of this system is the hyphal radius, therefore we choose $[r] = r_0$. In addition, let us scale the solution concentration with the Michaelis Menten constant, $[C_l] = K_m$ and the

adsorbed concentration with the adsorbed concentration which is in equilibrium with $C_l = K_m$, $[C_a] = \frac{k_a \theta}{k_d \rho_b A_s} K_m$. Time scales of interest are the time scale of the life of a hypha, which is in the order of several days, the reaction time scale that determines how fast the adsorbed solute is available for the fungus, and the diffusion time scale. On the diffusion time scale, $[t] = \frac{r_0^2}{D}$, and the non-dimensional model in radial polar coordinates is (dropping asterisks)

$$\frac{\partial C_l}{\partial t} = \frac{1}{r} \frac{\partial}{\partial r} (r \frac{\partial C_l}{\partial r}), \tag{4.35}$$

$$\frac{\partial C_l}{\partial r} = \lambda \frac{C_l}{1 + C_l} \qquad \text{at} \ , \qquad r = 1, \tag{4.36}$$

$$\begin{cases} \frac{\partial C_l}{\partial r} = -\delta_1 (C_l - C_a), \\ \delta_2 \frac{dC_a}{dt} = C_l - C_a, \qquad \text{at} \qquad r = r_{end}, \end{cases} \tag{4.37}$$

$$C_l = C_a = c_\infty, \quad \text{at } t = 0. \tag{4.38}$$

The dimensionless parameters are $\lambda = \frac{F_m r_0}{D K_m}$, $\delta_1 = \frac{k_a \theta r_0}{\rho_b A_s D}$, $c_\infty = \frac{C_{l0}}{K_m}$, $r_{end} = \frac{r_1}{r_0}$ and $\delta_2 = \frac{D}{k_d r_0^2}$, where λ is the dimensionless uptake parameter, c_∞ is the dimensionless solute concentration in the bulk solution, r_{end} is the dimensionless distance to the pore wall, and δ_1 and δ_2 are the dimensionless ad- and desorption parameters.

4.3.3 Parameter estimation

Approximate values for the dimensional parameters in the model are given in table 4.2. Mycorrhiza experiments are often performed using a substrate of sandy soil, which has a small specific surface area. It is therefore reasonable to assume a specific surface area of 200 $cm^2 g^{-1}$. Not many values for the uptake parameters F_m and K_m are available. It is often assumed that they are the same as the values for roots. Schweiger & Jakobsen (1999) estimated uptake parameters that are an order of magnitude larger than root values. If we assume that the desorption of phosphate is fast, so that $k_d = 10^{-2}\ s^{-1}$, the dimensionless parameters λ, δ_1 and δ_2 are $\lambda = 0.03 - 0.75$, $\delta_1 = 5.86 \times 10^{-1}$ and $\delta_2 = 4000$. The values of r_0 and r_1 in table 4.2 suggest that r_{end} can be either $r_{end} = O(1)$ or $r_{end} >> 1$. In the second case, we can treat the domain as semi-infinite, so that the outer boundary has no influence on the flux at the hyphal

Table 4.2: Typical values of the dimensional parameters for the pore scale model.

Parameter	Units	Value for P	Reference
D_l	$cm^2\ s^{-1}$	10^{-5}	Lide (2000)
r_0	cm	5×10^{-4}	Ezawa *et al.* (2002)
r_1	cm	1.2×10^{-1}-3.5×10^{-3}	$r_1 = d_p/2 = d_w \frac{2}{3} \frac{n}{1-n}$, $d_w = \frac{6(1-n)}{A_s \rho_b}$ *
F_m	$\mu mol\ cm^{-2}\ s^{-1}$	$3.26 \times 10^{-6} - 2.55 \times 10^{-5}$	Tinker & Nye (2000); Schweiger & Jakobsen (1999)
K_m	$\mu mol\ cm^{-3}$	$5.8 \times 10^{-3} - 1.7 \times 10^{-3}$	Tinker & Nye (2000); Schweiger & Jakobsen (1999)
b	$cm^3 cm^{-3}$	239	Barber (1995)
k_d	s^{-1}	$5.94 \times 10^{-5} - 2.72 \times 10^{-2}$	Chen *et al.* (1996)
k_a	s^{-1}	$4.73 \times 10^{-2} - 1.95$	$k_a = k_d \frac{b}{\theta}$
θ	$cm^3 cm^{-3}$	1	assumption on the single hyphal scale
A_s	$cm^2\ g^{-1}$	< 1000	for sands (Kammerer & Loiskandl 2003)
ρ_b	$g\ cm^{-3}$	1.02	calculated from Jakobsen *et al.* (1992)
C_{l0}	$\mu mol\ cm^{-3}$	6×10^{-4} -3×10^{-3}	low to medium concentration (Barber 1995)

*where d_p is the effective pore diameter and d_w is the effective particle diameter (Kammerer & Loiskandl 2003).

surface. Rescaling the concentration $C_l = c_\infty c$ and $C_a = c_\infty c_a$, the model becomes

$$\frac{\partial c}{\partial t} = \frac{1}{r}\frac{\partial}{\partial r}(r\frac{\partial c}{\partial r}), \tag{4.39}$$

$$\frac{\partial c}{\partial r} = \lambda \frac{c}{1 + c_\infty c}, \qquad r = 1, \tag{4.40}$$

$$\begin{cases} \frac{\partial c}{\partial r} = -\delta_1 (c - c_a), \\ \delta_2 \frac{dc_a}{dt} = c - c_a, & r = r_{end}, \end{cases} \tag{4.41}$$

$$c = c_a = 1, \qquad t = 0. \tag{4.42}$$

Mycorrhizas are said to increase plant phosphate nutrition in particular when the soil concentration is low. The values for C_{l0} in table 4.2 suggest that in this case we have $c_\infty << 1$. We will assume that this is the case in all subsequent calculations. When $c_\infty << 1$, the boundary condition at $r = 1$ can be approximated at leading order by the linear equation

$$\frac{\partial c}{\partial r} = \lambda c, \qquad r = 1. \tag{4.43}$$

In summary, the model which we wish to solve is

$$\frac{\partial c}{\partial t} = \frac{1}{r}\frac{\partial}{\partial r}(r\frac{\partial c}{\partial r}), \tag{4.44}$$

$$\frac{\partial c}{\partial r} = \lambda c, \qquad r = 1, \tag{4.45}$$

$$\begin{cases} \frac{\partial c}{\partial r} = -\delta_1(c - c_a), \\ \delta_2 \frac{dc_a}{dt} = c - c_a, \qquad \text{at} \quad r = r_{end}, \end{cases} \tag{4.46}$$

$$c = c_a = 1, \qquad t = 0. \tag{4.47}$$

4.3.4 Approximate analytical solution for bounded domain

When the domain is bounded, *i.e.*, $r_{end} = O(1)$, the effect of desorption of solute from the pore wall is included into the model in the form of the boundary condition (4.46). In this section, we develop an approximate analytical solution for this model. We seek an approximate solution to the model described by (4.44)-(4.47). Because $\delta_2 >> 1$, we use an asymptotic expansion in $\frac{1}{\delta_2} << 1$. This solution is valid for all $t << \delta_2$. We call this the inner solution. We seek solutions of the form

$$c \approx c_0 + \frac{1}{\delta_2}c_1 + ... \tag{4.48}$$

$$c_a \approx c_{a,0} + \frac{1}{\delta_2}c_{a,1} + ... \tag{4.49}$$

Substituting equations (4.48) and (4.49) into equations (4.44)-(4.47) and collecting the terms of $O(\frac{1}{\delta_2}^0)$, we get

$$\frac{\partial c_0}{\partial t} = \frac{1}{r}\frac{\partial}{\partial r}(r\frac{\partial c_0}{\partial r}), \tag{4.50}$$

$$\frac{\partial c_0}{\partial r} = \lambda c_0, \qquad r = 1, \tag{4.51}$$

$$\begin{cases} \frac{\partial c_0}{\partial r} = -\delta_1(c_0 - ca_0), \\ \frac{dc_{a,0}}{dt} = 0, \qquad r = r_{end}, \end{cases} \tag{4.52}$$

$$c_0 = c_{a,0} = 1, \qquad t = 0. \tag{4.53}$$

Because $\frac{dc_a}{dt} = 0$ it follows from the initial condition that $c_a(t) = 1$. Therefore we are left with a model in c_0 only:

$$\frac{\partial c_0}{\partial t} = \frac{1}{r}\frac{\partial}{\partial r}(r\frac{\partial c_0}{\partial r}), \tag{4.54}$$

$$\frac{\partial c_0}{\partial r} = \lambda c_0, \qquad r = 1, \tag{4.55}$$

$$\tfrac{\partial c_0}{\partial r} = -\delta_1(c_0 - 1), \qquad r = r_{end}, \tag{4.56}$$

$$c_0 = 1, \qquad t = 0. \tag{4.57}$$

The solution to this model can be found using Laplace transformation. Crank (1975) (p. 86) gives the solution to the diffusion equation in a hollow cylinder with general linear boundary conditions and zero initial condition. If we put $c_0(r,t) = 1 + \tilde{c}(r,t)$ in equations (4.54)-(4.57), we get the initial condition $\tilde{c}(r,0) = 0$ so that we can apply this general solution to our model. The solution is

$$\begin{aligned} \tilde{c} &= \frac{\lambda[1 - r_{end}\delta_1 \ln(r/r_{end})]}{-\lambda - r_{end}\delta_1 + r_{end}\lambda\delta_1 \ln(1/r_{end})} - \\ &- \pi \sum_{n=1}^{\infty} e^{-\alpha_n^2 t} F(\alpha_n) C_0(r;\alpha_n)[\lambda\{\delta_1 J_0(r_{end}\alpha_n) - \alpha_n J_1(r_{end}\alpha_n)\}] \end{aligned} \tag{4.58}$$

where the α_n are the roots of

$$\begin{aligned} &[(-\lambda J_0(\alpha) - \alpha J_1(\alpha)][\delta_1 Y_0(r_{end}\alpha) - \alpha Y_1(r_{end}\alpha)] - \\ &-[\delta_1 J_0(r_{end}\alpha) - \alpha J_1(r_{end}\alpha)][\lambda Y_0(\alpha) - \alpha Y_1(\alpha)] = 0, \end{aligned} \tag{4.59}$$

$$\begin{aligned} F(\alpha_n) = \frac{\delta_1 J_0(r_{end}\alpha_n) - \alpha_n J_1(r_{end}\alpha_n)}{\{[\delta_1 J_0(r_{end}\alpha_n) - \alpha_n J_1(r_{end}\alpha_n)]^2(\lambda^2 + \alpha_n^2) - \\ -[-\lambda J_0(\alpha_n) - \alpha_n J_1\alpha_n]^2(\delta_1^2 + \alpha_n^2)\}, \end{aligned} \tag{4.60}$$

and

$$\begin{aligned} C_0(r,\alpha_n) = J_0(r\alpha_n)[-\lambda Y_0(\alpha_n) - \alpha_n Y_1(\alpha_n)] - \\ -Y_0(r\alpha_n)[-\lambda J_0(\alpha_n) - \alpha_n J_1(\alpha_n)]. \end{aligned} \tag{4.61}$$

The approximate solution c_0 is

$$c_0 = 1 + \tilde{c}. \tag{4.62}$$

In the limit $t \to \infty$, the solution is

$$c_{lim} = 1 + \tilde{c}|_{t\to\infty} = \frac{r_{end}\delta_1 + r_{end}\delta_1\lambda \ln(r)}{\lambda + r_{end}\delta_1 + r_{end}\delta_1\lambda \ln(r_{end})}. \tag{4.63}$$

In figure 4.3, equation (4.62) was plotted against the numerical solution of the full non-linear problem. The numerical scheme was obtained using a finite difference scheme with a centered discretisation in space and the θ-method in time. Due to the non-linear boundary condition, we have an implicit non-linear expression, which we solved using fixed-point iteration. The scheme is given in appendix A. The numerical and analytical solutions agree well, so we are confident in our use of the approximate analytical solution below. At $t = 100$, the solution has already reached the limit. This is consistent with the condition for the validity of this approximate solution, that $t << \delta_2$, where $\delta_2 = 4000$.

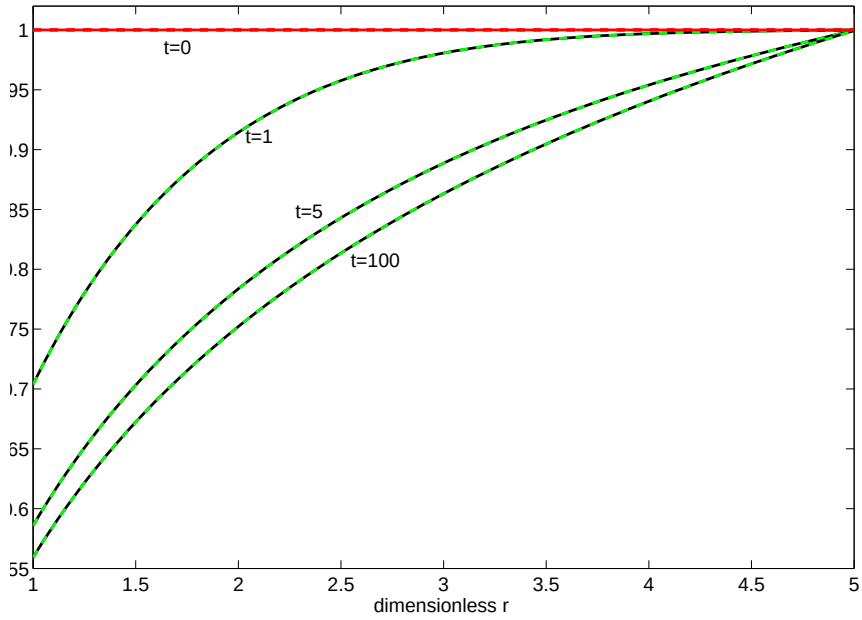

Figure 4.3: Plot of equation (4.62) (green line) against numerical solution of full non-linear model (4.39)-(4.42) (black dashed line). Model parameters: $\lambda = 0.5$, $\delta_1 = 0.6$, $\delta_2 = 4000$, $r_0 = 1$, $r_1 = 5$. Numerical parameters: $\Delta x = 0.04$, $\Delta t = 0.0016$.

To get the solution for times $t >> \delta_2$, we rescale time and let $t = \delta_2 \tau$, so that the model becomes

$$\frac{1}{\delta_2}\frac{\partial c}{\partial \tau} = \frac{1}{r}\frac{\partial}{\partial r}(r\frac{\partial c}{\partial r}), \tag{4.64}$$

$$\frac{\partial c}{\partial r} = \lambda c, \qquad r = 1, \tag{4.65}$$

$$\begin{cases} \frac{\partial c}{\partial r} = -\delta_1(c - c_a), \\ \frac{dc_a}{d\tau} = c - c_a, & r = r_{end}, \end{cases} \tag{4.66}$$

$$c \approx c_{lim}, \quad c_a, \approx 1 \quad \tau \approx 0. \tag{4.67}$$

The initial conditions come from matching with the diffusion time scale model as $t \to \infty$. There we saw that, at leading order, $c_{a,0} = 1$ for all times, and $c_0 = c_{lim}$ as $t \to \infty$.

Using asymptotic expansions in $\frac{1}{\delta_2} << 1$, we obtain an approximate solution which we call the outer solution. We seek solutions of the form

$$c \approx c_0 + \frac{1}{\delta_2} c_1 + ... \tag{4.68}$$

$$c_a \approx c_{a,0} + \frac{1}{\delta_2} c_{a,1} + ... \tag{4.69}$$

Substituting equations (4.68) and (4.69) into equations (4.64)-(4.67) and collecting the terms of $O(\frac{1}{\delta_2}^0)$, we get

$$0 = \frac{1}{r}\frac{\partial}{\partial r}(r\frac{\partial c_0}{\partial r}), \tag{4.70}$$

$$\frac{\partial c_0}{\partial r} = \lambda c_0, \qquad r = 1, \tag{4.71}$$

$$\begin{cases} \frac{\partial c_0}{\partial r} = -\delta_1(c_0 - c_{a,0}), \\ \frac{dc_{a,0}}{d\tau} = c_0 - c_{a,0}, \end{cases} \qquad r = r_{end}, \tag{4.72}$$

$$c_{a,0} = 1, \quad \tau \approx 0. \tag{4.73}$$

The solution of equation (4.70) is

$$c_0(r,t) = B_1 \ln(r) + B_2, \tag{4.74}$$

where B_1 and B_2 are constants of integration to be determined from the two boundary conditions. From the boundary condition at $r = 1$ we get that

$$\frac{dc_0}{dr}|_{r=1} = B_1(t) = \lambda c_0(1,t). \tag{4.75}$$

Because $\ln(1) = 0$, we get also that at $r = 1$, equation (4.74) becomes $c(1,t) = B_2$. Hence $B_1 = \lambda B_2(t)$ so that we can express the solution as

$$c_0(r,t) = B_2 \lambda \ln(r) + B_2. \tag{4.76}$$

From the boundary condition at $r = r_{end}$, we get that

$$\frac{dc_0}{dr}|_{r=r_{end}} = \frac{\lambda B_2}{r_{end}} = -\delta_1(\lambda B_2 \ln(r_{end}) + B_2) - c_{a,0}). \tag{4.77}$$

Hence, we obtain an expression for B_2 with respect to $c_{a,0}$:

$$B_2 = \frac{\delta_1 r_{end}}{\lambda + \delta_1 r_{end} \lambda \ln(r_{end}) + \delta_1 r_{end}} c_{a,0}. \tag{4.78}$$

Substituting equation (4.78) into equation (4.76) and substituting the result into the equation for $c_{a,0}$ in equation (4.72), we get the following linear ordinary differential equation

$$\frac{dc_{a,0}}{d\tau} + \gamma c_{a,0} = 0, \tag{4.79}$$

with initial condition $c_{a,0}(0) = 1$, where

$$\gamma = 1 - \frac{(\lambda \ln(r_{end}) + 1)\delta_1 r_{end}}{\lambda + \delta_1 r_{end}\lambda \ln(r_{end}) + \delta_1 r_{end}}. \tag{4.80}$$

The solution is

$$c_{a,0} = e^{-\gamma\tau}. \tag{4.81}$$

Substituting this into equation (4.78), B_2 is

$$B_2 = \frac{\delta_1 r_{end}}{\lambda + \delta_1 r_{end}\lambda \ln(r_{end}) + \delta_1 r_{end}}\, e^{-\gamma\tau}, \tag{4.82}$$

and the solution for c_0 becomes

$$c_0 = \frac{\delta_1 r_{end}\,[\lambda \ln(r) + 1]}{\lambda + \delta_1 r_{end}\lambda \ln(r_{end}) + \delta_1 r_{end}}\, e^{-\gamma\tau}. \tag{4.83}$$

This approximate analytical solution was compared to the numerical solution of the full non-linear model (4.39)-(4.42) but with the time expressed in terms of τ. The result is shown in Figure 4.4; the analytical solution agrees well with the numerical solution. Therefore, we are confident in our use of this approximate analytical solution in the following. The equilibrium concentration $c_0 = 0$ is reached fast; after approximately 1.5 hrs, the fungus has taken up all available solute. This is due to our assumption that reaction time is fast. The fungus would require a longer time to take up all available solute if the desorption reaction was slower.

The composite solution is obtained as the sum of the outer and the inner solution minus the common part, *i.e.* the concentration at $r = 1$ is

$$\begin{aligned} c &= 1 + \frac{\delta_1 r_{end}[e^{-\gamma\tau} - 1 - \lambda \ln(r_{end})] - \lambda}{\lambda + r_{end}\delta_1 + r_{end}\lambda\delta_1 \ln(r_{end})} - \\ &- \pi \sum_{n=1}^{\infty} e^{-\alpha_n^2 \delta_2 \tau} F(\alpha_n) C_0(1;\alpha_n)[\lambda\{\delta_1 J_0(r_{end}\alpha_n) - \alpha_n J_1(r_{end}\alpha_n)\}], \end{aligned} \tag{4.84}$$

where the α_n are the positive roots of equation (4.59) and $F(\alpha_n)$ and C_0 are given by equations (4.60) and (4.61) when $r = 1$.

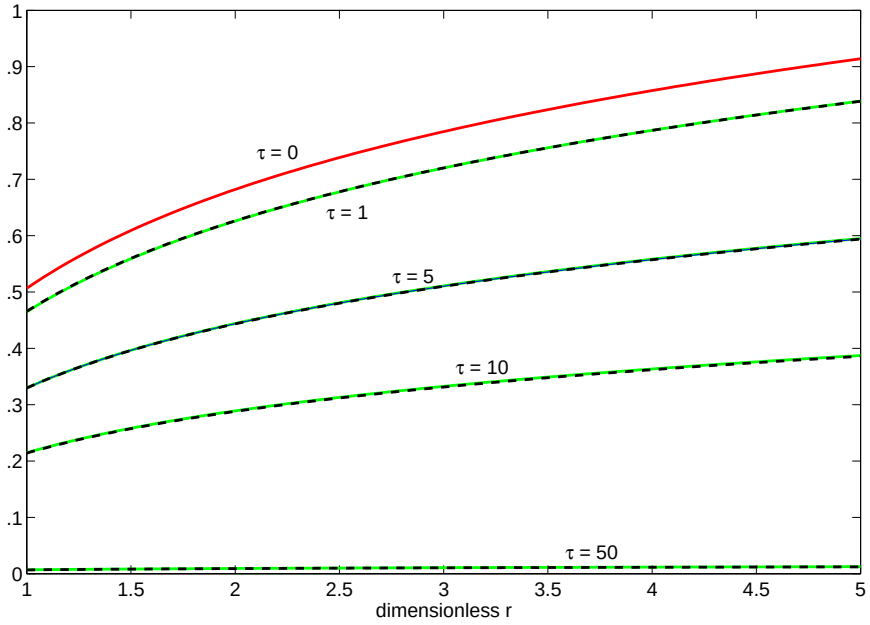

Figure 4.4: Plot of equation (4.83) (green line) against numerical solution of full model (4.39)-(4.42) (black dashed line). Model parameter: $\lambda = 0.5$, $\delta_1 = 0.6$, $\delta_2 = 4000$, $r_0 = 1$, $r_1 = 5$. Numerical parameter: $\Delta x = 0.04$, $\Delta\tau = 0.0016$.

The dimensionless influx into the hypha is given by

$$\begin{aligned} F(\tau) &= \lambda c_\infty c = \lambda c_\infty \left[1 + \frac{\delta_1 r_{end}[e^{-\gamma\tau} - 1 - \lambda \ln(r_{end})] - \lambda}{\lambda + r_{end}\delta_1 + r_{end}\lambda\delta_1 \ln(r_{end})} - \right. \\ &- \left. \pi \sum_{n=1}^{\infty} e^{-\alpha_n^2 \delta_2 \tau} F(\alpha_n) C_0(1;\alpha_n)[\lambda\{\delta_1 J_0(r_{end}\alpha_n) - \alpha_n J_1(r_{end}\alpha_n)\}]\right] \quad (4.85) \end{aligned}$$

The scale for the flux is $\frac{DK_m}{r_0} = \frac{F_m}{\lambda}$ and the scale for time in terms of τ is $\frac{1}{k_d}$. Therefore, the dimensional influx into the hypha is $F_D(t_D) = \frac{F_m}{\lambda} F(k_d\, t_D)$. The resulting dimensional influx into the hypha is shown in Figure 4.5 and compared to the numerical solution of the full non-linear model. It can be seen that the hypha takes up all available solutes at a time $t >> \delta_2$. The speed at which this takes place depends on the values of the dimensionless ad- and desorption parameters δ_1 and δ_2 as well as the uptake parameter λ. In figure 4.6, dimensional time is plotted on a logarithmic scale so as to point out the phases of solute uptake by a single hypha from a soil pore. At a time in the order of the diffusion time scale, the flux rapidly decreases as the hypha takes up solutes, creating a depletion zone around it. At a time in the order of the reaction time scale, the depletion zone has reached the outer boundary at the pore wall and the concentration in the pore water solution is sustained with

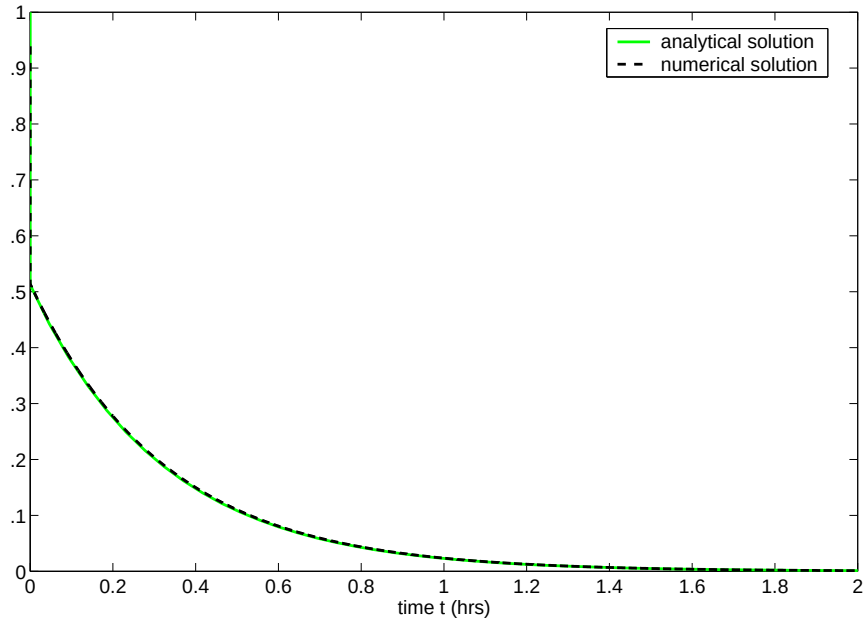

Figure 4.5: Approximate analytical and numerical solution for solute influx into hypha. Model parameters: $\lambda = 0.5$, $\delta_1 = 0.6$, $\delta_2 = 4000$, $r_0 = 1$, $r_1 = 5$. Numerical parameters: $\Delta x = 0.04$, $\Delta\tau = 0.0016$ and $\Delta\tau = 1 \times 10^{-6}$ during the first five seconds.

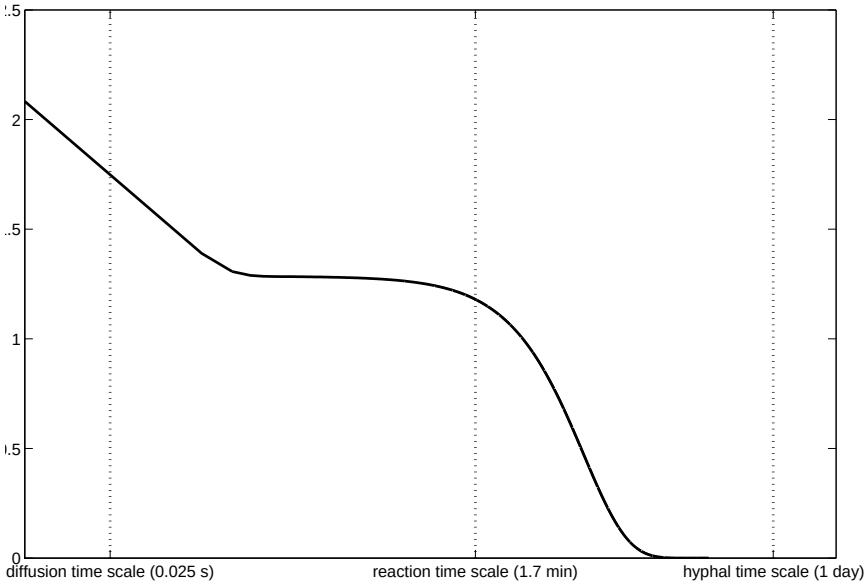

Figure 4.6: Phases of the solute influx into a single hypha as calculated by the bounded soil pore model.

solutes that are desorbed from the pore wall. After the adsorbed phase has also been depleted by the fungus, the concentration in the solution tends to zero, which is the

equilibrium concentration reached at a time in the order of the hyphal time scale.

4.3.5 Approximate analytical solution for semi-infinite domain

In section 4.3.3, we have shown that the dimensionless parameter r_{end} can be either of order 1 or much larger than 1, depending on the relative diameters of hyphae and soil pores. In this section, we deal with the case when $r_{end} >> 1$. Then the domain where radial flow of solutes towards the hyphal surface occurs can be treated as a semi-infinite domain. If we assume that r_{end} is big enough so that the solution concentration there stays unaffected by the presence of the hypha, the concentration at r_{end} stays constant. Therefore, our model becomes

$$\frac{\partial c}{\partial t} = \frac{1}{r}\frac{\partial}{\partial r}(r\frac{\partial c}{\partial r}), \tag{4.86}$$

$$\frac{\partial c}{\partial r} = \lambda c \quad \text{at} \quad r = 1, \tag{4.87}$$

$$\begin{cases} c = 1, \\ c_a = 1 \qquad \text{at} \quad r \to \infty, \end{cases} \tag{4.88}$$

$$c = c_a = 1 \quad \text{at} \quad t = 0 \tag{4.89}$$

As in section 4.2, we can use the solution provided by Roose *et al.* (2001),

$$F(t) = \frac{2\lambda c_\infty}{1 + c_\infty + \frac{\lambda}{2}\ln(4e^{-\gamma}t + 1) + \sqrt{4c_\infty + [1 - c_\infty + \frac{\lambda}{2}\ln(4e^{-\gamma}t + 1)]^2}}, \tag{4.90}$$

but with $\lambda = \frac{F_m r_0}{DK_m}$. The scale for the dimensional flux is $\frac{DK_m}{r_0} = \frac{F_m}{\lambda}$ and the scale for the dimensional time t_D is $t_D = \frac{r_0^2}{D}t$. The dimensional flux on the single hyphal scale for water filled pores only is hence given by $F_D(t_D) = \frac{F_m}{\lambda}F(\frac{D}{r_0^2}t_D)$.

4.4 Conclusions

We have found approximate analytical solutions describing the influx of solute into a cylindrical hypha. The influx for the continuum soil model is given by equation (4.19) or by equation equation (4.20), depending on the value of the dimensionless parameter λ. The solution for the bounded case in the soil pore model is given by equation (4.85) and the solution for the semi-infinite case is given by equation (4.90). In figure 4.7, the dimensional influxes based on equations (4.19), (4.85) and (4.90) are

compared. The differences in the three expressions are large. For the example given in figure 4.7, the cumulative uptake of one unit length of hypha of radius $5 \times 10^{-4}\, cm$ after $5\, hrs$ is $4.55 \times 10^{-7} \mu mol$ for the bounded soil pore model, $2.82 \times 10^{-6} \mu mol$ for the semi-infinite soil pore model and $7.50 \times 10^{-6} \mu mol$ for the continuum soil model. To test which expression is describing the system accurately, we would need to test them against experimental data. However, none are available, since it is difficult to measure influxes into or concentration profiles around single hyphae. So the models presented here are highlighting the need for experiments on the single hyphal scale.

In the next chapter, we are going to use the solutions found in this chapter to estimate uptake by a fungal colony.

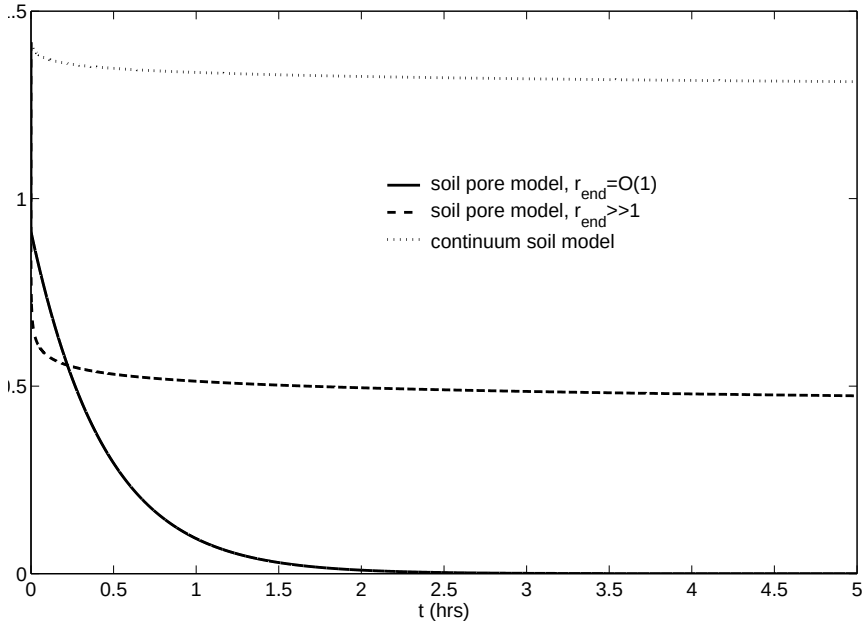

Figure 4.7: Comparison of influxes into hypha as obtained with equations (4.19), (4.85) and (4.90). Model parameters: $\lambda = 0.5$, $\delta_1 = 0.6$, $\delta_2 = 4000$, $r_0 = 1$, $r_1 = 5$

Chapter 5

Solute uptake by a mycorrhizal root

5.1 Introduction

In this chapter, we develop a model for solute uptake by a mycorrhizal root. Mycorrhizas have been recognized as an important means of plant phosphorus nutrition (Tinker & Nye 2000). External fungal hyphae take up phosphate from soil solution and contribute to the overall plant uptake. The starting point for model development is the model for root solute uptake on the single root scale as described by Barber (1995); Tinker & Nye (2000). The expressions developed in the previous chapters provide a basis to develop a sink term to account for solute uptake by the fungal mycelium. In this first model, we will not consider competition between mycorrhizal roots. We are interested in the effect of the fungal mycelium on total nutrient uptake of one root, based on the assumption that external hyphae offer a spatial advantage to access non-mobile nutrients such as phosphorus. The model is motivated by the experiment of Drew *et al.* (2003) described in section 1.1.2. A root free side arm filled with soil is attached to a root compartment and growth of fungal hyphae as well as phosphorus uptake are observed. We take that the interface between root and fungal compartment mimics the "root surface", and aim to estimate the contribution of mycelial solute uptake to the total uptake.

The experiment of Drew *et al.* (2003) cannot be used to test our model because it does not offer all the necessary information, but it serves as motivation for model development and the choice of coordinate system. We will use the model to present numerical experiments based on different standard assumptions. Firstly, uptake parameters for hyphae have not been measured. It is often claimed that it is reasonable

to assume that they are the same as for the root. Schweiger & Jakobsen (1999) estimated uptake parameters that are an order of magnitude larger than root values. We will look at the effect on soil solution concentration and solute uptake when we use the one or the other uptake parameter estimation. Secondly, we will compare calculated uptake based on the different influx models on the single hyphal scale developed in chapter 4.

5.2 Model formulation

Our starting point is the nutrient uptake model on the scale of a single root described by Barber (1995); Tinker & Nye (2000). It models transport and reaction of nutrients through soil towards the root surface and uptake by the root according to prescribed uptake kinetics. Because the root diameter is large compared to most soil pores, the soil can be described as a continuum. Thus, for solute transport in soil, we can in principal use the model developed in section 4.2.1. However, if a root develops mycorrhizas, the external hyphae may grow up to several centimeters away from the root surface and form a mycelial network. We consider this as an additional "mycelial" phase in soil.

Let us assume that there is one characteristic average hyphal diameter r_m. We can then use the equations for hyphal length density developed in chapters 2 and 3 to calculate the total volume of mycelium per unit volume of soil. The volume fraction of mycelial phase, θ_m, is hence given by

$$\theta_m(t, r) = r_m^2 \pi \rho(t, r), \tag{5.1}$$

where t is the time, r_m is the radius of the external hyphae and ρ is the hyphal length density given by one of the equations derived in chapters 2 or 3.

Fungi require large amounts of water for their growth. It seems reasonable to think that locally available water is mainly used for growth rather than water being translocated from within the mycelial network. As the simplest approach, we assume that the volume fraction of fungal biomass replaces part of the volume fraction of water in soil, θ_l, so that $\theta_l = \theta_l(t)$ and the overall volume conservation relation becomes

$$\theta_s + \theta_l(r, t) + \theta_g + \theta_m(r, t) = 1, \tag{5.2}$$

where $\theta_l(r, t) = \theta_{l,0} - \theta_m(r, t)$, $\theta_{l,0}$ is the initial water content, and θ_s and θ_a are the volume fractions of the soil solid and gas phase, respectively. However, we have seen

in chapter 3 that the hyphal length density was of order $10^3\ cm\,cm^{-3}$ for the fungi studied. With a hyphal radius of $5 \times 10^{-4}\,cm$ (table 4.2), we find that θ_m is of order 10^{-4}. Typical values for θ_l in soil are $0.15 - 0.4$. Thus, we may assume

$$\theta_l(t) \approx \theta_{l,0}. \tag{5.3}$$

We assume that, in addition to the solid (C_s) and liquid (C_l) phase, the solute is also present in the mycelial (C_m) phase. As described in section 4.2, C_s is expressed in moles per unit total soil volume whereas C_l is expressed in moles per unit volume of liquid phase. We express C_m in moles per unit volume of mycelial phase. In section 4.2, we developed an equation for solute movement in soil, equation (4.5), which we now extend with a sink term F_{myc} to account for the removal of solutes from liquid phase by external fungal hyphae. Thus, the equation is

$$\frac{\partial((b_p + \theta_l)C_l)}{\partial t} = \nabla \cdot (\theta_l D_l f_l \nabla C_l) - \nabla \cdot (\mathbf{v}\, C_l) - F_{myc}(t), \tag{5.4}$$

where D_l is the diffusion coefficient in free water, $\mathbf{v}$ is the Darcy flux of water, f_l is the impedance factor of solute in the liquid phase and b_p is the buffer power.

The fate of solutes within the mycelial phase varies strongly for different solutes since it is dependent on its biological function and biochemical form. Phosphate is thought to be taken up in excess of the fugal need and transported towards the root surface where it is transferred into the root cells. We will not go into the detail of the biochemical processes of this. However we will use the information that phosphate is thought to be transported due to cytoplasmic streaming. Cytoplasmic streaming is a bulk flow of the cytoplasm, the semi-fluid matter contained within the cell's plasma membrane, which is caused by cytoskeletal forces (Bago *et al.* 2002). Hence, we assume in our model that solute transport within the mycelial phase is mainly by convection. However, quantitative information about this process is scarce. In addition, we include diffusion as another possible form of transport in our model. We expect the impedance factor of any solute in the mycelial phase to be smaller or equal than the one in the soil liquid phase, *i.e.* $f_m \leq f_l$. A relationship between the impedance factor in porous media and the volume fraction has been found empirically in form of a power law, also called "Archie's law" (Kume-Kick *et al.* 2002),

$$f_m = \theta_m^p. \tag{5.5}$$

In soils, we can mostly assume that $1 \leq p \leq 2$ (Roose *et al.* 2001). Kume-Kick *et al.* (2002) present the values $0.5 \leq p \leq 0.7$ for brain tissues. Another relationship, based

on geometrical considerations, was derived by Tao & Nicholson (2004) to estimate the tortuosity of brain extracellular space. The impedance factor f_m is related to the tortuosity λ by $f = \frac{1}{\lambda^2}$. Their equation for the impedance factor is

$$f_m = \frac{2}{3 - \theta_m}. \tag{5.6}$$

Note that in this case, a limiting value of 2/3 is reached as $\theta_m \to 0$. Tao & Nicholson (2004) argue that this limit corresponds to an infinitesimal particle traversing vanishingly thin sheets of extra cellular space. This value is therefore very specific to brain tissue and is not applicable to soil because the fluid pore space in soils does not have this type of sheet structure. In absence of other data, we will use equation (5.5) to estimate the impedance factor of the mycelial phase.

The equation for the mycelial phase is due to diffusive and convective transport of solute through the mycelial phase and a source term to account for solute uptake by the mycelium from soil solution,

$$\frac{\partial(\theta_m C_m)}{\partial t} = \nabla \cdot (D\theta_m^{p+1} \nabla C_m) - \nabla \cdot (\theta_m \mathbf{v}_m C_m) + F_{myc}(t), \tag{5.7}$$

where $\mathbf{v}_m$ is the velocity of the cytoplasm.

5.2.1 The sink term for solute uptake by fungal mycelium

Local solute uptake by fungal mycelium depends on hyphal surface area and influx. Assuming an average hyphal radius, r_m, we calculate the surface area at any given position and time using one of the expressions for hyphal length density developed in chapters 2 and 3. In chapter 4, we present approximate analytical solutions for hyphal influx on the single hyphal scale and show that the differences between them can be more than an order of magnitude. In this chapter, we consider the two expressions that predict the largest and smallest influx for comparison.

The influx is largest if we assume that the fungi can be modelled as sinks in a continuum soil. Under the assumption that the dimensionless uptake parameter $\lambda = \frac{F_{m,h} r_m}{D K_{m,h}}$ is small, where $F_{m,h}$ is the maximal influx rate of hyphae and $K_{m,h}$ is the Michaelis Menten constant of hyphae, the influx into one cylindrical hypha is given by equation (4.21),

$$F_{hom}(C_l) = \frac{F_{m,h} C_l}{K_{m,h} + C_l}, \tag{5.8}$$

where C_l is the local bulk solute concentration in the liquid phase. This model assumes that there is a continuous resupply of solute to the depleted pores. Assuming the

hyphal length density ρ is known, the local uptake rate of external hyphae is given by

$$F_{myc}(x,t;C_l) = 2\pi r_m \rho(x,t) F_{hom}(C_l). \tag{5.9}$$

In chapter 4, we showed that influx into a single hypha is smallest when the soil is not regarded as continuum and when the dimensionless parameter $r_{end} = \frac{r_p}{r_m}$ is of order 1, where r_p is the soil pore radius. Under the assumption that the dimensionless parameter $c_\infty = \frac{C_l}{K_{m,h}} << 1$, the dimensionless influx is given by equation (4.85). However, consider that equation (4.85) is an approximate analytical solution obtained by matching the solution for the model on the diffusion time scale with the solution on the reaction time scale. The solution on the diffusion time scale requires solving an infinite series and calculating roots of a relatively complicated expression, which can take a long time. We have shown that the diffusion time scale model is only valid for the first few seconds, depending on how fast the desorption reaction is. Because we are interested in a time scale of several weeks, the large time behavior of the flux is adequately well described by the solution on the reaction time scale only. We do this to compute the sink term, which we wish to develop, faster. The dimensional analytical expression for influx becomes thus

$$F_{nonhom}(t;C_l) \;=\; F_{m,h}\frac{C_l}{K_{m,h}}\frac{\delta_1 r_{end}\left[\lambda \ln(r)+1\right]}{\lambda+\delta_1 r_{end}\lambda\ln(r_{end})+\delta_1 r_{end}}\, e^{-\gamma k_d t}, \tag{5.10}$$

where $\gamma = 1 - \frac{(\lambda\ln(r_{end})+1)\delta_1 r_{end}}{\lambda+\delta_1 r_{end}\lambda\ln(r_{end})+\delta_1 r_{end}}$, k_d is the desorption rate constant, and δ_1, δ_2, λ are the dimensionless parameters described in section 4.3.2. To calculate the local uptake rate of external hyphae, we also have to take into account that the model on the single hyphal scale was developed for fully saturated pores. If the soil is only partially saturated, we introduce an additional factor θ_l to account for the volume fraction where uptake can occur. We also need to consider that uptake only starts after external hyphae first appear at a given point. Hyphae are thought to spread through the soil due to a flux of tips, where the paths behind the tips represent the newly created hyphae. The time when the tips first reach a given position can be calculated from the characteristic equations of the hyperbolic equation for the hyphal tip density n. Let us call this time t_c. Then the source term for hyphal solute uptake is

$$F_{myc}(x,t;C_l) = \begin{cases} 0, & t - t_c < 0, \\ 2\pi r_m \rho(x,t)\theta_l F_{nonhom}(t-t_c;C_l), & t - t_c \geq 0. \end{cases} \tag{5.11}$$

This model assumes that a pore can be depleted completely by a hypha and that replenishment can be neglected.

The source terms described by equations (5.9) and (5.11) will represent an upper and lower bound for solute uptake by the mycelium. Having developed equations for transport of solute in soil and mycelial phase, we need to apply initial and boundary conditions to complete the model.

5.2.2 Initial and boundary conditions

Let us assume that the solute concentration in soil solution, C_l, is initially constant and uniform and that there are no external hyphae present, so that we have

$$C_l = C_{l,0}, \qquad t = 0, \tag{5.12}$$

$$C_m = 0, \qquad t = 0. \tag{5.13}$$

We assume that the root takes up nutrients according to Michaelis Menten kinetics. At the root-soil interface, $\partial\Omega_1$, we define a flux boundary condition

$$\theta_l D f \frac{\partial C_l}{\partial n} - v_n C_l = \frac{F_m C_l}{K_m + C_l}, \tag{5.14}$$

where $\frac{\partial}{\partial n}$ is the outward normal derivative and v_n is the Darcy flux of water normal to the root surface. As we assume no competition between roots, we can write

$$C_l = C_{l,0}, \qquad |\mathbf{x}| \to \infty. \tag{5.15}$$

The mechanisms of solute transfer across the fungus-root interface are not very well understood. It is thought to be the limiting step for phosphate transfer into plant root cells, rather than the translocation within the mycelium. As a first attempt, we will assume that the flux at the fungus-root interface is linearly dependent on the concentration in the mycelial phase at the interface,

$$\theta_m^{p+1} D \frac{\partial C_m}{\partial n} - \theta_m v_{m,n} C_m = k_h C_m, \tag{5.16}$$

where k_h is the mycelium root transfer rate. The other boundary condition for solute in the mycelium, C_m, has to be applied at the edge of the colony, which consists of tips only. This boundary is moving forward into the soil with time, and therefore we have to consider it as a moving boundary, $\partial\Omega_m$. We assume that hyphae take up solutes everywhere except exactly at the tip, so that we have at the edge of the colony

$$\theta_m^{p+1} D \frac{\partial C_m}{\partial n} - \theta_m v_{m,n} C_m = 0 \qquad \text{at } \mathrm{x} \in \partial\Omega_m. \tag{5.17}$$

In summary, we have developed the following model for solute uptake by a mycorrhizal root,

$$\frac{\partial((b_p+\theta_l)C_l)}{\partial t} = \nabla\cdot(\theta_l D_l f_l \nabla C_l) - \nabla\cdot(\mathbf{v}\,C_l) - F_{myc}(t), \tag{5.18}$$

$$\frac{\partial(\theta_m C_m)}{\partial t} = \nabla\cdot(D_m\theta_m^{p+1}\nabla C_m) - \nabla\cdot(\theta_m \mathbf{v}_m C_m) + F_{myc}(t), \tag{5.19}$$

$$C_l = C_{l,0}, \quad \mathrm{x}\in\Omega,\ t=0, \tag{5.20}$$

$$C_m = 0, \quad \mathrm{x}\in\Omega,\ t=0, \tag{5.21}$$

$$\theta_l D f \frac{\partial C_l}{\partial n} - v_n C_l = \frac{F_m C_l}{K_m C_l}, \quad \mathrm{x}\in\partial\Omega_1,\ t>0 \tag{5.22}$$

$$C_l = C_{l,0} \quad |\mathbf{x}|\to\infty,\ t>0 \tag{5.23}$$

$$\theta_m^{p+1} D\frac{\partial C_m}{\partial n} - \theta_m v_{m,n} C_m = k_h C_m, \quad \mathrm{x}\in\partial\Omega_1,\ t>0 \tag{5.24}$$

$$\theta_m^{p+1} D\frac{\partial C_m}{\partial n} - \theta_m v_{m,n} C_m = 0, \quad \mathrm{x}\in\partial\Omega_m,\ t>0 \tag{5.25}$$

where F_{myc} is given by either equation (5.9) or (5.11). In the next section, we will apply the model to a specific example motivated by the model of Drew *et al.* (2003).

5.3 Example simulations: Mycorrhizal solute uptake

To apply the model to a specific problem, we need to decide on the appropriate coordinate system, as well as the expressions for hyphal length density and the sink term. We are interested in applying our model to an experiment such as the one described in section 1.1.2. We can not test our model against the data of Drew *et al.* (2003), since it does not provide us with all the necessary information, such as the boundary condition for the hyphal length density, but the experiment serves for our motivation. In this experiment, a root free side arm filled with soil is attached to a root compartment and fungal hyphae are allowed to grow into this side arm and take up isotopically labeled solutes. We assume that the interface between root and hyphal compartment mimics the root surface. Hyphal length density is only dependent on the horizontal distance to the root compartment and we can describe this experiment using one-dimensional cartesian coordinates.

In the following, we need to select the appropriate expressions for hyphal length density and influx. Drew *et al.* (2003) only present one average value of hyphal length density in the hyphal compartment at the end of their experiment. Therefore, we cannot calibrate any of the models for hyphal length density developed in chapters 2 of 3. We choose the simplest model, which is the Boundary Flux Model of chapter

2 with linear branching and constant flux of tips at the boundary. It is given by equation (2.46), and in dimensional form, it is

$$\rho(x,t) = \begin{cases} \frac{k}{d} e^{\frac{b}{v}x} \left(1 - e^{\frac{d}{v}(x-tv)}\right), & 0 \le x \le tv, \\ 0, & tv \le x < \infty, \end{cases} \tag{5.26}$$

where k is the constant tip flux, v is the fungal growth constant, b is the tip branching rate and d is the hyphal death rate. We estimate the values for these parameters from chapter 3. The moving boundary in this case is located at $x_c = vt$.

Assuming that the interface between root and hyphal compartment is located at $x = 0$, the model in one-dimensional cartesian coordinates is

$$(b + \theta_l)\frac{\partial C_l}{\partial t} = \theta_l D_l f_l \frac{\partial^2 C_l}{\partial x^2} + v\frac{\partial C_l}{\partial x} - F_{myc}(t), \tag{5.27}$$

$$\frac{\partial(\theta_m C_m)}{\partial t} = D_m \frac{\partial}{\partial x}(\theta_m^{p+1}\frac{\partial C_m}{\partial x}) + v_m \frac{\partial}{\partial x}(\theta_m C_m) + F_{myc}(t), \tag{5.28}$$

$$\theta_m(t,r) = r_m^2 \pi \begin{cases} \frac{k}{d} e^{\frac{b}{v}x} \left(1 - e^{\frac{d}{v}(x-tv)}\right), & 0 \le x \le tv, \\ 0, & tv \le x < \infty, \end{cases} \tag{5.29}$$

with initial conditions

$$C_l = C_{l,0}, \qquad t = 0, \tag{5.30}$$

$$C_m = 0, \qquad t = 0, \tag{5.31}$$

and boundary condition

$$\theta_l D_l f_l \frac{\partial C_l}{\partial x} + vC_l = \frac{F_m C_l}{K_m + C_l}, \qquad x = 0, \tag{5.32}$$

$$C_l = C_{l,0}, \qquad x \to \infty, \tag{5.33}$$

$$D_m \theta_m^{p+1} \frac{\partial C_m}{\partial x} + v_m \theta_m C_m = k_h C_m, \qquad x = 0, \tag{5.34}$$

$$D_m \theta_m^{p+1} \frac{\partial C_m}{\partial n} + v_m \theta_m C_m = 0, \qquad x = x_c. \tag{5.35}$$

Let x_{max} be the maximal distance of fungal growth in the experiment. Let

$$g(x,t) = \begin{cases} e^{\frac{b}{v}(x-x_{max})} \left(1 - e^{\frac{d}{v}(x-vt)}\right), & 0 \le x \le tv, \\ 0, & tv \le x < \infty. \end{cases} \tag{5.36}$$

Then $\rho(x,t)$ can be expressed as

$$\rho(x,t) = \frac{k}{d} e^{\frac{b}{v}x_{max}} g(x,t), \tag{5.37}$$

where $0 \le g(x,t) \le 1$. The source term F_{myc} is given by either equation (5.9) or (5.11).

5.3.1 Non-dimensionalisation

Let $x = [x]x^*$, $t = [t]t^*$, $C_l = K_m C_l^*$ and $C_m = K_{m,h} C_m^*$. Because we are interested in solute diffusion in soil and the duration of relevant experiments is in the order of weeks. Because of this, we have chosen a length scale which is based on the distance the solute can diffuse in a given soil in one week. So, $[x] = 2\sqrt{6.0 \times 10^5 D_e}$, where D_e is the effective diffusion coefficient of a solute in soil, $D_e = \frac{\theta_l D_l f_l}{b_p + \theta_l}$. Let us choose the time scale such that the coefficient in front of the diffusion term in the equation for C_l is equal to 1, *i.e.* $[t] = \frac{[x]^2(b_p+\theta_l)}{\theta_l D_l f_l}$. Then the non-dimensional model is (dropping asterisks)

$$\begin{aligned} \frac{\partial C_l}{\partial t} &= \frac{\partial^2 C_l}{\partial x^2} + Pe\frac{\partial C_l}{\partial x} - S_1 F_{myc}(x,t;C_l), && (5.38) \\ \delta\,\frac{\partial (g(x,t)C_m)}{\partial t} &= \epsilon\,\frac{\partial}{\partial x}\left(g(x,t)^{p+1}\frac{\partial C_m}{\partial x}\right) + \\ &+ \frac{\partial}{\partial x}\left(g(x,t)C_m\right) + S_2 F_{myc}(x,t;C_l), && (5.39) \end{aligned}$$

where $Pe = \frac{v[x]}{\theta_l D f}$, $S_1 = \frac{2r_m \pi k F_{m,h}[x]^2}{dK_m \theta_l D f} e^{\frac{b}{v}x_{max}}$, $\delta = \frac{\theta_l D f}{[x](b_p+\theta_l)v_m}$, $\epsilon = \frac{D}{[x]v_m}\left(\frac{r_m^2 \pi k}{d}\right)^p e^{\frac{b}{v}x_{max}p}$ and $S_2 = \frac{2F_{m,h}[x]}{K_{m,h} r_m v_m}$. The dimensionless sink term F_{myc} is one of the equations

$$\begin{aligned} F_{myc}(x,t;C_l) &= g(x,t)\frac{C_l}{\kappa + C_l}, && (5.40) \\ F_{myc}(x,t;C_l) &= \begin{cases} 0, & t - t_c < 0, \\ g(x,t)\frac{C_l}{\kappa}\frac{\delta_1 r_{end}[\lambda \ln(r)+1]}{\lambda + \delta_1 r_{end}\lambda \ln(r_{end}) + \delta_1 r_{end}}\, e^{-\gamma k_d (t[t]-t_c)} & t - t_c \geq 0, \end{cases} && (5.41) \end{aligned}$$

where $\kappa = \frac{K_{m,h}}{K_m}$ and $g(x,t) = e^{\frac{b}{v}([x]x - x_{max})}\left(1 - e^{\frac{d}{v}([x]x - vt[t])}\right)$. The boundary conditions become

$$\begin{aligned} \frac{\partial C_l}{\partial x} + PeC_l = \lambda_1 \frac{C_l}{1+C_l}, \quad x = 0, && (5.42) \\ C_l = c_\infty, \quad x \to \infty, && (5.43) \\ g(x,t)^{p+1}\epsilon\frac{\partial C_m}{\partial x} + g(x,t)\,C_m = \lambda_2 C_m, \quad x = 0, && (5.44) \\ g(x,t)^{p+1}\epsilon\frac{\partial C_m}{\partial x} + g(x,t)\,C_m = 0, \quad x = \hat{x_c}, && (5.45) \end{aligned}$$

where $\hat{x_c} = \frac{(b_p+\theta_l)v}{\theta_l D f}t[x]$, $\lambda_1 = \frac{[x]F_m}{\theta_l D f K_m}$, $\lambda_2 = \frac{k_h}{v_m}\frac{d}{k r_m^2 \pi}e^{-\frac{b}{v}x_{max}}$ and $c_\infty = \frac{C_{l,0}}{K_m}$. The dimensionless initial conditions are

$$\begin{aligned} C_l = c_\infty, \quad t = 0, && (5.46) \\ C_m = 0, \quad t = 0. && (5.47) \end{aligned}$$

5.3.2 Parameter estimation

Approximate values for the dimensional parameters in the model are given in table 5.1. The parameters for soil and solute influx on the single hyphal scale have already been discussed in previous chapters. We take the parameters for the fungal growth model from the application to *S. calospora* in chapter 3, because the linear growth model could be fitted to this fungal species. The parameters of most uncertainty are the ones for the mycelial phase, D_m, v_m and k_h and we will now discuss how we estimate them. Given that the fungal cell mainly consists of water, we assume that the diffusion coefficient in the mycelial phase is equal to the diffusion coefficient in water. We estimate the parameter v_m by the velocity of cytoplasmic streaming. Data for this are very scarce. Bago *et al.* (2002) gave estimates for the cytoplasmic streaming of $4.0 \times 10^{-4} - 1.1 \times 10^{-3}\ cm\, s^{-1}$. Nielsen *et al.* (2002) gave estimates for net phosphate flux within arbuscular mycorrhizal hyphae towards the root surface of $F_P = 1.5\, \mu mol\, cm^{-2} s^{-1}$. Assuming that the concentration of P in the hyphae is $C_m = 10.0\ \mu mol\, cm^{-3}$ (Ezawa *et al.* 2002), and that the translocation is due to convection only, the estimated velocity is $v_m = \frac{F_P}{C_m} = 1.5 \times 10^{-3}\ cm\, s^{-1}$. This value is an upper bound for the range given by Bago *et al.* (2002). A third method to estimate v_m is as follows: When we assume a low soil solution concentration of $10^{-4}\, \mu mol\, cm^{-3}$, that the uptake properties of the hyphae are the same as for the root and that the solute is transported away through the cross-sectional area of the hypha at the same rate it is taken up, the velocity is $v_m = 2.21 \times 10^{-5}$. This is lower than the range given by Bago *et al.* (2002), which could be due to the fact that the two experiments above have been conducted under non-limiting solute concentrations. The parameter k_h, accounting for the transfer of solute from the mycorrhiza phase into the root, is completely unknown. Since the hyphae enter the root cells at the so called 'entry points', the value of k_h is likely to be dependent on the number of entry points per unit root surface area. However, we do not have any indication what value k_h could have. As a first guess, we will choose its value so that the dimensionless parameter λ_2 is of order one. It would be interesting to look at the effect of varying k_h, because from experimental evidence, we know that the transport within the hyphal phase is fast and thus the transfer rate at the root-fungus interface may be a limiting step in overall contribution of hyphae to root solute uptake.

Assuming that the uptake characteristics of fungi are the same as for the root, all other parameters are as listed in table 5.1, and k_h is such that $\lambda_2 = O(1)$, the coefficients of the dimensionless model are given in table 5.2.

Table 5.1: Typical values of the dimensional parameters for the mycorrhizal root model.

Parameter	Units	Value	Reference
D_l	$cm^2\ s^{-1}$	10^{-5}	Lide (2000)
q	$cm^2\ s^{-1}$	10^{-7}	Barber (1995)
D_m	$cm^2\ s^{-1}$	10^{-5}	$= D_l$, given that 90% of cell consists of water
f_l	$cm^2\ s^{-1}$	0.308	$f_l = 1.6\,\theta_l - 0.172$ (Barber 1995)
f_m	$cm^2\ s^{-1}$	$\approx< 2 \times 10^{-3}$	equation (5.5)
θ_l	$cm^3 cm^{-3}$	0.3	Barber (1995)
v_m	$cm\,s^{-1}$	$2.21 \times 10^{-5} - 1.5 \times 10^{-3}$	cytoplasmic streaming
r_m	cm	5×10^{-4}	Ezawa *et al.* (2002)
$F_{m,hypha}$	$\mu mol\ cm^{-2}\ s^{-1}$	$3.26 \times 10^{-6} - 2.55 \times 10^{-5}$	Tinker & Nye (2000); Schweiger & Jakobsen (1999)
$K_{m,hypha}$	$\mu mol\ cm^{-3}$	$5.8 \times 10^{-3} - 1.7 \times 10^{-3}$	Tinker & Nye (2000); Schweiger & Jakobsen (1999)
$F_{m,root}$	$\mu mol\ cm^{-2}\ s^{-1}$	3.26×10^{-6}	Tinker & Nye (2000)
$K_{m,root}$	$\mu mol\ cm^{-3}$	5.8×10^{-3}	Tinker & Nye (2000)
k_h	cms^{-1}	-	chosen s.t. $\lambda_2 = O(1)$
b_p	$-$	239	Barber (1995)
k_d	s^{-1}	$5.94 \times 10^{-5} - 2.72 \times 10^{-2}$	Chen *et al.* (1996)
k_a	s^{-1}	$4.73 \times 10^{-2} - 1.95$	$k_a = k_d \frac{b}{\theta}$
A_s	$cm^2\ g^{-1}$	< 1000	for sands (Kammerer & Loiskandl 2003)
ρ_b	$g\ cm^{-3}$	1.02	calculated from Jakobsen *et al.* (1992)
C_{l0}	$\mu mol\ cm^{-3}$	1×10^{-4}	low concentration
b	s^{-1}	5.59×10^{-7}	from *S. calospora*, chapter3
v	$cm\,s^{-1}$	2.89×10^{-6}	from *S. calospora*, chapter3
d	s^{-1}	2.89×10^{-6}	from *S. calospora*, chapter3
k	$cm^{-2}s^{-1}$	2.89×10^{-3}	from *S. calospora*, chapter3

Table 5.2: Values of the dimensionless parameters for the mycorrhizal root model.

	P_e	S_1	λ_1	δ	ϵ	S_2	λ_2	c_∞
$v_m = 2.21, \times 10^{-5}$								
$k_h = 4.0 \times 10^{-7}$	1.05×10^{-2}	196.78	58.79	1.81×10^{-3}	4.05×10^{-2}	9832.36	2.09	0.017
$v_m = 1.50, \times 10^{-3}$								
$k_h = 4.0 \times 10^{-5}$	1.05×10^{-2}	196.78	58.79	3.63×10^{-5}	8.14×10^{-4}	197.54	4.20	0.017

Since the Péclet number P_e is small, we neglect the convection term in equation (5.38), and the model for the soil solution concentration becomes at leading order

$$\frac{\partial C_l}{\partial t} = \frac{\partial^2 C_l}{\partial x^2} - S_1 F_{myc}(x, t; C_l), \tag{5.48}$$

$$\frac{\partial c}{\partial x} = \lambda_1 c, \qquad x = 0, \tag{5.49}$$

$$C_l = c_\infty, \qquad x \to \infty, \tag{5.50}$$

$$C_l = c_\infty, \qquad t = 0. \tag{5.51}$$

The smallest parameter in equation (5.39) is δ. Neglecting the time derivative in the equation for C_m, the model for the concentration in the mycelial phase becomes at the leading order

$$0 = \epsilon \frac{\partial}{\partial x}\left(g(x,t)^{p+1}\frac{\partial C_m}{\partial x}\right) + \\ + \frac{\partial}{\partial x}\left(g(x,t)C_m\right) + S_2 F_{myc}(x,t;C_l), \tag{5.52}$$

$$g(x,t)^{p+1}\epsilon\frac{\partial C_m}{\partial x} + g(x,t)\, C_m = \lambda_2 C_m, \qquad x = 0, \tag{5.53}$$

$$g(x,t)^{p+1}\epsilon\frac{\partial C_m}{\partial x} - g(x,t)\, C_m = 0, \qquad x = \hat{x_c}. \tag{5.54}$$

We solve equations (5.48)-(5.51) numerically, using a finite difference scheme with a centered discretisation in space and the θ-method in time. The implicit non-linear expression due to the sink term is solved using fixed-point iteration. In the case where we use the sink term based on the soil pore model, we have to deal with time delay. The critical time when the external hyphae appear at a given position does not necessarily coincide with the discretisation of time. We approximate the sink term in this case using a finite volume method. The scheme is given in appendix B.

Integrating the right hand side of equation (5.52) from 0 to $\hat{x_c}$, we get an expression for the influx of solute into the root from the mycelial phase,

$$\lambda_2 C_m = \int_0^{\hat{x_c}} S_2 F_{myc}(x,t;C_l)dx, \tag{5.55}$$

which we can compute from the numerical solution of equations (5.48)-(5.51). An upper bound of this influx is provided by the removal of solute by hyphae at any given time t,

$$\int_0^{\hat{x_c}} S_1 F_{myc}(x,t;C_l)dx. \tag{5.56}$$

In the next section, we assess the effect of the two estimates for the hyphal uptake parameters $F_{m,h}$ and $K_{m,h}$ on soil solution concentration as well as solute uptake by mycelium is assessed and the effect of the different expressions for hyphal influx on the single hyphal scale on total solute uptake. Finally, we would like to know the effect of varying the parameters for transport in the mycelial phase, v_m and k_h.

5.3.3 Results

First, we shall consider the results when the sink term based on the continuum soil model is used. Figures 5.1(a)-5.1(b) show the solute concentration in solution, C_l,

for the case when the uptake parameters of the hyphae were assumed to be equal to those of the root and as estimated by Schweiger & Jakobsen (1999), respectively. The width of the depletion zone without mycorrhizas is only approximately $2\,mm$. This value is typical for non-mobile ions such as phosphorus. This corresponds to a relatively small soil volume from which the plant can access this nutrient. Including mycorrhizas shows that the depletion zone reaches as far as the fungal mycelium grows. In this example, it is about $2.5\,cm$ wide after 10 days. If we assume that most of the solute taken up is eventually transferred to the plant, the volume from which the plant can access the solute increases enormously. In figure 5.1(a) we show the concentration in soil solution when the uptake parameters are assumed to be the same as for roots. The depletion in soil is hardly visible, although the total uptake may still be significant. In figure 5.1(b), the concentration in soil solution when uptake parameters are as estimated by Schweiger & Jakobsen (1999) is shown. Here, the external hyphae completely take up all the solutes that are available. The difference between the two results is large and it should be possible to test this with an experiment. The corresponding hyphal length densities are shown in figure 5.1(c).

We wish to asses the contribution of external fungal hyphae to the total influx of solutes into the root. Because the influx into root from soil liquid phase and from mycelial phase come from two differently scaled equations, we bring them into dimensional form before comparing them. The scale for the influx into the root from liquid phase is

$$\frac{K_m \theta_l D_l f}{[x]} = \frac{F_m}{\lambda_1},$$

and the scale for the influx into the root from mycelial phase is

$$K_{m,h} v_m r_m^2 \pi \frac{k}{d} e^{\frac{b}{v} x_{max}} = \frac{k_h}{\lambda_2} K_{m,h}.$$

Integrating the source term F_{myc} over the length of the domain gives the total removal of solute by the mycelium. It is an upper bound for the cumulative influx into root from the mycelial phase. The dimensional equation is

$$J_{upper}(t_D) = \frac{F_m}{\lambda_1} S_1 \int_0^\infty F_{myc}(x,t) dx. \tag{5.57}$$

Figures 5.2(a) and 5.2(b) show the influx of solute into the root from mycelial phase for the two regimes of uptake parameters. In figure 5.2(a), we show the influx when the hyphal uptake parameters are assumed to be the same as for roots. It increases with time, which we expect for an growing fungal mycelium. In figure 5.2(b), we show

the influx when the uptake parameter values are larger. It reaches a constant value, because the mycelium depletes all the available solutes and can access new ones only as it is growing further. It can also be seen in the figures that influx into the root from the mycelial phase is equal to the total removal of solutes from soil. This is independent of the values of the parameters v_m and k_h (graphs not shown), which is why we do not describe the effects of these values further. Transport by convection is so fast that accumulation within the mycelial phase is negligible with respect to influx into the root. It also means that this model does not provide us with the possibility of "regulating" the influx into mycelial phase by means of varying the parameter k_h. We would have to model the transfer from fungus to root in more detail to achieve this (see chapter 6 for suggestions). Figures 5.3(a)-5.3(b) show the cumulative influxes by root, mycelium and in total for the two uptake parameter regimes. In the case when we assume that the hyphal uptake parameters are the same as the ones for the root, hyphal influx becomes important when the root influx starts to level off. In the case of the large uptake parameters, hyphal uptake dominates the total uptake. The cumulative uptake by hyphae of the two parameter regimes are compared in figure 5.3(c). After 10 days, hyphal influx is an order of magnitude larger when the parameters according to Schweiger & Jakobsen (1999) are used.

We shall now consider results for the case when the hyphal influx is based on the soil pore model. Uptake occurs only over a short period of time, until the fungi have completely deplete the pore they are in. For fast reaction times, the period of uptake is very short. In this case, we needed to use a very fine spatial grid to avoid numerical oscillations when computing the influx into the root from the mycelial phase. In figure 5.4(a), small oscillations are still visible even though 10000 grid points were used. The reason for this is that the sink term is like a spike at each grid point around the time t_c, the time when the first external hyphae arrive at a given position (figure 5.4(b)). As can be expected, the contribution of hyphae to total root uptake is much smaller, because only the edge of the colony is taking up as it is foraging into new, undepleted soil. In figure 5.4(c), we show the cumulative influxes due to root, mycelium and in total when the larger uptake parameters as estimated by Schweiger & Jakobsen (1999) are used. In the case when the uptake parameters are the same as the ones for the root, uptake was negligibly small.

5.4 Conclusions

In this section, we have developed a model for solute uptake by a mycorrhizal root. Our main goal was to estimate the contribution of external fungal hyphae to total root uptake.

Based on the assumption that transport within the mycelial phase is dominated by convection and very fast, we arrived at a model where almost all solutes that have been taken up by the hyphae are almost instantaneously translocated to the root surface and transferred into the root. The fast translocation is in accordance with experimental evidence. However, the transfer from fungus into root needs a more detailed model.

We compared the use of two different expressions for solute uptake by a single hypha as developed in chapter 4 to create the sink term that accounts for solute uptake by the fungal mycelium. Using the sink term based on the continuum soil model is straight forward and was used to assess the effect of varying hyphal uptake parameters. We found that when the hyphal uptake parameters of Schweiger & Jakobsen (1999) were used, uptake was completely dominated by the fungi. This would support a recent article by Smith *et al.* (2003), who claime that, under certain conditions, plants may depend completely on the mycorrhizal pathway for their phosphorus nutrition.

When we used the sink term based on the soil pore model, we needed ten times more spatial grid points for the numerical solution so as to avoid numerical oscillations. We also found that, according to this model, the contribution of the mycelium to total uptake is small.

In summary, the differences between the expressions we have developed are large and this highlights the need to test the model against experimental data. Our simulation results confirm that mycorrhizas provide the root with a big spatial advantage to access non-mobile solutes in soil. They also confirm that under certain conditions, mycorrhizal fungi may dominate solute uptake completely and make root uptake negligible.

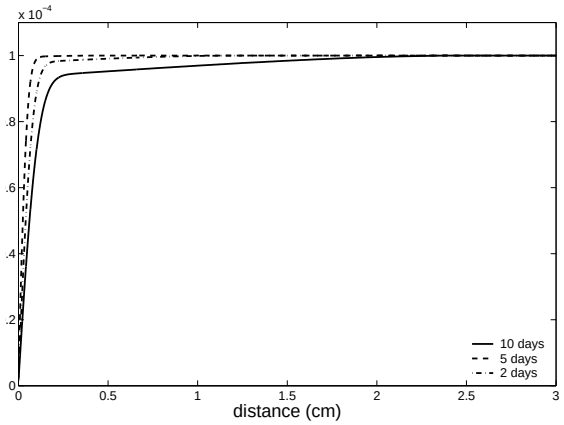

(a) Uptake parameters as root values: $F_{m,h} = 3.26 \times 10^{-6}\,\mu mol\,cm^{-2}s^{-1}$, $K_{m,h} = 5.80 \times 10^{-3}\,\mu mol\,cm^{-3}$.

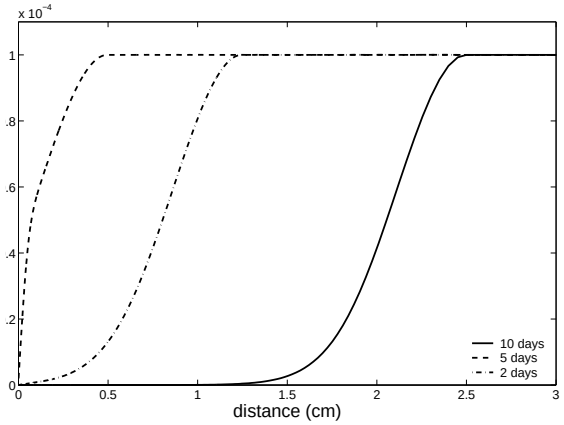

(b) Uptake parameters as given by Schweiger & Jakobsen (1999): $F_{m,h} = 2.55 \times 10^{-5}\,\mu mol\,cm^{-2}s^{-1}$, $K_{m,h} = 1.7 \times 10^{-3}\,\mu mol\,cm^{-3}$.

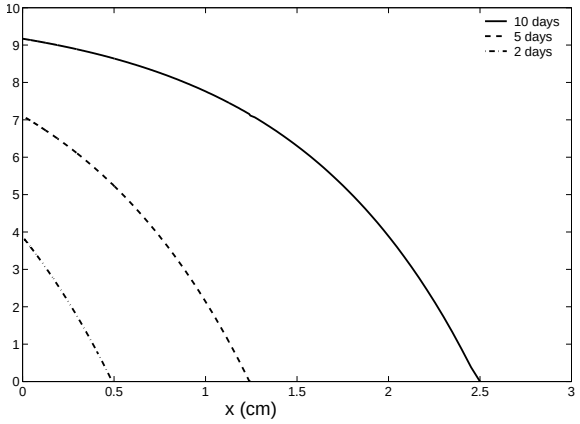

(c) Hyphal length densities corresponding to figures 5.1(a)-5.1(b)

Figure 5.1: Solute concentration in soil solution when uptake by mycelium is based on the continuum soil model. Parameter values as in table 5.1, $v_m = 2.21E-5\,cm\,s^{-1}$, $k_h = 4E-7\,cm\,s^{-1}$, simulation time: 10 days, J=1000, dt=0.001.

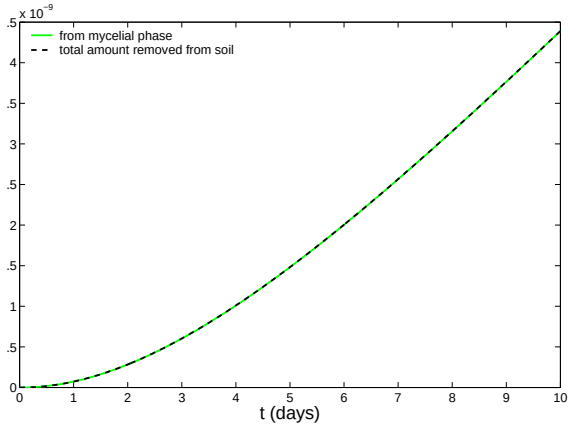

(a) Uptake parameters as root values: $F_{m,h} = 3.26 \times 10^{-6}\,\mu mol\,cm^{-2}s^{-1}$, $K_{m,h} = 5.80 \times 10^{-3}\,\mu mol\,cm^{-3}$.

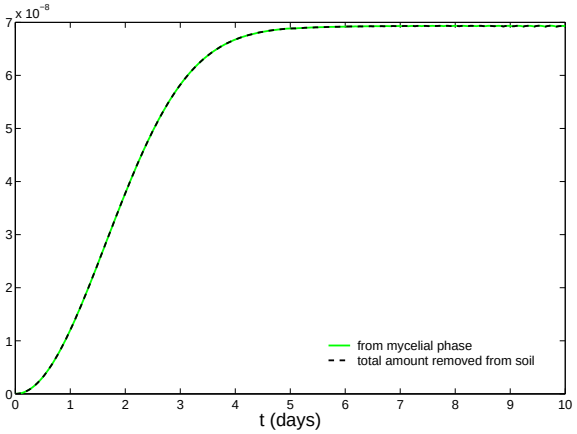

(b) Uptake parameters as given by Schweiger & Jakobsen (1999): $F_{m,h} = 2.55 \times 10^{-5}\,\mu mol\,cm^{-2}s^{-1}$, $K_{m,h} = 1.7 \times 10^{-3}\,\mu mol\,cm^{-3}$.

Figure 5.2: Influx of solute into the root from mycelial phase when uptake by mycelium is based on the continuum soil model. Parameter values as in table 5.1, $v_m = 2.21E-5\,cm\,s^{-1}$, $k_h = 4E-7\,cm\,s^{-1}$, simulation time: 10 days, J=1000, dt=0.001.

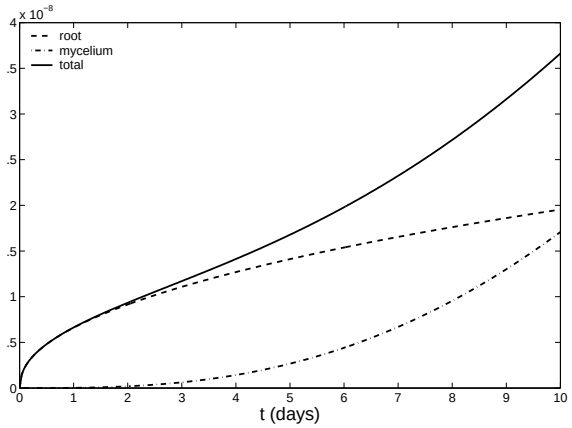

(a) Uptake parameters as root values: $F_{m,h} = 3.26 \times 10^{-6}\,\mu mol\,cm^{-2}s^{-1}$, $K_{m,h} = 5.80 \times 10^{-3}\,\mu mol\,cm^{-3}$.

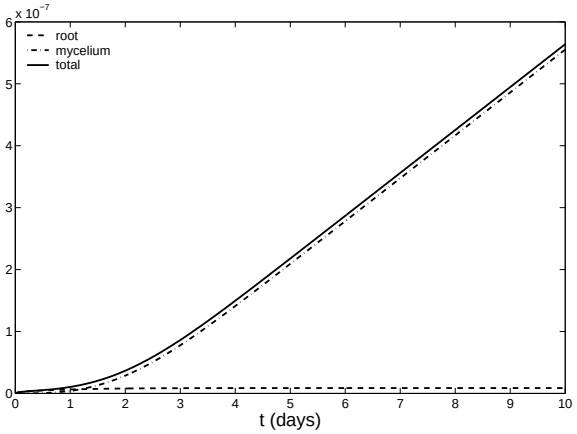

(b) Uptake parameters as given by Schweiger & Jakobsen (1999): $F_{m,h} = 2.55 \times 10^{-5}\,\mu mol\,cm^{-2}s^{-1}$, $K_{m,h} = 1.7 \times 10^{-3}\,\mu mol\,cm^{-3}$.

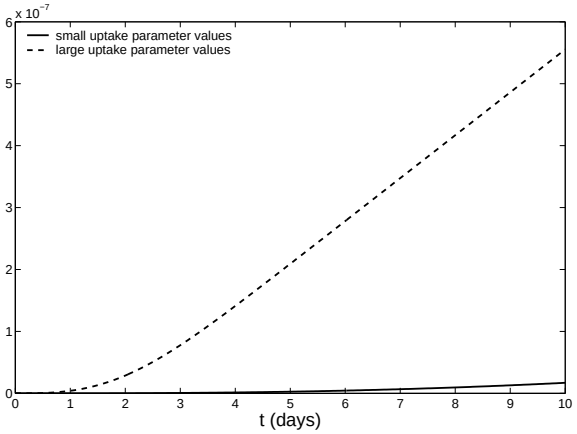

(c) Comparison of hyphal cumulative influx due to the two uptake parameter regimes.

Figure 5.3: Cumulative solute influx into root from soil, mycelium and in total when uptake by mycelium is based on the continuum soil model. Parameter values as in table 5.1, $v_m = 2.21E-5\,cm\,s^{-1}$, $k_h = 4E-7\,cm\,s^{-1}$, simulation time: 10 days, J=1000, dt=0.001.

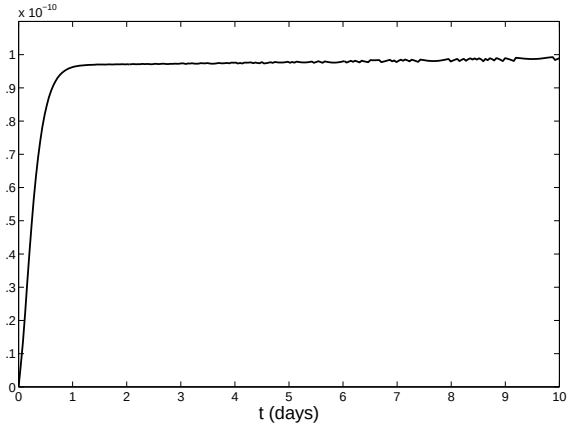

(a) Influx into root from mycelial phase.

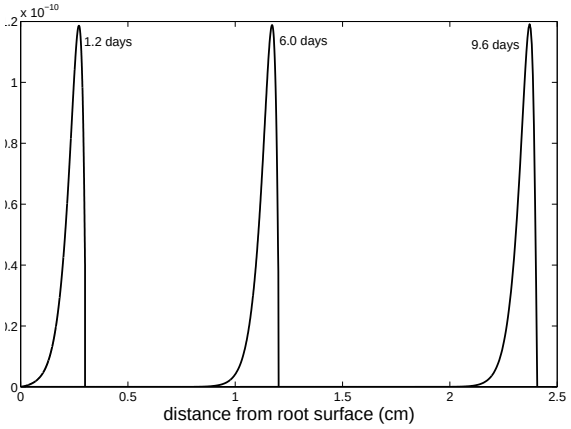

(b) Local hyphal uptake rate.

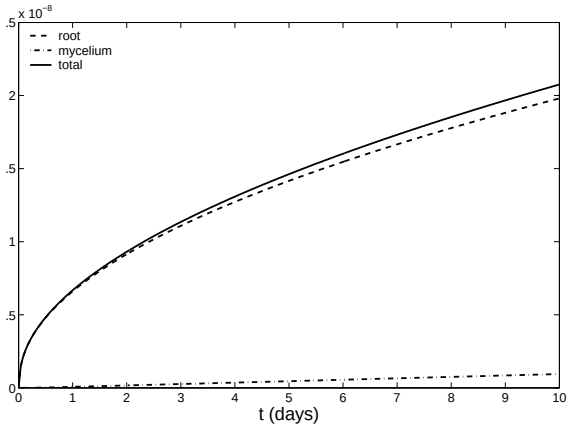

(c) Cumulative solute influx into root.

Figure 5.4: Solute uptake by mycelium due to source term based on the soil pore model. Parameter values as in table 5.1, $F_{m,h} = 2.55 \times 10^{-5}\,\mu mol\,cm^{-2}s^{-1}$, $K_{m,h} = 1.7 \times 10^{-3}\,\mu mol\,cm^{-3}$, $k_d = 6.35 \times 10^{-3}\,s^{-1}$, simulation time: 10 days, J=10000, dt=0.001.

Chapter 6

Conclusions and future work

In this thesis, we developed a model for solute uptake by a mycorrhizal root. It was motivated by the fact that mycorrhizas are important for the mineral nutrition, in particular phosphorus, of many plants. We developed the model for a general solute, and applied it to the special case of phosphorus. A mycorrhizal root is colonized by a soil fungus that grows external hyphae into the soil, several centimeters away from the root surface. These external hyphae can forage for mineral nutrients, translocate them within the hyphal network and transfer them to the plant root. In our model, we accounted for this by means of a sink term which we used to extend a standard single root uptake model. This sink term was derived by scaling from a single hyphal scale to a colony (mycelium) scale.

The fungal growth model is a colony scale model, but its parameters relate to growth, death and branching of individual hyphae. Considering an average value for these properties for all hyphae within the mycelium, we were able to derive analytical and numerical solutions for different initial and boundary conditions, which are presented in chapters 2 and 3. The feature which enabled us to apply this fungal growth model to the specific case of arbuscular mycorrhizal fungi was by means of a boundary condition for tip flux across the root surface. By fitting a function to given boundary data for hyphal length density, we were able to test our model against experimental data of Jakobsen *et al.* (1992). We found that the basic linear fungal growth model, which was developed by Edelstein (1982), could be applied to one of the fungal species considered, *S. calospora*. For the other two fungal species, it was necessary to include additional processes. We tested the effect of non-linear branching and anastomosis. The non-linear branching model could be fitted to the data for the fungal species *Glomus sp.*, but not to *A. laevis*. Including anastomosis could only partly explain the behavior of *A. laevis*. Hence it remains undetermined whether this process is important for this fungal species. In conclusion, this is the first time

a spatially explicit growth model for mycelial fungi has been applied to arbuscular mycorrhizal fungi. It was generally applicable, but had to be modified carefully for each fungal species.

In chapter 4, we presented approximate analytical expressions describing the influx of solute into a cylindrical hypha. These expressions were based on different assumptions about the soil in which the fungi are growing. The standard assumption is that the soil can be described as a continuum. For this case, we showed that we can apply the approximate analytical solution that Roose *et al.* (2001) developed for a single cylindrical root to calculate influx into a single cylindrical hypha. Considering the fact that, for most soils, the hyphal diameter is much smaller than the soil pore diameter, we developed a model for solute influx into a single cylindrical hypha when the soil cannot be described as a continuum, but assuming that the fungi grow in the pore space between the soil solid particles. We presented approximate analytical solutions for this model. All approximate analytical solutions were compared with the numerical solutions of the full models and good agreement was found. This provides confidence that the solutions are correctly derived. However, in our examples considered, the differences between the expressions were up to an order of magnitude, and we have no means of testing them against experimental data, as there are none available on the single hyphal scale. This highlights the fact that experiments on the single hyphal scale would be beneficial. The pore scale model could serve to determine hyphal uptake parameters in an experiment conducted on the single hyphal scale.

The upscaling to solute uptake by the whole mycelium is done by assuming average values of hyphal diameter and uptake parameters for all hyphae within the mycelium. Using the expressions for hyphal length density and solute influx on the single hyphal scale for either the continuum soil model or the soil pore model, we can create different sink terms accounting for solute uptake by hyphae. We carried out example simulations in chapter 5, where we were interested in assessing solute removal from soil by a fungal mycelium, as well as translocation and transfer of solute within the mycelial phase. Based on the assumption that transport within the mycelial phase is dominated by convection and is very fast, we arrived at a model where all solutes that had been taken up by the hyphae were almost instantaneously translocated to the root surface and transferred into the root. The fast translocation is in accordance with experimental evidence. This model, however, does not provide us with a means of estimating whether transfer from fungus to root could be a limiting step for the contribution of fungi to plant mineral nutrition. This was true for all models considered.

The quantity of interest in terms of plant mineral nutrition is the cumulative influx of solute into the root. We compared cumulative influxes of root and mycelium for the model based on both the continuum soil model and the soil pore model. In the first case, the fungi take up nutrients as long as they are available in the soil. When we assume that the fungi have the same uptake properties as the root, cumulative influx was first dominated by the root until the mycelium grew larger. When the root influx started to level off, the mycelium took over and dominated total cumulative influx. When we assumed that the fungi had larger uptake properties than the root, as estimated by Schweiger & Jakobsen (1999), uptake was completely dominated by the mycelium. This would support a recent article by Smith *et al.* (2003), who claims that, under certain conditions, plants may depend completely on the mycorrhizal pathway for their phosphorus nutrition. In the case of the pore scale model, only the first hyphae to arrive at a given position take up nutrients. Influx due to that source term is like a spike that travels through the soil. In this case, we had to use a very fine space grid so as to avoid oscillations in the numerical solution. The contribution of hyphae to total cumulative influx was found to be much less than that of the root. In summary, the models for solute uptake by a mycorrhizal root that we have developed here give largely different results. We would need to test the model against experimental data to find out which model describes the system most adequately. However, our simulation results confirm that mycorrhizas provide the root with a spatial advantage to access non-mobile solutes in soil. They also confirm that under certain conditions, mycorrhizal fungi may dominate plant solute uptake.

Our suggestion for future work regarding the fungal growth model relates to the fact that the model we developed here is dependent on boundary data for the hyphal length density that may not always be available. Root colonisation by mycorrhiza is typically measured in percentage of root length infected. If it was possible to infer the hyphal length density from this data, we could replace our boundary condition with a model for root infection. Two approaches to model colonization of roots have been proposed. McGonigle (2001) used non-linear regression with the logistic equation for changes with time of percentage root length colonized. This would be similar to the boundary condition we used here. Allen (2001); Neuhauser & Fargione (2004) proposed to use Lotka-Volterra type models. The basic idea is to model two interactive but distinct entities (root and fungus) instead of a lumped variable such as infection. From this, infection can still be inferred and be used to compare with experimental data.

Regarding the transport of solute within the mycelial phase, we suggest modelling the transfer from fungus into root in more detail. Tinker & Nye (2000) suggest a model for transfer from fungus to plant that takes into account the two plasmalemmas and transfer processes across them. Another approach would be to include the arbuscules into the model, those fungal structures within root cells developed by arbuscular mycorrhizal fungi, where the transfer of phosphorus from fungus to root is thought to occur.

For upscaling hyphal influx of the soil pore model to mycelium scale, we used the local hyphal length density as well as a factor θ, to account for the volume from which hyphae can take up solutes. However, we suggest a different type of upscaling that is linked with turnover of external hyphae. In particular, we suggest accounting for the fact that, after the first appearance of external hyphae at a given position, new hyphae are created by branching. If we assume that they grow into a new, undepleted soil pore, uptake would not stop as fast as it did in our model.

A further extension would be a model on the root system scale, in which case we would also have to deal with competition between mycorrhizal roots.

Appendix A

Numerical solution of the full non-linear model in chapter 4

For the numerical solution of Equations (4.39)-(4.42), we use a finite difference scheme with a centered discretisation in space and the θ-method in time. Let h be the step size of a uniform mesh in space and let Δt be the time step. Let $J+1$ be the number of grid points. Let $c(jh,\, n\Delta t) \approx U_j^n$ and $c_a(n\Delta t) \approx V^n$. Then the numerical scheme is given by

$$\frac{U_j^{n+1} - U_j^n}{\Delta t} = \theta \left[\frac{1}{r}\frac{\partial}{\partial r}\left(r\frac{\partial U}{\partial r}\right)\right]^{n+1} + (1-\theta)\left[\frac{1}{r}\frac{\partial}{\partial r}\left(r\frac{\partial U}{\partial r}\right)\right]^{n} \quad n = 0, 1, ..., N-1, \quad \text{(A.1)}$$

where

$$\frac{1}{r}\frac{\partial}{\partial r}\left(r\frac{\partial U}{\partial r}\right) \approx \frac{1}{r_j\, h}\left[r_{j+\frac{1}{2}}\frac{U_{j+1} - U_j}{h} - r_{j-\frac{1}{2}}\frac{U_j - U_{j-1}}{h}\right] \qquad j = 1, ..., J-1. \quad \text{(A.2)}$$

This scheme can be rewritten as

$$\begin{aligned} -\frac{r_{j+\frac{1}{2}}}{r_j}\theta\mu U_{j+1}^{n+1} + \left(1 + \frac{r_{j+\frac{1}{2}} + r_{j-\frac{1}{2}}}{r_j}\theta\mu\right) U_j^{n+1} - \frac{r_{j-\frac{1}{2}}}{r_j}\theta\mu U_{j-1}^{n+1} = \\ \frac{r_{j+\frac{1}{2}}}{r_j}(1-\theta)\mu U_{j+1}^{n} + \left(1 - \frac{r_{j+\frac{1}{2}} + r_{j-\frac{1}{2}}}{r_j}(1-\theta)\mu\right) U_j^{n} + \frac{r_{j-\frac{1}{2}}}{r_j}(1-\theta)\mu U_{j-1}^{n} \quad \text{(A.3)} \\ j = 1, ..., J-1 \end{aligned}$$

where $\mu = \frac{\Delta t}{h^2}$. We solve the tridiagonal system of equations

$$(I - \theta\mu D)U^{n+1} = (I + (1-\theta)\mu D)U^n + b, \qquad j = 1, 2, ..., J-1, \qquad \text{(A.4)}$$

where I is the $(J+1) \times (J+1)$ unit matrix, b is $(J+1) \times 1$ zero-vector used to implement the boundary conditions, U is the vector $(U_0, U_1, ..., U_J)^T$ and D is the

differential operator, a tridiagonal $(J+1)\times(J+1)$ matrix whose entries are zero except for

$$\left[\frac{r_{j-\frac{1}{2}}}{r_j}, -\frac{r_{j+\frac{1}{2}}+r_{j-\frac{1}{2}}}{r_j}, \frac{r_{j+\frac{1}{2}}}{r_j}\right] \quad \text{at} \quad j=1,...,J-1.$$

Let LHS be the matrix $(I-\theta\mu D)$ of the left hand side of equation (A.4) and RHS the matrix $(I+(1-\theta)$ of the right hand side. The first and last rows of LHS and RHS have to be modified according to the boundary conditions. The initial condition is

$$U_j^0 = 1 \quad \text{at} \quad j=0,1,...,J. \tag{A.5}$$

To implement the flux boundary conditions at $r=1$ and $r=r_{end}$, we use a grid such that the boundaries lie between the first and second, respectively between the two last grid points, *i.e.* we define the space grid vector as $r=(1-\frac{h}{2}, 1+\frac{h}{2}, ..., r_{end}+\frac{h}{2})$. Then we approximate the flux equations (4.40) and (4.41) with

$$\frac{U_1^{n+1}-U_0^{n+1}}{h} = \lambda\frac{\frac{1}{2}(U_0^n+U_1^n)}{1+c_\infty\frac{1}{2}(U_0^n+U_1^n)} \quad n=0,...,N-1 \tag{A.6}$$

and

$$\frac{U_J^{n+1}-U_{J-1}^{n+1}}{h} = -\frac{\delta_1}{2}(U_{J-1}^{n+1}+U_J^{n+1})+\delta_1 V^{n+1} \quad \text{at} \quad n=0,...,N-1. \tag{A.7}$$

At every time step, we approximate c_a in equation (4.41) with an explicit Euler scheme, $V^{n+1}=V^n+\frac{\Delta t}{\delta_2}(\frac{1}{2}(U_J^n+U_{J-1}^n)-V^n)$, where $V^0=1$.

The first row of LHS becomes

$$[-1,1,0,...,0] \tag{A.8}$$

and the first row of the RHS is a zero-vector. The last row of LHS becomes

$$[0,...,-1+0.5\delta_1 h, 1+0.5\delta_1 h] \tag{A.9}$$

and the last row of the RHS is a zero-vector. The entries of the vector b are zero, except the first entry is $(\lambda\frac{\frac{h}{2}(U_0^{n+1}+U_1^{n+1})}{1+c_\infty\frac{1}{2}(U_0^{n+1}+U_1^{n+1})})$ and the last entry is $(\delta_1 h V^{n+1})$. This non-linear expression requires values of the solution at time $n+1$. We solved this by a fixed point iteration, using the values at time n as initial guesses.

The solutions at $r=1$ and $r=r_{end}$ are given by

$$U(1,n\Delta t) = \frac{1}{2}(U_0^n+U_1^n) \tag{A.10}$$

and

$$U(r_{end},n\Delta t)) = \frac{1}{2}(U_J^n+U_{J-1}^n). \tag{A.11}$$

Appendix B

Numerical solutions for chapter 5

To deal with the semi-infinite domain, we define a new space variable $z = \frac{1}{x+1}$, so that $x \in [0, \infty)$ is mapped to $z \in (0, 1]$. The differential operator becomes

$$\frac{\partial}{\partial x} = -z^2 \frac{\partial}{\partial z}, \tag{B.1}$$

and $g(x, t)$ is transformed to

$$g(z, t) = e^{\frac{b}{v}\left([x]\frac{1-z}{z} - x_{max}\right)} \left(1 - e^{\frac{d}{v}\left([x]\frac{1-z}{z} - vt[t]\right)}\right). \tag{B.2}$$

B.1 Soil solution concentration, c, with sink term based on the continuum soil model

Rescaling $C_l = c_\infty c$, and transforming the space variable as outlined above, equations (5.48)-(5.51) become

$$\frac{\partial c}{\partial t} = z^2 \frac{\partial}{\partial z}\left(z^2 \frac{\partial c}{\partial z}\right) - S_1 F_{myc}(z, t, c), \tag{B.3}$$

$$\frac{\partial c}{\partial z} = -\lambda_1 \frac{c}{1 + c\, c_\infty}, \qquad z = 1, \tag{B.4}$$

$$c = 1, \qquad z \to 0, \tag{B.5}$$

$$c = 1, \qquad t = 0, \tag{B.6}$$

where

$$F_{myc}(z, t, c) = g(z, t) \frac{c}{\kappa + c_\infty c}$$

or

$$F_{myc}(z, t; c) = \begin{cases} 0, & t - t_c < 0, \\ g(z, t) \frac{c}{\kappa} \frac{\delta_1 r_{end}[\lambda \ln(r) + 1]}{\lambda + \delta_1 r_{end} \lambda \ln(r_{end}) + \delta_1 r_{end}} e^{-\gamma k_d (t[t] - t_c)}, & t - t_c \geq 0. \end{cases}$$

For their solution, we use a finite difference scheme with a centered discretisation in space and using the θ-method in time. Let h be the step size of a uniform mesh in space and let Δt be the time step. Let $J+1$ be the number of grid point and N be the number of time steps. Let the dimensionless concentration in soil be denoted by $c(z,t)$ where t is the dimensionless time and z is the dimensionless and transformed space variable such that $z=1$ at the root surface and $z=0$ infinitely far away from the root. Let $c(jh,\, n\Delta t) \approx U_j^n$ and ${F_{myc}}_j^n \approx F_{myc}(jh, n\Delta t, U_j^n)$. Then the numerical scheme is given by

$$\begin{aligned} \frac{U_j^{n+1}-U_j^n}{\Delta t} &= \theta\left(z^2\frac{\partial}{\partial z}z^2\frac{\partial c}{\partial z}\right)^{n+1} + (1-\theta)\left(z^2\frac{\partial}{\partial z}z^2\frac{\partial c}{\partial z}\right)^{n} - \\ &- \theta S_1 {F_{myc}}_j^{n+1} - (1-\theta)S_1 {F_{myc}}_j^{n},\ n=0,1,...,N-1 \end{aligned} \tag{B.7}$$

where

$$z^2\frac{\partial}{\partial z}z^2\frac{\partial c}{\partial z} \approx \frac{z_j^2}{h}\left(z_{j+\frac{1}{2}}^2\frac{U_{j+1}^n-U_j^n}{h} - z_{j-\frac{1}{2}}^2\frac{U_j^n-U_{j-1}^n}{h}\right), \qquad j=1,...,J-1. \tag{B.8}$$

The value of U_j^{n+1} is required for the non-linear sink term, if $\theta \neq 0$. We could either use Newton's method to solve this implicit equation, or, which is what we have used, a fixed-point iteration, with U_j^n as the starting value.

To implement the flux boundary condition at $z=1$, we use a spatial grid such that $z=1$ lies between the last and second to last grid point. The value at $z=1$, we approximate by $U(1, n\Delta t) \approx 0.5(U_J^n + U_{J-1}^n)$. The initial and boundary conditions are

$$U_j^0 = 1, \qquad j=0,...,J, \tag{B.9}$$

$$U_0^{n+1} = 1, \qquad n=0,...,N-1, \tag{B.10}$$

$$(1+0.5\lambda_1 h)U_J^{n+1} = (-1+0.5\lambda_1 h)U_{J-1}^{n+1} = 0, \qquad n=0,...N-1. \tag{B.11}$$

Expressed in matrix form, we solve

$$(I-\theta\mu D)U^{n+1} = (I+(1-\theta)\mu D)U^n + b, \tag{B.12}$$

where $\mu = \frac{\Delta t}{h^2}$, D is the differential operator

$$\begin{aligned} D &= \left(0,...,0, z_j^2 z_{j-\frac{1}{2}}^2, -z_j^2(z_{j-\frac{1}{2}}^2 + z_{j+\frac{1}{2}}^2), z_j^2 z_{j+\frac{1}{2}}^2, 0,...,0\right), \\ &\quad j=1,2,...,J-1. \end{aligned} \tag{B.13}$$

The vector b implements the source term and is

$$b = \left(-\theta S_1 {F_{myc}}_j^{n+1} - (1-\theta)S_1 {F_{myc}}_j^{n}\right), \qquad j=1,2,...,J-1. \tag{B.14}$$

Let LHS be $(I - \theta\mu D)$ and RHS be $(I - (1-\theta)\mu D)$. Then the boundary condition at $z = 0$ implies that the first line of LHS as well as RHS is $(1, 0...0)$. Due to the boundary condition at $z = 1$, the last line of LHS is $(0...0, (\frac{1}{2}\lambda h - 1), (\frac{1}{2}\lambda h + 1))$.

B.2 Sink term based on the soil pore model

In the case of the sink term based on the soil pore model, we need to deal with a time-delay. Equation 5.41 describes the time dependent hyphal solute uptake. It starts only at the critical time t_c, when external hyphae first appear at a given point. Since t_c may lay between two points of the time grid, t_n and t_{n+1}, we approximate the source term using finite volumes instead of finite differences, so that

$$\begin{aligned} {F_{myc}}_j^n &\approx \frac{\theta}{h\,\Delta t}\int_{z_j-\frac{h}{2}}^{z_j+\frac{h}{2}}\int_{t_n}^{t_{n+1}} F_{myc}(z,t;U_j^{n+1})\,dt\,dz + \\ &+ \frac{(1-\theta)}{h\,\Delta t}\int_{z_j-\frac{h}{2}}^{z_j+\frac{h}{2}}\int_{t_n}^{t_{n+1}} F_{myc}(z,t;U_j^{n})\,dt\,dz. \end{aligned} \tag{B.15}$$

References

Allen 2001 Modeling arbuscular mycorrhizal infection: is % infection an appropriate variable? *Mycorrhiza* **10**, 255 – 258.

Atkins, P. 1998 *Physical Chemistry*, 6th edn. Oxford University Press.

Bago, B., Zipfel, W., Williams, R., Jun, J., Arreola, R., Lammers, P., Pfeffer, P. & Shachar-Hill, Y. 2002 Translocation and utilization of fungal storage lipid in the arbuscular mycorrhizal symbiosis. *Plant Physiology* **128**, 109–124.

Barber, S. 1995 *Soil Nutrient Bioavailability: a mechanistic approach*. JohnWiley & sons, Inc. New York.

Chen, J., Mansell, R., Nkedi-Kizza, P. & Burgoa, B. 1996 Phosphorus transport during transient, unsaturated water flow in an acid sandy soil. *Soil Sci. Soc. Am. J.* **60**, 42–48.

Crank, J. 1975 *The Mathematics of Diffusion*. Clarendon Press, Oxford.

Drew, E., Murray, R., Smith, S. & Jakobsen, I. 2003 Beyond the rhizosphere: growth and function of arbuscular mycorrizal external hyphae in sands of varying pore sizes. *Plant and Soil* **251**, 105–114.

Edelstein, L. 1982 The propagation of fungal colonies: A model for tissue growth. *J. theor. Biol.* **98**, 679–701.

Ezawa, T., Smith, S. & Smith, F. 2002 P metabolism and transport in am fungi. *Plant Soil* **244**, 221–230.

Giovanetti, M., Fortuna, P., Citernesi, A. & Morini, S. 2001 The occurrence of anastomosis formation and nuclear exchange in intact arbuscular mycorrhizal networks. *New Phytol.* **151**, 717–724.

Jakobsen, I., Abbott, L. & Robson, A. 1992 External hyphae of vesicular-arbuscular mycorrhizal fungi associated with *Trifolium subterraneum* l. 1. spread of hyphae and phosphorus inflow into roots. *New Phytol.* **120**, 371–380.

Kammerer, G. & Loiskandl, W. 2003 Bodenphysik (Vertiefung). Lecture notes, BOKU-University of Natural Resources and Applied Life Sciences.

Kume-Kick, J., Mazel, T., Vorsek, I., Hrabetov, S., Tao, L. & Nicholson, C. 2002 Independence of extracellular tortuosity and volume fraction during osmotic challenge in rat neocortex. *Journal of Physiology* **542**, 515–527.

Lide, D. 2000 *Handbook of Chemistry and Physics*, 83rd edn. CRC Press LLC, Boca Raton, FL.

McGonigle, T. 2001 On the use of non-linear regression with the logistic equation for changes with time of percentage of root length colonized by arbuscular mycorrhizal fungi. *Mycorrhiza* **10**, 249–254.

Morton, K. & Mayers, D. 1994 *Numerical Solution of Partial Differential Equations*. Cambridge University Press.

Neuhauser, C. & Fargione, J. 2004 A mutualism-parasitism continuum model and its application to plant-mycorrhizae interactions. *Ecological Modelling* **177**, 337–352.

Nielsen, J., Joner, E., Declereck, S., Olsson, S. & Jakobsen, I. 2002 Phospho-imaging as a tool for visualization and noninvasive measurement of p transport dynamics in arbuscular mycorrhizas. *New Phytologist* **154**, 809–819.

Reginato, J., Palumbo, M., Moreno, I., Bernardo, I. & Tarzia, D. 2000 Modeling nutrient uptake using a moving boundary approach: Comparison with the barber-cushman model. *Published in Soil Sci. Soc. Am. J.* **64**, 1363–1367.

Roose, T., Fowler, A. & Darrah, P. 2001 A mathematical model of plant nutrient uptake. *J. Math. Biol.* **42**, 347–360.

Scheffer, F., Schachtschabel, P., Blume, H., Brmmer, G., Schwertmann, U., Horn, R., Kgel-Knabner, I., Stahr, K. & Wilke 2002 *Scheffer/Schachtschabel: Lehrbuch der Bodenkunde*. Spektrum Akademischer Verlag.

Schweiger, P. & Jakobsen, I. 1999 *Plant Nutrition - Molecular Biology and Genetics.*, chap. The role of mycorrhizas in plant P nutrition: Fungal uptake kinetics and genotype variation., pp. 277–289. Kluwer Academic Publishers, Dordrecht.

Smith, S., Smith, F. & Jakobsen, I. 2003 Mycorrhizal fungi can dominate phosphate supply to plants irrespective of growth responses. *Plant Physiology* **130**, 16–20.

Staddon, P., Bronk Ramsey, C., Ostle, N., Ineson, P. & Fitter, A. 2003 Rapid turnover of hyphae of mycorrhizal fungi determined by ams microanalysis of ^{14}C. *Science* **300**, 1138–1139.

Tao, L. & Nicholson, C. 2004 Maximum geometrical hindrance to diffusion in brain extracellular space surrounding uniformly spaced convex cells. *Journal of Theoretical Biology* **229**, 59–68.

Tinker, P. & Nye, P. 2000 *Solute Movement in the Rhizosphere*. Oxford University Press, New York, Oxford.